

AIX-MARSEILLE UNIVERSITE
FACULTE DES SCIENCES MEDICALES ET PARAMEDICALES
Ecole doctorale Sciences de la Vie et de la Santé

THESE

De doctorat spécialité Biologie et Santé

Characterizing the role of epithelial cells at transition
zones in normal and disease state

Soutenue publiquement le 13 octobre 2021

Louciné MITOYAN

En vue de l'obtention du grade de Docteur en Sciences

Membres du jury:

Dr. Audrey FERRAND	Rapporteuse
Pr. Cédric BLANPAIN	Rapporteur
Dr. Béatrice ROMAGNOLO	Examinatrice
Pr. John DE VOS	Président
Dr. Géraldine GUASCH	Directrice de thèse

ACKNOWLEDGMENTS

First, I want to thank Pr. Cédric BLANPAIN, Dr. Audrey FERRAND, Dr. Béatrice ROMAGNOLO and Pr. John De Vos for accepting to be part of my thesis jury.

I want to thank Pr. Jean-Paul BORG for accepting me in the CRCM.

I want to thank la Ligue Nationale Contre le Cancer for funding my fourth year of Ph.D. This year has been crucial for the achievement of many projects.

I would like to thank our team leaders, Emmanuelle CHARAFE-JAUFFRET and Christophe GINESTIER for their relevant advices during these years that really helped my project to mature. Thank you both for supporting me during hard times. I will be forever grateful for what you have done.

I genuinely want to thank Géraldine GUASCH, my mentor, for everything she taught me, her involvement and her availability. You helped me to mature and grow in many ways; scientifically, professionally and personally. Thank you for being such a good example. I will miss our long discussions in your office (so long that my coffee was actually getting cold). I think we made a great team together. I truly wish you the best.

I also want to thank Véronique CHEVRIER for everything she did for me during my time in the lab. Thank you for your daily advices that helped me and the nice moments we shared together.

Thank you to all my coworkers Julien, Alexane, Célia, Martin, Mary-Loup, Mauro and the last to arrive in the lab, Manon, Eddy, Sarah and Chloé. Thank you all for the good times spent together, especially nice lunches we shared together. Special mention to Julien and his blind tests that bring everyone together. I also want to thank Robin, Lauriane and Tiphaine that stayed for shorter periods in the lab. I will remember all of you.

I would like to thank Sébastien, Françoise, Florence, Stéphane and Marion without whom lab life would not have been the same. Thank you for all good memories and the joy you brought me.

I thank all the people I interacted with on a daily basis, Jean-Christophe, Arnaud, Jean-Baptiste and Cyril from the mouse facility, Manon and Françoise from the flow cytometry

facility, Emilie from the experimental histopathology (ICEP) and Magda from the microscopic core facility. It was a real pleasure to work with you.

I am grateful for my incredibly supportive friends Mélina, Bella, Hripsimé, Eugénie, Gayané, Sabria, Evelyne and Lola that keep encouraging me in all aspect of my life, particularly during my Ph.D, I wouldn't have made it without you.

I am unconditionally grateful for my parents, brother and family that made everything in order to let me achieve my goals. Thank you to my grandparents that taught me hard work and never stopped pushing me, especially my grandfather that sadly passed away during my Ph.D.

Finally, the last (but not the least) my husband-to-be, Antoine, who helps me and motivates me daily to achieve my goals and to improve myself. Thank you for making life easier.

Thank you to everyone I had the chance to share a little moment with. This Ph.D journey has been an incredible life experience. I learned so much during the last four years and not only professionally but also humanly and personally.

*To my People,
To my Family,
To my Grandparents,*

Résumé

Les zones de transition (TZ) représentent la jonction entre deux types d'épithéliums et sont retrouvées à différents endroits dans notre corps. Ces zones sont susceptibles de développer des cancers de très mauvais pronostic, mais les mécanismes cellulaires et moléculaires responsables de cette susceptibilité tumorale sont peu connus. Ces régions contiennent des cellules ayant des caractéristiques communes avec des cellules souches provenant d'autres tissus. Cependant, le rôle de cette population cellulaire unique est peu connu dans un contexte d'homéostasie, de blessure et dans le processus d'initiation tumorale. Notre hypothèse de travail est donc que les cellules présentes dans les zones de transition contribuent au maintien des différents épithéliums et représentent des cellules actrices de l'initiation tumorale. Durant ma thèse, j'ai analysé et suivi le devenir de ces cellules dans un contexte de développement normal et de blessure en me focalisant sur la TZ anorectale. Un modèle génétique unique de traçage cellulaire utilisant le marqueur spécifique de TZ, la Kératine 17, a été utilisé permettant de suivre *in vivo* le devenir ces cellules en condition physiologique et de blessure. De plus, nous avons établi un modèle de culture cellulaire en 3Dimensions, dit d'organoïdes, à partir de cellules de la TZ anorectale récapitulant la hiérarchie et les marqueurs retrouvés *in situ*. Ces modèles, combinés à des analyses transcriptomiques, nous ont permis de mettre en lumière l'hétérogénéité cellulaire de la TZ anorectale ainsi que les propriétés des cellules souches qui s'y trouvent. Ces cellules souches montrent des capacités d'unipotence en condition d'homéostasie en maintenant l'épithélium du canal anal mais également de multipotence en condition de stress leur conférant la capacité de participer à la réparation tissulaire du rectum.

De récentes observations ont montré que des mutations dans les lymphocytes T menaient spontanément à l'apparition de tumeurs au niveau de la TZ anorectale suggérant une forte interaction entre les cellules immunes et les cellules épithéliales. J'ai mis au point un modèle murin unique de pré-néoplasie utilisant l'oncogène KRas dans sa forme mutée G12D spécifiquement dans les cellules de la TZ. Ce modèle est unique car il permet de suivre de façon séquentielle les différentes étapes de la progression tumorale spécifiquement à la TZ anorectale. Du séquençage sur cellule unique sera réalisé à partir des cellules épithéliales et immunes de ce modèle et permettra d'identifier les gènes impliqués dans la susceptibilité tumorale de ces régions.

Abstract

Transition zones (TZ) are special regions in the body at the junction between two different types of epithelium. These zones harbor a unique cell population with stem cell properties and may be the target of early transformation as they are frequently associated with cancer. The mere fact that transition zone cells can merge different architecture with separate functions implies for a unique plasticity that these cells must display in steady state. However, their roles during tissue regeneration in normal and injured states and their role in tumorigenesis remain unknown. Using *in vivo* lineage tracing, single-cell transcriptomics, computational modeling and a three-dimensional organoid culture system of anorectal transition zone cells, we identified a population of Keratin 17⁺ (Krt17) basal cells at the squamo-columnar anorectal junction that maintain a squamous epithelium during homeostasis. When challenged, a minority of Krt17⁺ TZ cells showed unexpected plasticity and participated to the repair of a glandular epithelium by giving rise to a fully differentiated crypt. Single cell RNAsequencing analysis unraveled the heterogeneity of anorectal TZ with differentially expressed genes and properties.

Recent observations showed that mutations specifically in T lymphocytes led to spontaneous tumors in anorectal transition zone suggesting an important interplay between immune and epithelial cells. We developed a unique mouse model of neoplasia with the oncogene KRas^{G12D} mutated in Krt17⁺ transition zones cells that recapitulate anorectal TZ hyperplasia when activated and *in situ* carcinoma when subjected to chronic mechanical wounds. This mouse model will be further used to investigate early events of oncogenic transformation and unveil key tumor susceptibility regulators with transcriptomic analysis. Regulators candidates will be tested on organoids derived from these mice to modulate tumor phenotype. Ultimately, this study will help identify cell populations responsible of tumor initiation.

Abbreviations.....	8
List of figures	11
INTRODUCTION.....	12
I. Cell: basic unit of Life.....	12
I.1. From zygote to a full body.....	13
I.2. Adult stem cells	14
I.2.1. Definition	14
I.2.2. Adult stem cells identification and isolation	15
I.2.3. Lineage tracing to follow the fate of adult stem cells	16
II. Epithelia: guardians of tissue integrity	18
II.1. Epithelial diversity and functions	18
II.2. Epithelial dynamics.....	20
II.2.1. Epithelial renewal.....	20
II.2.2. Epithelial differentiation	21
II.2.3. Cytokeratins: guardians of epithelial homeostasis	23
II.2.4. Epithelial regeneration	24
III. Epithelial transition zones: connecting tissues	25
III.1. Anatomy of transition zones.....	25
III.2. Molecular characteristics of transition zones	27
IV. Epithelial stem cells and their neighbors	30
IV.1. Stem cell niche	30
IV.1.1. Microenvironment role during homeostasis.....	30
IV.1.2. Pathways involved in stem cell determination.....	32
IV.2. Epithelial stem cells: state or fate?	36
V. Epithelial transition zone: a stem cell niche associated with pathogenesis.....	39
V.1. Transition zone: naturally prone to aggressions	39
V.1.1. Transition zone and bacterial stress.....	39
V.1.2. Mechanical and chemical stress: hallmark of transition zones	39
V.2. Transition zone microenvironment: One of a kind	40
V.2.1. Transition zone stromal stiffness.....	40
V.2.2. The transition zone niche	41
V.2.3. Transition zone and immune cells.....	41
V.3. Transition zone and cancer susceptibility	42
OBJECTIVE.....	46
RESULTS.....	47

I. A stem cell population at the anorectal junction maintains homeostasis and participates in tissue regeneration after injury	47
II. SUPPLEMENTARY RESULTS 1.....	85
III. SUPPLEMENTARY RESULTS 2.....	88
CONCLUSION.....	100
DISCUSSION/PERSPECTIVE	101
I. Cellular plasticity and transition zone heterogeneity	101
I.1. Heterogeneity of anorectal transition zone	101
I.2. Genetic ablation of transition zone	102
II. Regulation of transition zone cells by external stimuli	103
II.1. Niche signaling in TZ.....	103
II.2. Transition zone and epigenetics	104
III. Immunity and KRas mutation in anorectal transition zone	105
III.1. Immune infiltration of anorectal transition zone	105
III.2. KRas-induced carcinoma	106
III.3. Epithelial and immune cells interplay.....	106
REFERENCES	108
ANNEXE	125

Abbreviations

ABCB5: ATP-binding cassette sub-family B member 5

ADAM10: A Disintegrin and Metalloprotease

ALDH1: Aldehyde dehydrogenase 1

ALK: anaplastic lymphoma kinase

APC: Adenomatous polyposis coli

BFP: Blue Fluorescent Protein

BMI1: B lymphoma Mo-MLV insertion region 1 homolog

BMP: Bone morphogenetic protein

BMPRI1A: Bone Morphogenetic Protein Receptor Type 1A

BrdU: 5-Bromo-2'-Deoxyuridine

CD34: Cluster of differentiation 34

CK1: Casein kinase 1

CSF: Colony Stimulating Factor

DKO: Double Knock-out

DNA: Deoxyribonucleic acid

DNMT: DNA methyltransferase

DOX: Doxycycline

DSS: Dextran sulfate sodium

DTA: diphtheria toxin fragment

DTR: Diphtheria toxin receptor

DVL: Dishevelled

ECM: Extracellular Matrix

EDTA: Ethylenedinitrilo tetraacetic acid

EdU: 5-ethynyl-2'-deoxyuridine

ER: Estrogen Receptor

FGF: fibroblast growth factor

FoxP3: Forkhead box P3

Fz: Frizzled

GFP: Green Fluorescent Protein

GPC3: Glypican-3

GSK3: glycogen synthase kinase 3

H.pylori: Helicobacter pylori

HSC: Hematopoietic stem cells

HPV: Human Papilloma Virus

ICM: Inner cell mass

IPSC: Induced Pluripotent Stem cells

Krt: Keratin (or cytokeratin)

LGR5: Leucine-rich repeat-containing G protein-coupled receptor 5

LRC: Label-retaining cells

LRP: lipoprotein receptor-related protein

LSL: Lox-Stop-Lox

MMP7: Matrix metalloproteinase 7

MSC: Mesenchymal stem cells

NICD: Notch intracellular domain

PDGFR α : Platelet-derived growth factor receptor A

RFP: Red Fluorescent Protein

SCC: Squamous cell carcinoma

α SMA: α -smooth muscle actin

TA: Transit-amplifying cells

TAM: Tamoxifen

TGF β : Transforming growth factor beta

TGF β RII: Transforming growth factor beta receptor II

Tif-1 γ : Transcriptional intermediary factor-1 gamma

TnC: TenascinC

TRE: Tetracyclin-responsive regulatory element

TZ: Transition zone

List of figures

Figure 1: Evolution of microscopes.	13
Figure 2: From zygote to specialized organs.....	14
Figure 3: Genetic mouse models used to trace cell with tamoxifen and doxycycline	17
Figure 4: Cell shape and number of layers define epithelia.	19
Figure 5: Cell differentiation during homeostasis.	21
Figure 6: Organization of epithelia	22
Figure 7: Cytokeratin family members	23
Figure 8: TZ represent the junction between two different types of epithelium and are found throughout the body	26
Figure 9: Anatomical difference between human and mouse stomach.....	26
Figure 10: Different way to define transition zones.....	29
Figure 11: Hematoxylin & Eosin staining of human gastro-duodenal junction.....	30
Figure 12: Overview of cells composing innate and adaptive immunities	31
Figure 13: Canonical Wnt/ β -catenin signaling pathway	33
Figure 14: Notch signaling pathway in intestinal epithelium.....	34
Figure 15: TGF β and BMP signaling pathways.....	35
Figure 16: Cellular plasticity. Dedifferentiation and transdifferentiation.....	37
Figure 17: Scheme depicting extracellular matrix (ECM) stiffness in transition zone of the eye	41
Figure 18: Overview of microenvironment populations present in the anorectal transition zone region during homeostasis	42
Figure 19: Tumor arise at the anorectal transition zone following mutations in T lymphocytes.	45
Figure 20: Anorectal TZ heterogeneity	101
Figure 21: Mouse genetic to specifically delete TZ Krt17 ⁺ cells.....	103

INTRODUCTION

From time immemorial, Man's quest has focused on understanding what Life was, how it worked and why it was as it was as well as its inexorable ending while keeping in mind the idea of immortality and eternal youth. From Ancient times to our modern society, hundreds of examples illustrate the tireless race against time. The quest of the famous Fountain of Youth that restores the youth of anyone who drinks its water has made more than one dream. In modern days, it is reflected in books, movies and even cosmetics. In a famous episode of *The Amazing Spiderman*, a desperate one-handed scientist injects himself with lizard DNA hoping to attribute himself its regenerative abilities to recover his lost hand. Recently, gene therapies have open new hopes in “correcting” diseases. At a more superficial level, and although anti-ageing creams were already used by Cleopatra, nowadays, thousands of creams and cosmetics procedures are elaborated with the promise to erase or delay signs of time.

Man has never ceased to test the limits its body and mind in order to be able to push them ever further. It remains a hot topic for our species, which once again hopes to push physical and psychical boundaries with technology and other transhumanist principles to become faster, smarter and stronger.

While theories vary and evolve over centuries, humanity's thirst for knowledge remains eternal.

I. Cell: basic unit of Life

Embryology, science focused on embryo formation and development, can be traced back to the Ancient Greece. Philosophers referred to embryology as “generation”. Aristotle described two models of “generation” called preformation and epigenesis. Epigenesists considered embryo as an undifferentiated “mass” present in the female. New parts were added to this “mass” by male and guided embryo development. In contrast, preformation theory described the embryo as a miniature individual that already exists in mother's egg or father's sperm. This theory persisted during centuries but the invention of microscopes has revolutionized our understanding of development. In 1665, the English scientist Robert Hooke observed cork tissue through the lens of this homemade microscope (**Figure 1**). Cork is composed of structures that reminded him of the small rooms where monks used to live in called “cell”. Twelve years after that, in 1677, Antoine van Leeuwenhoek observed sperm

under a microscope and described them as “animalcules” (little animals) as he believed in preformation.

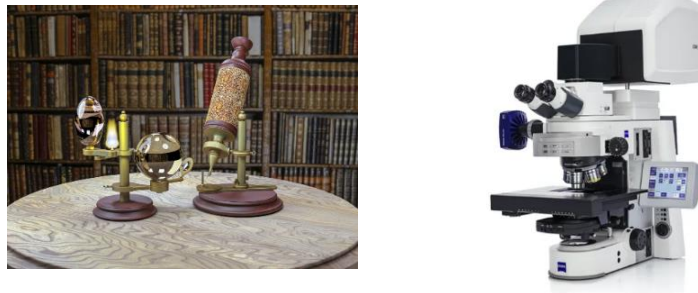


Figure 1: Evolution of microscopes. Robert Hooke's Microscope from 1665 (left) compared to a ZEISS confocal microscope from 2020 (right).

Tons of observations were made thanks to microscopy and cells were described in plants, fungi, animals, yeast, all living organisms and cells were then considered as basic unit of Life. In mammals, more precisely humans, a new born baby is composed of approximately 26 000 000 000 cells. In the XXIth century, development processes are well studied and understood and nor preformation nor epigenesis are favored theories.

I.1. From zygote to a full body

During fertilization, a fusion between a spermatozoid and an egg occurs leading to the formation of a structure called zygote (**Figure 2**). The fertilized egg is **totipotent** which means these cells can give rise to all cells of the future embryo but also cells that will support embryo development such as placenta and umbilical cord. Totipotency persists until the 8-cells stage Morula and after few days of cell divisions, a new structure composed of around 150 cells appears called a Blastocyst that is no longer totipotent. Blastocyst is composed of two compartments: an enveloping layer of cells and the Inner Mass Cells (ICM). ICM are known as **pluripotent** stem cells (they can give rise to all cell types of the embryo proper) and rearrange themselves and differentiate into the three germ layers during a process called gastrulation^{1,2}. The three germ layers called ectoderm, mesoderm and endoderm are composed of **multipotent** cells that can yield a more limited number of cell lineages. Each layer will give rise to different tissues and organs during morphogenesis. Mesoderm gives rise to muscles, bones, cartilages and blood. Epithelial tissues derive from either ectoderm or endoderm. For example, epidermis, mammary glands and nervous system arise from the

ectoderm whereas endoderm gives rise to the pre-gut including digestive tract, pancreas and liver (**Figure 2**). In adult organism, tissue-specific stem cells (also called adult stem cells) are present in each tissue in order to maintain them.

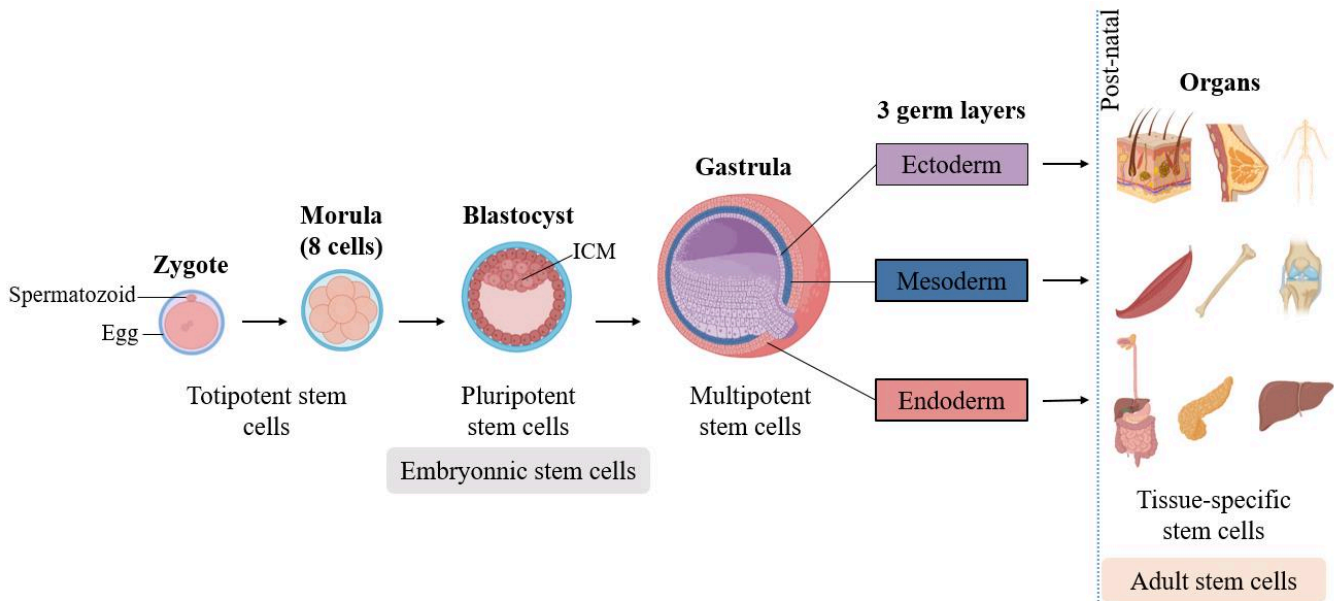


Figure 2: From zygote to specialized organs. Across development, stem cells with different potencies lead to the formation of different organs constituting the organism. ICM: Inner Cell Mass

I.2. Adult stem cells

I.2.1. Definition

Adult stem cells are defined by their ability to self-renew and differentiate. Although all adult stem cells are able to self-renew, they distinguish one another from their differentiation ability. There are many adult stem cells, for example, Hematopoietic Stem Cell (HSC), Mesenchymal Stem Cells (MSC), neural stem cells and epithelial stem cells. Adult stem cells can display a **multipotent** feature which allow them differentiate into different cell lineages. The best example is the HSC able to supply all blood cell types³. Tragedies of Hiroshima and Nagasaki in 1945 killed hundreds of thousands of people in Japan because of myelosuppression induced by radiation. These tragic consequences accelerated research on hematopoietic system. Few years after those events, in 1956, human bone marrow was successfully transplanted from a healthy donor to his leukemic identical twin that was previously treated with radiotherapy. In the meantime, a mouse model of leukemia supralethal

irradiation (above the lethal dose) and bone marrow grafts was developed⁴. In 1960s, Till and McCulloch studies showed for the first time that cells with stem cell properties in the marrow existed. Indeed, these cells were able to self-renew *in vitro* and could give rise to mixed myeloerythroid progeny (granulocytes, macrophages, red cells, megakaryocytes)⁵⁻⁷. The ability of bone marrow to repopulate the entire blood system suggested the presence of stem cells.

Tissues can contain stem cells called **oligopotent** stem cells also able to differentiate into multiple cell types but their differentiation potential is more restricted compared to multipotent stem cells. For example, multipotent HSC give rise to the common myeloid progenitor that is oligopotent able to differentiate into the myeloid lineage including granulocytes and monocytes⁸. Stem cells with the less differentiation potential are **unipotent** stem cells that give rise to only one cell type such as cells within the interfollicular epidermis^{9,10}.

Every tissue has its own adult stem cells pool and stem cells are restricted to a specific tissue. Stem cells are found in almost all tissues. Although it seems very compartmentalized and immutable, recent studies have shown that unipotent stem cells can maintain homeostasis and can also participate to injury repair in different tissues such as in the sweat gland¹¹, mammary gland¹² or skin¹³. This notion will be further developed in Chapter IV part 2. In the present manuscript, we will focus on the adult stem cells only.

Stem cells are essential to maintain tissues and organs, providing new cells to preserve them. Because of their crucial role, it is essential to understand their biological properties. In order to understand stem cell properties and better characterize them, they need to be isolated first.

I.2.2. Adult stem cells identification and isolation

During few decades, quiescence, which is a state of low proliferative activity, was used as one specific characteristic of adult stem cells. Adult stem cells were hypothesized to be slow-cycling in order to preserve their proliferative potential and minimize DNA errors during replications. A method called “pulse and chase” was designed to identify slow-cycling cells. This method consists of injection(s) of a thymidine analog (ex. BrdU or EdU) will incorporate into the newly synthesized DNA of replicating cells; this is the “pulse phase”. Cells that continue to divide after the pulse of thymidine analog will dilute out the incorporated

thymidine analog through cell division during the “chase phase”. Cells where the thymidine analog is not diluted are called “label-retaining cells” (LRC) and are thus considered as stem cells. However, using this technique does not allow the molecular analysis of cells as cells need to be fixed to detect thymidine analog. Tumbar and colleagues used a clever system to isolate LRC from mice hair follicle bulge based on their slow-cycling property¹⁴. They used the H2B-GFP system, where the histone H2B is fused to the green fluorescent protein (GFP) under the control of tetracyclin-responsive regulatory element (TRE). This mouse was then crossed with a mouse bearing the transcription factor Tet-VP16 under the control of a protein expressed in all stratified cells of the epidermis and hair follicle, keratin 5. In the absence of doxycycline, an analog of tetracyclin, GFP is expressed. When doxycycline is added, Tet is repressed and, subsequently, led to repression of GFP expression. Cells where GFP was expressed before the doxycycline injection will retain their GFP. Cells that proliferate will dilute their GFP by half across divisions and rarely dividing cells will retain the GFP. This system with Krt5 promoter in other tissues allowed to identify LRC such as the eye to isolate LRC that lay in a special region called the limbus between the cornea and the conjunctiva¹⁵ or in mammary gland¹⁶. This powerful tool can be used in a wide range of tissues with the use of a tissue-specific promoter, for example in prostate with the specific promoter Probasin to label LRC luminal cells¹⁷. This technique has allowed the characterization of stem cells and led to the discovery of cell surface marker such as CD34 in the hair follicle that provide tool to further analyze the heterogeneity within a stem cell population¹⁸.

However, some stem cells show low proliferative activity like the liver, lung and pancreas whereas stem cells in the skin and gut are constantly proliferative and so property is tissue-dependent and is no longer systematically used as an essential stem cell feature.

I.2.3. Lineage tracing to follow the fate of adult stem cells

Since late XIXth century, genetic fate mapping tools were developed using mouse models to trace cells and their offspring cells in order to understand their properties. This is the principle of lineage tracing where animals are genetically modified to express/inactivate/mutate a specific gene in cell populations of interest. Lineage tracing has become a gold standard to study cell fate and dynamics of tissue-specific cells during development, homeostasis, regeneration and tumorigenesis. Different models of transgenic mice were developed over time; mouse models can be constitutive (also called conventional models) or conditional and

genes can be knocked-in or knocked-out. One of the most widely used system in the Cre/Lox system that involves the excision of LoxP sequences (small DNA sequences) by the enzyme Cre recombinase¹⁹. In conventional knock-out models, a target gene is inactivated in all tissues at all times, from development through adult life. In some conditional models, an inducer is essential in order to delete (knock-out) or introduce (knock-in) specific genes in a tissue-specific and time-dependent fashion. Few models can be used for this purpose using tamoxifen or doxycycline induction. In the example of tamoxifen induction, Cre recombinase is fused with the Estrogen Receptor (ER) that can bind to tamoxifen once administrated. After binding, Cre recombinase translocate into the nucleus where it cuts LoxP sequences and, subsequently, the target gene between them. The target gene is initially inhibited by the presence of a stop cassette. To follow visually cells of interest upon induction, a fluorescent reporter gene is used; a “floxed” stop cassette upstream of a fluorescent reporter gene by Cre recombinase expressed under the control of a cell type-specific promoter. This technique allows genetically and irreversibly labeling of cells of interest and following these cells and their progeny fate over time in situ (**Figure 3**). The induction allows controlling when the gene of interest will be expressed/deleted/mutated. To really follow the fate of cells and their progeny, a tracker is needed. Most of the time a fluorescent protein is used, multiple choices exist going from Red to Green or Blue Fluorescent Protein (respectively RFP, GFP or BFP), tomato, etc.... However, in these models labelling occurs in all cells of the same population making difficult to follow the fate of different clones within the population of interest. To overcome this issue, another model, called Confetti, was created²⁰. In this model, a combination of fluorescent proteins is expressed in cells in a stochastic manner allowing the labelling (thereby the following) of cells and their progeny in a more clonal way.

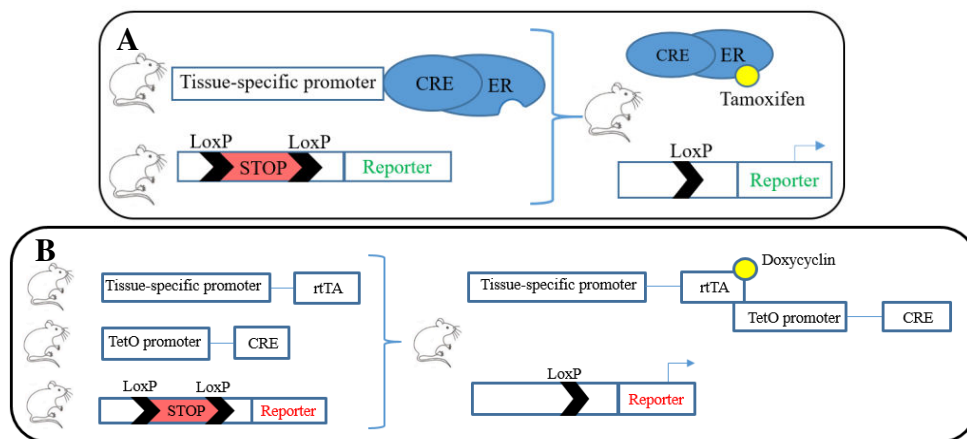


Figure 3: Genetic mouse models used to trace cell with tamoxifen (A) and doxycycline (B)

Across discoveries, many markers had become hallmarks of stem cells. One of them, the membrane protein CD34, a marker of hair follicle and human HSC. Other example, LGR5 is expressed in intestinal crypts²¹ but also hair follicles. In mammary gland, Ginestier et al. identified stem cells using ALDH1, an enzyme specifically active in mammary stem cells²².

The expression of a stem cell marker in one tissue does not implies that this marker could be used as a stem cell marker in other tissues. The surface marker CD34 is a good example as it is a stem cell marker in the hair follicle and the hematopoietic system but fibroblasts and endothelial cells, which are not stem cells, also express it. Usually, stem cells are identified based on functional assays (further developed in Chapter II, Part 2) and a combination of markers. For example, in hair follicle, epithelial stem cells and fibroblasts populations are both CD34+, to separate these two populations and isolate epithelial stem cells only, CD34 is combined with $\alpha 6$ -integrin²³.

The diversity of tools developed over centuries has made it possible to better understand the properties of these special cells called stem cells. Particularly, their involvement in the generation of epithelia that they maintain.

II. Epithelia: guardians of tissue integrity

Epithelial tissue is one of the four basic types of animal tissues along with connective tissue, muscle tissue and nervous tissue. Epithelial tissues line the external part of our body and also the internal cavities throughout the body. The word “epithelium” is the combination of two Ancient Greek words “ἐπί (epí, “around”) and θηλή (thēlē, “nipple”) as it was first used to describe the mammary gland. Epithelia constitute an effective protective barrier regularly renewed by stem cells to ensure their functions. Therefore, epithelial integrity is essential to prevent leakage of materials to the lumen and to prevent the intrusion of foreign bodies²⁴.

II.1. Epithelial diversity and functions

By definition, epithelium is a group of cells arranged in a specific manner to fulfill a specific function. Epithelial tissue is, therefore, classified by the shape and the arrangement of its cells. There are three main shapes of epithelial cells: squamous, cuboidal and columnar.

These can be arranged in a single layer of cells as a simple epithelium where all cells rest on basal membrane or in two or more layers of cells classified as stratified epithelium where only basal cells rest on basement membrane. Epithelium can also be pseudostratified where all nuclei are at different levels giving the illusion of a multilayered epithelium when in reality all cells rest on basement membrane. Pseudostratified epithelium can be ciliated for example in the respiratory tract. Glandular epithelium is a simple layer of columnar cells arranged in structures called glands. Finally, transitional epithelium is composed of different cell shapes, this kind of epithelium is found in the urinary tract. A summary of different epithelium is illustrated in **Figure 4**.

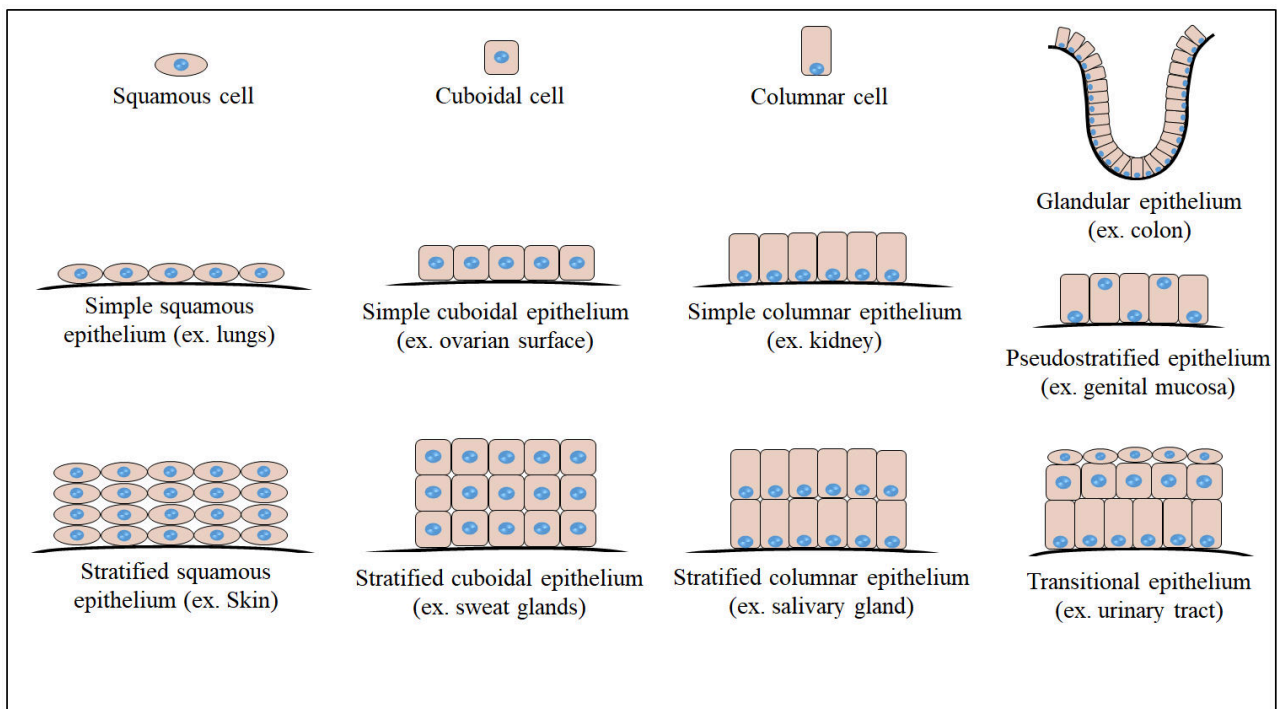


Figure 4: Cell shape and number of layers define epithelia. Epithelia are composed of squamous, cuboidal or columnar cells arranged in simple or multi-layered manner.

Shape and number of layers are directly linked to epithelial functions. They range from protection to secretion and absorption. We distinguish epithelium of coating, which constitute the superficial layer of the skin (epidermis) and of the mucous membranes, and the glandular epithelium, which have a function of secretion. Epithelial cells display a wide range of functions including selective absorption, protection and sensing^{25,26}. As an example, skin is an epithelium composed of squamous cells organized in multiple layers to provide an effective protective barrier against external aggressions (virus, bacteria, UV) and avoid dehydration. *A contrario*, lungs and blood vessels are lined with a simple layer of squamous

cells to ease gas exchanges during respiration. Epithelium can also have a secretory function such as sweat glands and salivary glands that are cuboidal stratified epithelia.

II.2. Epithelial dynamics

II.2.1. Epithelial renewal

Epithelium turnover varies from one epithelium to another and within each epithelium different cell types displays different lifespan. These differences are due to proliferation rates and differentiation path each cell will take; longer the path, longer the turnover!

Globally, in mice, the simple columnar epithelium lining the intestine is renewed every 5 days. Differentiated cells of the intestine such as mucous-secreting cells are renewed every 3 days and Paneth cells renewal can extend to 3 weeks²⁷. The interfollicular epidermis needs 4 weeks to turn over a new leaf²⁸. Finally, the alveolar region of lungs needs between 28 and 35 days to renew whereas ciliated epithelial cells renewal can take as long as 17 months^{29,30}.

Stem cells properties of self-renewal has been the basis of numerous experiments to identify them. The limited dilution assay is a technique to determine the frequency of stem cells in a mixed population of cells. The idea is to dilute, by serial dilution, the mixed population of cells. Below a certain dilution, the obtained population is derived from a single stem cell^{31,32}.

In the same objective to identify stem cells, a clonogenicity assay can be performed where the number of passages of colonies is recorded. If a cell has stem cell properties, then it can be passed for an unlimited number of times. This method is available in numerous ways; can be done with mammospheres to study mammary glands cells potential, can be done in 2Dimensional cultures and more recently, in 3-Dimensional cultures allowing the culture of mini-organs called organoids. Organoids story began back in the early XXth century, in 1906 more precisely, with R.G. Harrison and his “hanging drop cell culture method”. Through the XXth century the progressive use of collagen led to the current organoids matrigel-based cultures³³. Organoid cultures had marked a critical turning point in cell culture as it allows cells to grow cells in a more physiologically-faithful environment and are now defined as “3D structures grown from *stem cells* and consisting of organ-specific cell types that *self-organizes*”³⁴ recapitulating the hierarchy of the tissue they come from.

II.2.2. Epithelial differentiation

One of the main features of stem cells is their ability to give rise to differentiated cells. Stem cells are at the top of the hierarchy and can either undergo symmetrical division to renew itself to maintain the stem cell pool or undergo asymmetrical division to differentiate. Cells take a differentiation path and differentiate; they run down the valley designed by C.H. Waddington in 1957, to reach a terminally differentiated state³⁵ (**Figure 5**) and acquire specialized functions like secretion and absorption.

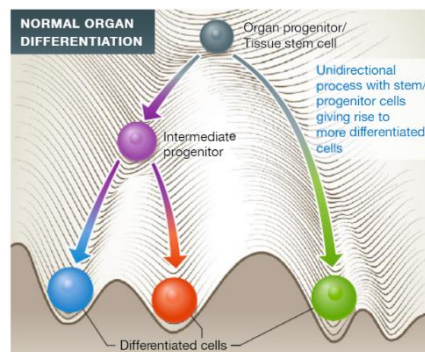


Figure 5: Cell differentiation during homeostasis schematized by C.H. Waddington in 1957 and called Waddington hills.

Differentiated cells maintain their features under stable condition called homeostasis and give a heterogeneous tissue called epithelium. Differentiated cells able to proliferate are referred to as “intermediate progenitors” (**Figure 5**). When a cell reaches the end of the differentiation path, it cannot proliferate and is therefore called “terminally differentiated cell”. These cells are present in particular in the intestine such as goblet cells and enteroendocrine cells³⁶ (**Figure 6A**). Differentiated cells of the intestine, in contrast with stem cells, have limited self-renewal ability and are restricted to their lineage. Simple glandular epithelium constituting intestinal crypts are well segmented; the base of the crypt is the starting point of differentiation, where stem cells reside. Cells are “pushed” to upper locations as they differentiate. Between the stem cells and differentiated cells compartments, there are Transit-Amplifying cells (TA cells) which are the direct progeny (or intermediate progenitors) of stem cells. TA cells divide 4-5 times before differentiation into specialized intestinal cell types, which are enteroendocrine cells, paneth cells, enterocytes and mucous-secreting goblet cells¹⁴. Squamous epithelium organization is also well described. In 2008, Elaine Fuchs, gave a very detailed epidermal differentiation stages of skin epidermis³⁷. Stratified epithelium is divided in 4 layers from basal to outer layer: Basal layer, spinous layer, granular layer and the last

layer called stratum corneum. Epidermal differentiation starts from basal cells to the outer layers, the acquisition or loss of particular keratins occurs for each layer. Each layer is defined by layer-specific proteins; as an example, integrin $\alpha 6$ is expressed exclusively by basal cells whereas filaggrin is specific to the outer layer of the stratified epithelium (**Figure 6B**). This differentiation pattern is similar in the stratified squamous epithelium lining the esophagus and the anal canal³⁸.

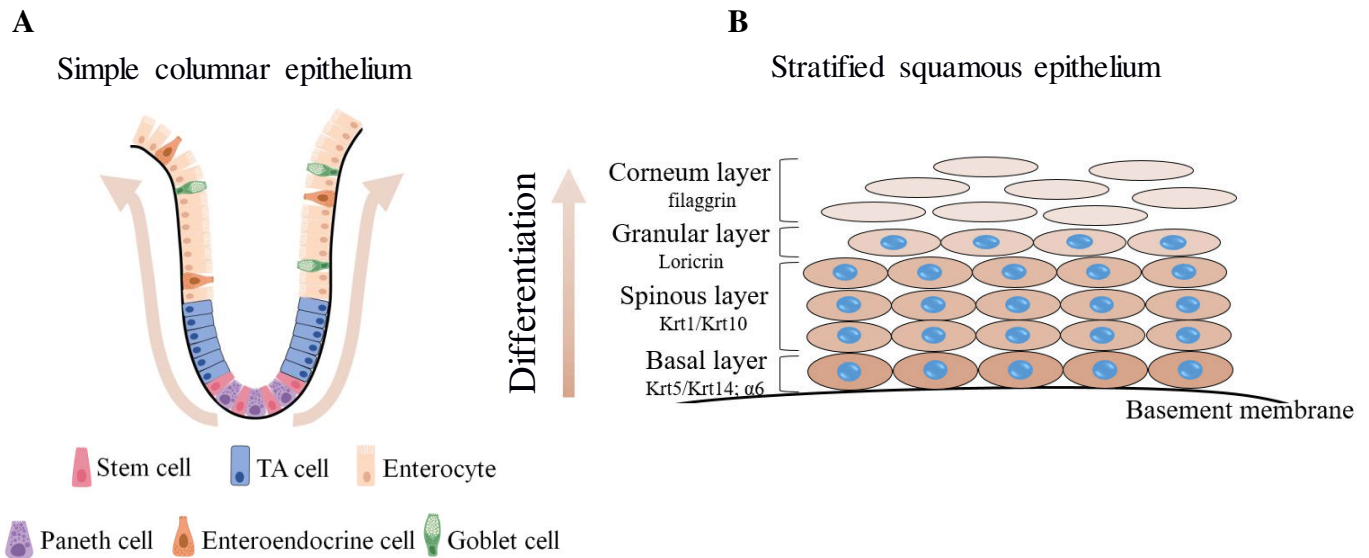


Figure 6: Organization of epithelia. Example of the simple columnar epithelium (ex. intestinal crypt) (A) and stratified squamous epithelium (ex. skin) (B) and how they differentiate. TA: Transit-Amplifying cells; $\alpha 6$: $\alpha 6$ integrin

Based on the presence of cytokeratins (or keratins) in the outer layer of cells, epithelial tissues can be categorized as keratinized and non-keratinized. The corneum layer of keratinized epithelium consists essentially of dead cells and is impervious to water providing a better protective barrier against abrasions compared to non-keratinized epithelium. The outer layer of non-keratinized epithelium is composed of living cells and is pervious to water. As an example, epidermis and ectocervix are respectively keratinized and non-keratinized epithelium.

II.2.3. Cytokeratins: guardians of epithelial homeostasis

Eukaryotes cytoskeletons are mainly composed of proteinaceous structures from 3 filament families: actin microfilaments (~7nm), intermediate filaments (~10nm) and microtubules (~25nm). Cytokeratins belong to the large intermediate filament family and provide rigidity and strength to cells while remaining flexible thus representing an internal cell support. In 2006, a consensus was established to classify intermediate filaments into 2 groups according to their structures and sequences homologies: intermediate filament types I and type II (**Figure 7A**). This large family is composed of 54 keratins separated in two groups based on their chemical properties and gene sequence homologies. Type I family counts 28 keratins that are acidic in charge whereas the 26 members of type II keratins are basic-neutral in charge. Because of their chemical properties, a keratin monomer from type I (acid) is paired with a keratin monomer from type II (basic), the assembly of these two monomers creates a heterodimer. Formed heterodimers bind each other by their extremities to form a structure called proto-filaments. The association of multiple proto-filaments constitutes the final intermediate filament (**Figure 7B**).

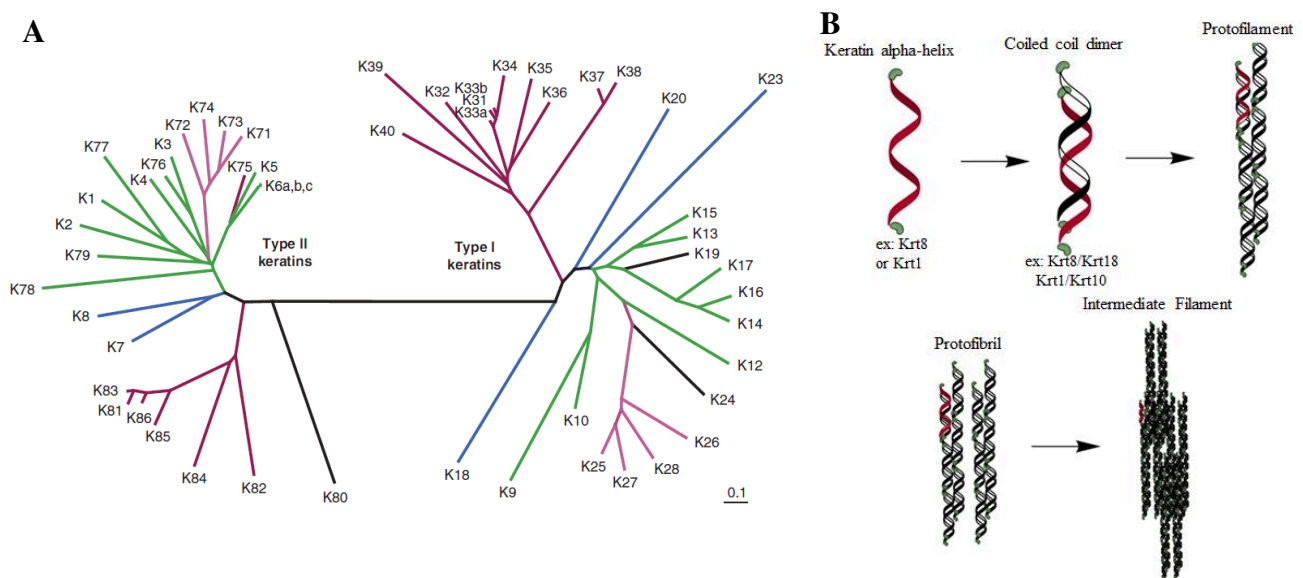


Figure 7: Cytokeratin family members. **A.** Overview of intermediate filaments family type I and type II members from Jacob et al. **B.** Intermediate filament assembly steps.

Keratins are involved in a wide range of biological functions. Consequently, mutations in keratin genes were shown to be responsible for a variety of diseases grouped under the term “keratinopathies”³⁹. Mutations and knock-out models showed the implication of keratins in crucial cell functions and diseases. Mutations of Krt14 and Krt5 expressed in stratified

squamous epithelia cause Epidermolysis Bullosa Simplex (EBS), a disease where the skin is weakened, blisters easily and in some cases, lead to dehydration and infections. Moreover, Mutations in Krt8 and Krt18, expressed in simple columnar epithelia, represent a risk factor for inflammatory bowel disease patients.

Several studies on mouse models of Krt17 deletion showed alteration in wound healing⁴⁰ and proper epithelial differentiation. Krt17 was also associated with the pathogenesis of psoriasis⁴¹, another skin disease. Finally, each keratin pair is specific to epithelial differentiated layer for example Krt1 and Krt10 are associated with suprabasal layers.

Keratins are important to ensure proper function of epithelia. As important as the balance between cell loss and new cells that is crucial to maintain epithelial homeostasis. In some cases (e.g. stress, infection, inflammation or injuries) epithelial homeostasis is perturbed and needs to be restored properly to keep doing its function.

II.2.4. Epithelial regeneration

An essential feature of stem cells is their ability to reconstruct injured tissue. The concept of regeneration is maybe as old as mankind. Aristotle in Ancient Greek already noticed that lizards were able to regrowth their tail after amputation. Numerous examples were illustrated in both Greek and Roman mythologies. Lernaean Hydra, a mythological creature composed of more than 50 heads according to some writers. Every time a head was cut off, two would grow back. In the XVIII century, Réaumur demonstrated regeneration of limb and claws of crayfish after amputation⁴². Almost 2000 years after Aristotle's observations, an Italian biologist, Lazzaro Spallanzani, reported regeneration of tails and limbs of salamanders after amputation^{43,44}.

Physical wounds are defined as a damage or a disruption of the normal and anatomical structure and function. They can be superficial by breaking epithelial integrity or more profound wounds damaging bones, cartilages and tendons⁴⁵. Wounds can be separated into acute and chronic wounds according to their time frame of healing. In acute wounds, a full restoration of function and anatomy is achieved when in chronic wounds; normal stages of wound healing fail to be accomplished and is incomplete or disturbed by diverse factors such as infection, hypoxia and excessive inflammation.

Wound healing is divided in four steps well-coordinated and precisely regulated requiring the cooperation of several cellular components; each step paving the way for the following one⁴⁶⁻⁴⁸. In the first hours after the injury, the emergency is to prevent blood and fluid loss. During **hemostasis**, platelets and endothelial cells work together to form a clot. Once the wound is clotted, during 2-3 days, the inflammatory cells neutrophils are recruited to take over to create an immune barrier preventing from infection by removing foreign micro-organisms and damaged tissues. This constitutes the early phase of **inflammation**. Then, monocytes are recruited on injury site and differentiate into macrophages that continue the phagocytosis process started by neutrophils. Two days after the injury, when fluid loss is stopped and immune system is successfully set up, **regeneration** phase starts and lasts until day 10 post-injury. During regenerative phase, for about two weeks, new tissues are formed through proliferation that allows re-epithelialization of the wound and the creation of new epithelial cells and angiogenesis which is the creation of new blood vessels⁴⁸. Regeneration time frame is different depending on tissues as already showed in page 13. Finally, **tissue remodeling** takes place and represent the balance between matrix degradation and synthesis and can last from few weeks to more than a year.

Throughout the body, epithelia from different shapes and different embryonic origins (see Chapter I Part 2 and Chapter II Part 1) form an uninterrupted lining of epithelial tissue that show differences in regeneration time frame. But did you ever wonder how all these different epithelia are connected? If we imagine our body as a piping network, where every single pipe represents an epithelium and where these pipes need to be connected to ensure sealing and communication between them. How these pipes (epithelia) are linked together? What is the centerpiece allowing the uninterrupted lining of tissues?

III. Epithelial transition zones: connecting tissues

III.1. Anatomy of transition zones (TZ)

The meeting of two different kind of epithelium is not a simple junction, it's a special region called epithelial transition zone (TZ). These TZ are found in numerous places throughout the body, for example in the eye, a region called the limbus located between the cornea and the conjunctiva. TZ are also found between the esophagus and the stomach and at the end of the digestive tract between the anal canal and the rectum. TZ are found in the

female reproductive system between the endocervix and the ectocervix and in the ovary⁴⁹. TZ represent an abrupt junction between two different types of epithelium that are easily visible histologically and are conserved among species as shown in **Figure 8**.

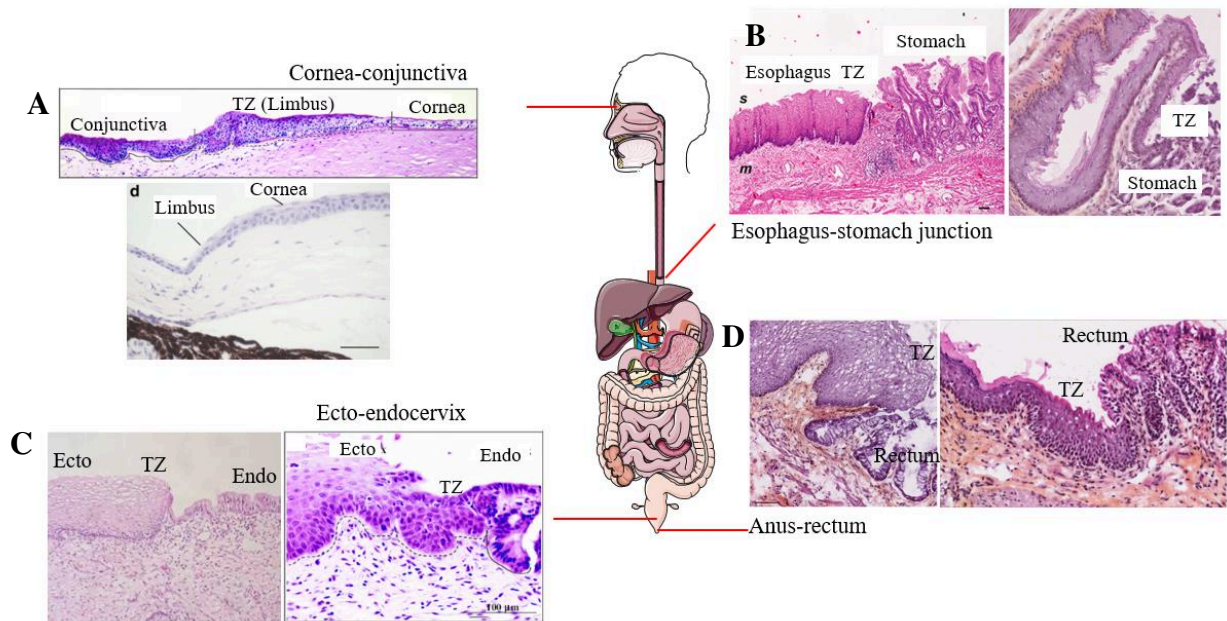


Figure 8: TZ represent the junction between two different types of epithelium and are found throughout the body. Hematoxylin & Eosin staining of human and mice transition zones found in the eye (A)²², between the esophagus and the stomach⁵⁰ (B), in the cervix (C)²³ (human cervix image from Ed Uthman at Flickr), and between the anus and the rectum (D)⁵¹

TZ are conserved among species but some anatomical differences exist. Indeed, human and mouse stomachs are not perfectly similar. The fundus region in human is replaced by the forestomach in mouse. This implies that TZ is not exactly located to the same place in both species; human stomach TZ is located between the esophagus and the corpus stomach whereas in mouse, it is located between the forestomach and the corpus⁵² (**Figure 9**).

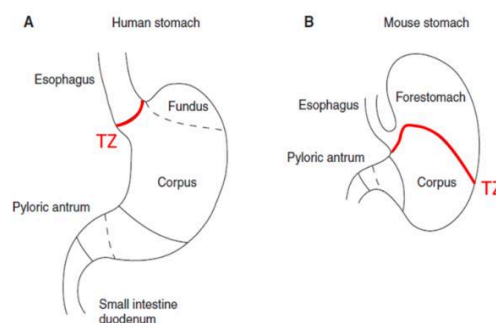


Figure 9: Anatomical difference between human (A) and mouse stomach (B). Scheme adapted from Schepers & Clevers⁵²

III.2. Molecular characteristics of transition zones

In some studies, this particular region is described as the reminiscent of embryonic tissue. During human development, at 16 weeks of gestation, the cervix epithelium is positive for Keratin7. At 20 weeks of gestation, Keratin5 positive cells emerge below this Krt7⁺ population and in adult humans, the Krt7⁺ population is restricted to a small region distinct from Krt5⁺ epithelium defined as the squamo-columnar junction. Similar observations in stomach from mice embryos and humans showed the emergence of Krt5⁺ cells at E15 (embryonic day 15) in mice and at 21 weeks of gestation for humans and the restriction of Krt7⁺ population in adult junctions^{53,54}.

Molecularly, TZ share common characteristics. Several studies had shown similarities in expressed keratins in mice such as Keratin17 that is expressed in stomach, cervix, limbus and anal TZ^{15,51,55,56}. Krt5 and Krt14, known to be expressed in squamous stratified epithelia are found in the limbus, stomach TZ, anal TZ and cervix TZ^{53,54,57-59}. Keratin7 was found in cervix, stomach and anal TZ^{53,55,60,61}. Keratin15 was found in the limbus, cervix and stomach TZ⁶²⁻⁶⁵.

However, while sharing common characteristics, TZ found in different locations display different markers. Some stem cell-associated markers are expressed in certain TZ in contrast with other TZ. Runck et al. identified a label-retaining population at the anorectal TZ back in 2010 suggesting the presence of stem cells in this region⁵⁶. LGR5, stem cell marker in intestinal crypts is expressed only in the limbus and ovary TZ^{51,66-69}. The anorectal TZ hosts a CD34⁺ population⁵⁶, a common stem cell marker in HSC, when it is not expressed in the stomach TZ (unpublished data **Annexe 1**). A summary of known markers for anal, stomach, cervical, limbal and ovary TZ is provided in **Table 1**.

	Anal TZ	Stomach TZ	Cervix TZ	Eye TZ	Ovary TZ	REF
Keratin5	✓	✓	✓	✓		53,54,57–59
Keratin14	✓	✓	✓	✓		
Keratin7	✓	✓	✓			53,55,60,61
Keratin17*	✓	✓	✓	✓		15,51,55,56
Keratin6 (a or b)	✓	✓	✓		✓	51,62–64,66
Keratin15		✓	✓	✓		62–65
ALDH1					✓	66
LGR5*	✗	✗	✗	✓	✓	51,66–69
CD34	✓	✗				56
Sox2*	✓	✓	✓	✓		56,70–72
ABCB5				✓		73
p63*	✓	✓	✓	✓		55,56,60,74

Table 1: Mouse transition zone share common markers while displaying specificities. Grey boxes highlight unknown status of markers in specified transition zones. Asterisks mark protein also present in human.

Despite the recent studies trying to characterize TZ, a clear definition of TZ has not been established yet and the way of defining TZ differs from one group to another. Chumduri and colleagues recently described cervix TZ as Krt5⁺ cells located below the columnar epithelium of endocervix⁵⁵ although Krt5 is a marker of basal cells all along stratified epithelia and not specific to TZ (**Figure 10A**). Another group, working on squamo-columnar junction of the stomach, define TZ as a small Krt7⁺ population located below columnar cells of corpus stomach⁶⁰ (**Figure 10B**). In our group, we define anorectal and stomach TZ as a larger region of approximately 200µm with a population overexpressing Krt17⁵¹ (**Figure 10C**). However, when trying to co-localize the two populations supposed to define TZ (Krt7 and Krt17) few

cells co-expressed both markers but the two populations do not completely overlap showing the importance of building consensus to define clearly TZ (**Figure 10**).

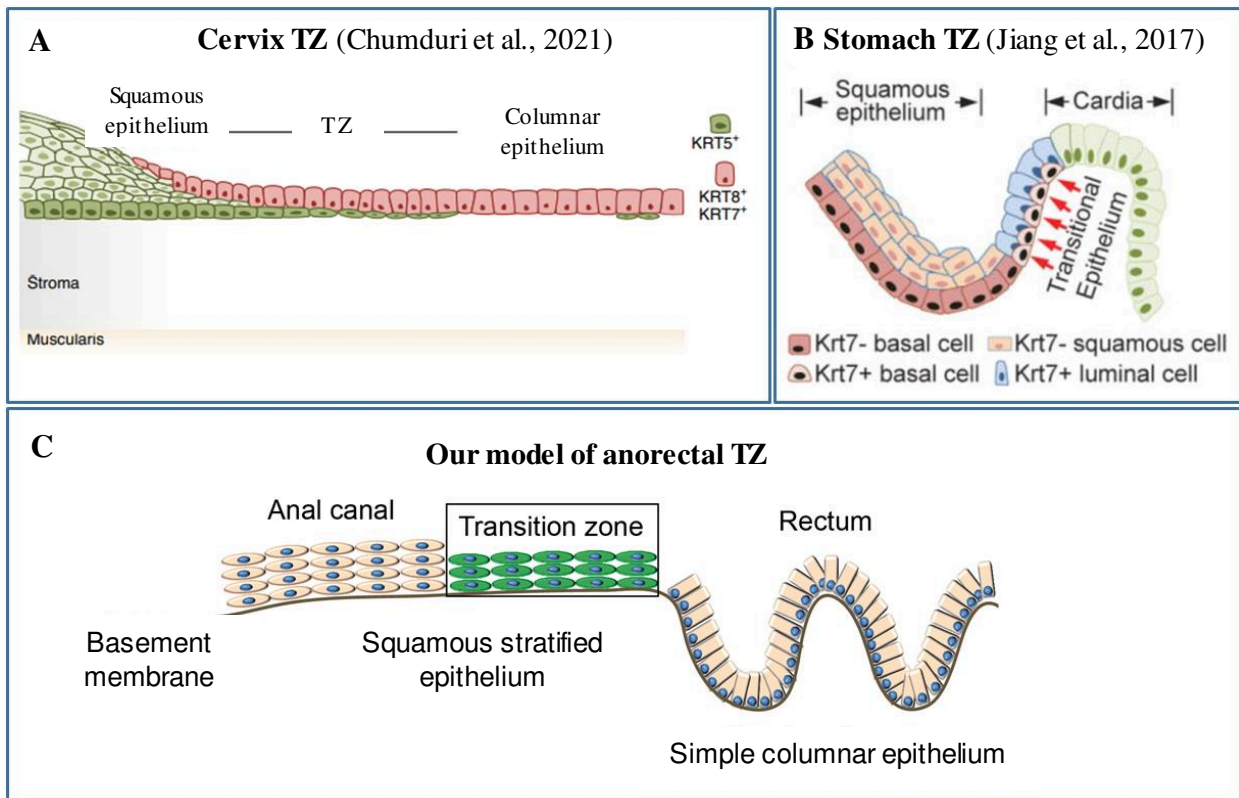


Figure 10: Different way to define transition zones. Examples of cervix TZ (A), stomach TZ (B) and anorectal TZ (C)

However, in other locations of the body, there are regions where slightly different epithelia meet that we do not consider as TZ. As an example, the junction between stomach and duodenum, both are simple glandular epithelia composed of columnar cells but structures called Brunner's glands are found specifically in the submucosal compartment of duodenum which differentiate it from the stomach⁷⁵. Hence they are both in the same epithelial category, we can not consider that there is a TZ in this location (**Figure 11**).

Therefore, we propose to define TZ as the junction between **two different types** of epithelia that displays specific markers associated with a pre-leisional state determined by the presence of wound-associated proteins.

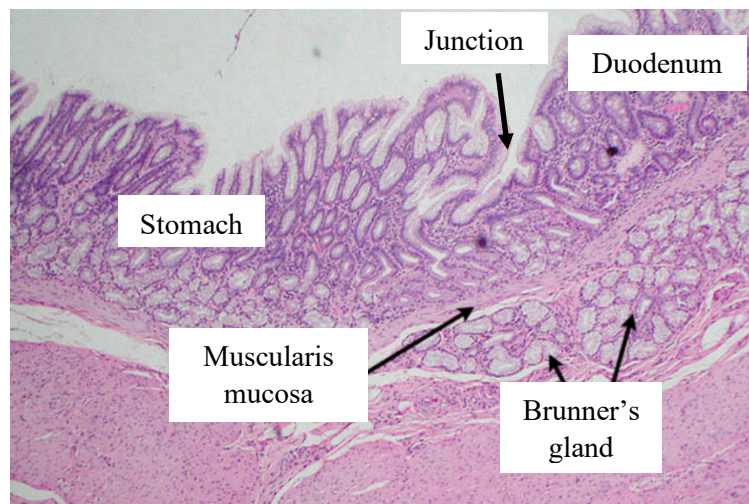


Figure 11: Hematoxylin & Eosin staining of human gastro-duodenal junction. From the Department of Anatomy of Geisel school of Medicine

IV. Epithelial stem cells and their neighbors

IV.1. Stem cell niche

Stem cells reside in specific places in tissues called stem cell niche where they receive stimuli from their microenvironment dictating their behaviors that are self-renewal, differentiation or maintenance of a dormant state. The first mention of stem cell niche concept appeared in 1978 in Schofield studies in HSC⁷⁶. Numerous studies in mouse and *Drosophila* allowed the identification of niches like the HSC niche among which intestinal niche, skin and hair follicle niche and germinal stem cell niche.

IV.1.1. Microenvironment role during homeostasis

Stem cells *in situ* are surrounded by numerous components whether they are cells or molecules. Stem cell microenvironment includes multiple cells types such as immune and stromal cells, other similar or dissimilar epithelial cells and the extracellular matrix.

Immune cells

Immunity is the guarding system of the body, soldiers that destroy any foreign bodies that may be harmful: bacteria, virus, parasites, abnormal cells, etc... Immune cells study started at

the end of XIXth century by the discovery of phagocytosis by E. Metchnikoff and neutralizing antibodies by E. Behring and P. Ehrlich⁷⁷. Generally, immune system is separated in two groups: innate and adaptive immunities. Innate immunity constitutes the rapid response and includes granulocytes (e.g. neutrophils, basophils, and eosinophils), monocytes, mast cells and natural killers. The adaptive immunity, slow response of the organism to a potential threat is constituted of B lymphocytes and T lymphocytes that is divided in 2 subtypes, CD8⁺ and CD4⁺. T lymphocytes positive for CD4 can differentiate into 4 subtypes with different roles: Th1, Th2, Th17 and T regulators (Treg). However, some immune cells stand right in the middle of these two compartments e.g. $\gamma\delta$ T lymphocytes and natural killer T cells (**Figure 12**).

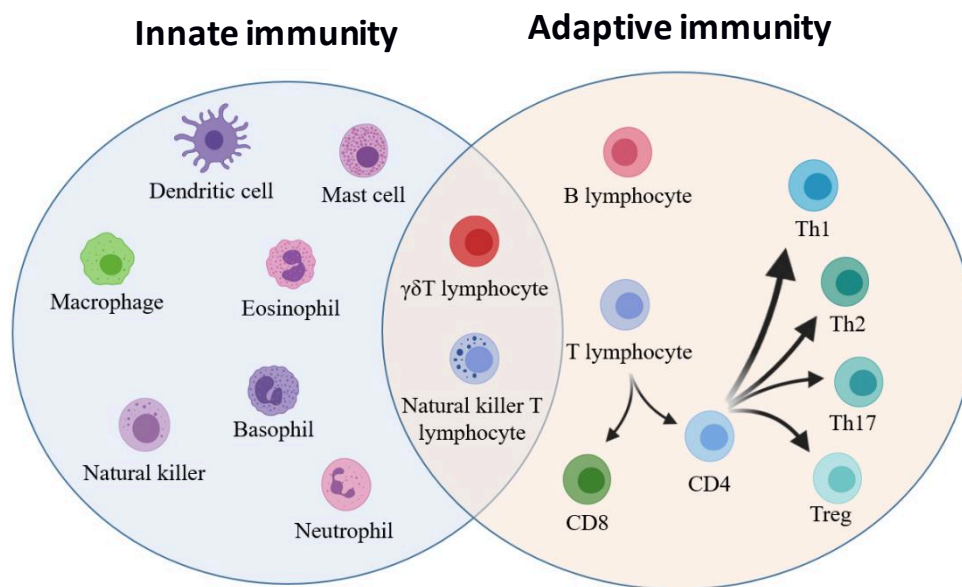


Figure 12: Overview of cells composing innate and adaptive immunities

Both cells from innate and adaptive immunity were proven to be important entities within stem cell niches. Tregs were shown to be implicated in stem cell pool maintenance in bone marrow and intestinal niches. Depletion of Tregs led to HSCs and intestinal stem cells diminution *in vivo*. When co-cultured with Tregs, intestinal cell cultures showed an enrichment in LGR5⁺ stem cells^{78,79}. Moreover, in intestinal stem cells microenvironment, macrophages are in close relationship with crypts. A study in mice reported that treatment with blocking antibodies against CSF receptor (expressed by macrophages) was responsible of stem cell pool diminution and differentiation alteration⁸⁰. Similar observations were done in mammary glands where mammary stem cells regenerative capacity was diminished in macrophage-deficient mice⁸¹.

Stromal cells

Stroma is a term referring to a vast and heterogeneous cell population encompassing fibroblasts subtypes, pericytes and endothelial cells. Stroma is often referred to as a mesenchymal compartment, a multipotential connective tissue able to give rise to all adult connective tissue. Mesenchymal cells (MCs) are commonly described as non-epithelial, non-hematopoietic and non-endothelial cells that support and connect tissues⁸². Stromal cells have been implicated in diverse functions such as extracellular matrix (ECM) regulation, support of blood vessel functions, immune regulation and stem cell maintenance⁸². They are identified with positive markers such as Vimentin, collagens and platelet-derived growth factor receptor (PDGFR). Fibroblasts are the main cells composing stroma; they produce collagens and other fibers to maintain the structural integrity of extracellular matrix and provide a solid support for tissues thus participating in homeostasis maintenance and wound healing. The last decades in stroma research, documented the heterogeneity of fibroblasts. Recently, single cell RNAsequencing analysis in mouse colon identified 4 subtypes of fibroblasts with differentially expressed genes and their spatial organization within the intestinal niche⁸³. Myofibroblasts are a subtype of fibroblasts often called activated fibroblasts. Upon activation, some fibroblasts differentiate and gain the myofibroblast marker α -smooth muscle actin (α SMA)⁸⁴. Myofibroblasts are present in organs with high remodeling ability such as kidney, lungs or in tissues following wounds. Indeed, they secrete collagen, fibronectin, tenascin, enzymes and cause the ECM to contract which are all implicated in tissue remodeling⁸⁵. In intestinal stem cell niche, PDGFR α^{high} cells called telocytes were described at the base of the intestinal villus, throughout the gastrointestinal tract, in lungs, esophagus and pancreas⁸⁶. In contrast, PDGFR α^{low} CD81⁺ cells called trophocytes are localized at the base of the intestinal crypt. *In vitro*, trophocytes were shown to expand intestinal stem cells and participate to stem cell maintenance *in vivo*⁸⁷. Moreover, In HSC niche, *in vivo* depletion of specific HSC stromal component, osteoblasts, led to a decrease of HSC number. *A contrario*, when osteoblasts were expanded, HSC pool size was increased showing the influence of stromal cells on HSC regulation⁸⁸.

IV.1.2. Pathways involved in stem cell determination

Numerous pathways involved in stem cell niches were documented over the years⁹, the most documented ones are described below:

The Wnt/ β -catenin signaling pathway implication in stem cell renewal was shown in hematopoietic and intestine stem cells^{89,90}. In the absence of Wnt, the signaling cascade is not activated and the cytoplasmic β -catenin protein is degraded by the action of the Axin complex, composed of Axin, the tumor suppressor Adenomatous polyposis coli (APC), casein kinase 1 (CK1), and glycogen synthase kinase 3 (GSK3); Wnt target genes are therefore repressed. The binding of Wnt ligands to the Frizzled (Fz) receptor and its co-receptor, lipoprotein receptor-related protein (LRP6 or LRP5) lead to the formation of the Wnt-Fz-LRP6 complex and the recruitment of Dishevelled (DVL) protein, results in the phosphorylation of DVL and LRP5/6. The Axin complex is then recruited and β -catenin degradation is prevented. Protein β -catenin accumulates and translocate into the nucleus to form complexes with TCF/LEF and activates Wnt target genes such as Axin and fibroblast growth factor (FGF) ^{91,92} (**Figure 13**).

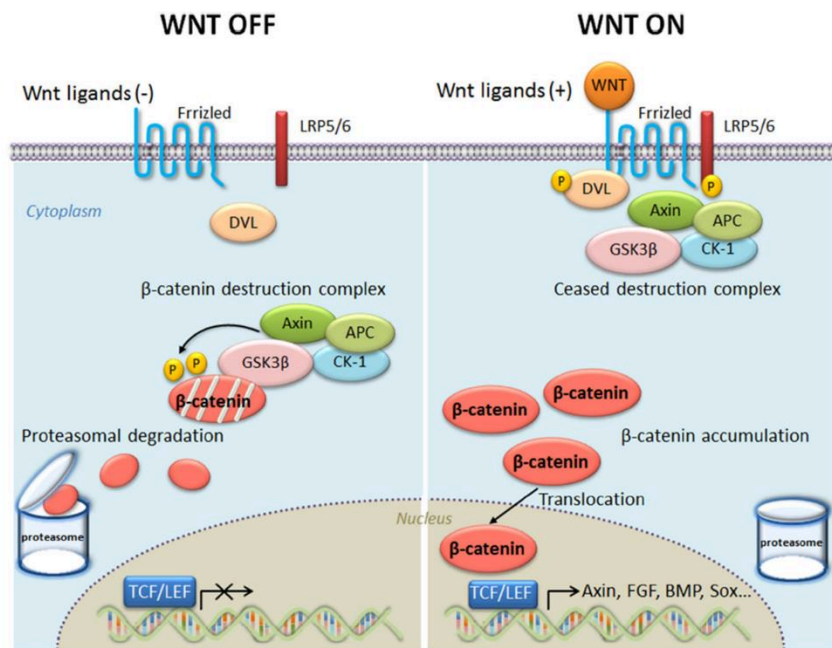


Figure 13: Canonical Wnt/ β -catenin signaling pathway. β -catenin protein is constantly degraded when Wnt pathway is not activated. In the presence of Wnt ligands, the cascade is activated leading to β -catenin accumulation in the cytoplasm. β -catenin translocates in the nucleus and activates Wnt target genes. Scheme from Ota et al.⁹²

Just as a marker can be specific to stem cells in one tissue and not at all in another tissue, signaling pathways can have opposite functions. Indeed, in the skin niche, Wnt/ β -catenin promotes differentiation of stem cells⁹³. In intestine, APC deficiency or β -catenin mutations, both downstream effectors of Wnt (**Figure 13**), destabilize homeostasis as stem cells self-renewal ability is increased⁹⁴. Furthermore,, LGR5⁺ stem cells are the target of Wnt/R-

spondin⁹⁵. Stromal compartments such as telocytes, trophocytes, fibroblasts and pericytes, all secrete R-spondin and Wnt that maintain LGR5⁺ cells. Overexpression of the Wnt activator R-spondin induces intestinal stem cell expansion *in vivo* showing its role in stem cell maintenance⁹⁶. Moreover, paneth cells (see **Figure 6A**), residing at the base of the intestinal crypt next to stem cells, is an important source of Wnt that participate in the stem cell pool maintenance⁹⁷.

Notch signaling is activated when a signal-sending cell that expresses Notch ligand (Dll1 and Dll4 in intestine), and a signal-receiving cell that expresses Notch receptor (Notch1 and Notch2 in intestine). After ligand/receptor binding, the Notch receptor is cleaved by ADAM10, and then by the γ -secretase complex, which cleaves the receptor at the cell membrane to release the Notch intracellular domain (NICD). NICD translocates into the nucleus and recruits a transcriptional co-activator complex that activates Notch target genes, such as Hes1 and Olfm4 (**Figure 14**)⁹⁸.

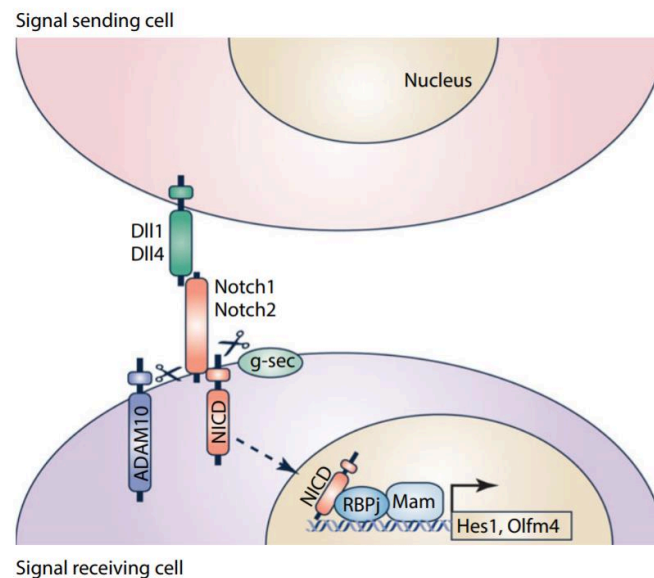


Figure 14: Notch signaling pathway in intestinal epithelium. Dll1 and Dll4 are ligands for Notch receptors (Notch1 and Notch2). Following binding, Notch is cleaved by ADAM10 and γ -secretase (g-sec) and NICD is liberated and activates Notch target genes. Scheme from Demitrack et al.⁹⁸

Notch signaling was widely studied in intestine and skin stem cell niche. In intestine, Notch signaling was shown to be essential to maintain the stem cell pool. Stem cells receive notch signaling input from Delta-like ligands Dll1 and Dll4⁹⁹. At the base of intestinal crypts, besides stem cells, reside Paneth cells which were known to express both Dll1 and Dll4 and

thus participating in stem cell maintain⁹⁷. Notch is also implicated in differentiation of intestinal cell with a process termed “lateral inhibition”¹⁰⁰. Inhibition of Notch signaling resulted in downregulation of stem cell markers *olm4* and *LGR5* and loss of stem cell pool leading to weight loss due to lack of nutrient absorption and fail to tissue replenishment and eventually death^{100,101}. In skin, Notch signaling was also shown to maintain the stem cell pool in hematopoietic niche^{102,103}.

Bone morphogenetic protein (BMP) and Transforming Growth Factor beta (TGF β) signaling pathways.

BMP are secreted members of the TGF β superfamily of signaling molecules. BMP ligands bind to activin-like kinase (ALK) 2, 3, or 6. This complex then binds to the BMP type II receptor (BMPRII), which phosphorylates the receptor. The activated receptor phosphorylates a set of Smad proteins called Smad (Smad1/5/8). In TGF β signaling pathway, TGF β RII and I dimerize and bind to TGF β which leads to Smad2/3 phosphorylation. In both pathways, Smad2/3 and Smad1/5/8 form a complex with Smad4, translocates into the nucleus and activates respectively TGF β and BMP-responsive genes (**Figure 15**)¹⁰⁴.

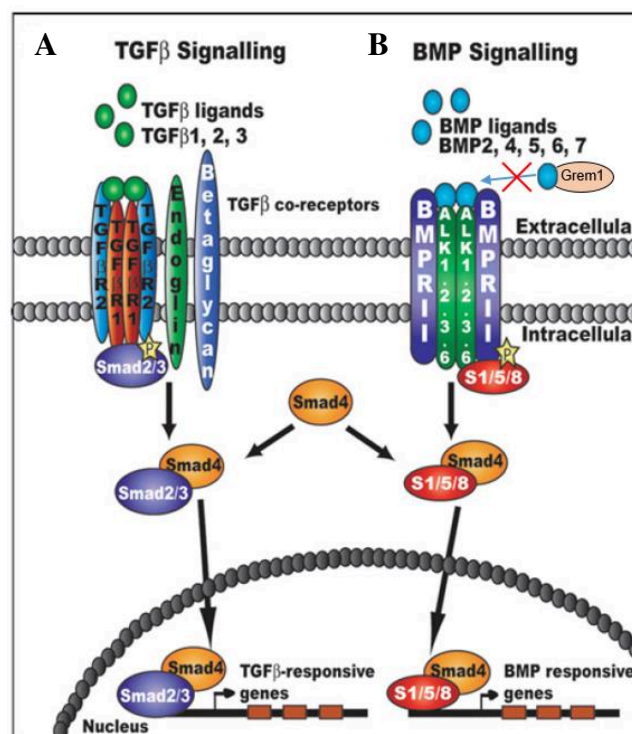


Figure 15: TGF β (A) and BMP (B) signaling pathways. After ligands/receptor binding, Smads get phosphorylated (Smad2/3 in TGF β pathway and Smad1/5/8 in BMP signaling). In both pathways, co-Smad4 form a complex with these smads and translocates into the nucleus to activate targeted genes for each pathways. S1/5/8: Smad1, 5 and 8; Greml1: Gremlin1. Scheme adapted from Garside et al.¹⁰⁴

BMP was shown to be a regulator of intestinal homeostasis. Indeed, using knock-out mouse models, Zhen Qi and colleagues showed that loss of BMP led to strong expansion of Lgr5⁺ stem cells and thus indicating BMP role in stem cell self-renewal restriction to avoid hyper-proliferation and ensure intestinal homeostasis¹⁰⁵. This role was also observed in hair follicle stem cell niche where inhibition of BMP activated stem cells and promoted their differentiation⁹. Similarly, in hair follicle niche, TGFβ was shown to activate hair follicle stem cells for regeneration¹⁰⁶.

Generally, signaling pathways involved in niche are cooperating as it was observed in intestinal niche⁸⁷. McCarthy and colleagues showed a gradient of Wnt expression between the base of the intestinal crypt and the base of the villus; Wnt expression at the base of the crypt decreases along the villus. Inversely, BMP signaling is present at the base of the villus and its signal is inhibited at the base of the crypt especially because of trophocytes, localized at the base of the crypt that secretes BMP inhibitor, Gremlin1 (Grem1). Grem1 binds to BMP ligands and prevents the ligand/receptor binding thereby inhibiting the BMP signaling pathway (**Figure 15**)^{87,107}.

All numerous studies I have described in this part showed the importance of niche cells in the maintenance of stem cell phenotype. Microenvironment maintains stem cells in their undifferentiated state. However, it can also play a critical role in cell fate by modulating stemness.

IV.2. Epithelial stem cells: state or fate?

Recent studies in mice have showed that when aged hematopoietic cells were exposed to younger environment, these cells actually rejuvenated proving the role of environment on cells behavior¹⁰⁸.

ECM is an important component of stem cell niches and is composed of several proteins among which fibronectins, collagens and laminins. These proteins are secreted by stromal cells such as fibroblasts and some epithelial cells. Epithelial cells and matrix collaborate to create a suitable environment for both. Cells elaborate their ECM by secreting proteins that will regulate stem cell behavior¹⁰⁹. ECM is implicated in many cellular processes ranging from migration to proliferation and apoptosis. ECM plays an important role in stem cell fate

decision. A deregulation in matrix-composing elements can impact stem cells behavior. As an example, a modified ratio in some laminins was shown to be critical to maintain stem cell homeostasis in hair follicle niche. Moreover, a reduction in collagen 17a1 levels led to stemness loss of hair follicle stem cells¹¹⁰. Upon mechanical stimulations, ECM stiffness can change affecting cell behavior¹⁰⁹. In 2016, H. Clevers and M. Lutolf collaborated to propose a custom made culture matrix designed according to different stages of intestinal stem cells organoids formation, aiming to enhance similarity between organoids and real organs¹¹¹.

When homeostasis is perturbed (e.g. infections, chemical or mechanical injuries, pH changes, etc...) cells can show plasticity. The first mention of such plasticity was described in 1886 by Rodolph Virchow that used/invented the term “Metaplasia” that literally means “mould into a new form”. Metaplasia is defined as a reversible process where one epithelium type can convert into another one. However, the definition of metaplasia is controversial; it is mainly used within a context of disease albeit metaplasia was also described as a physiological process. During puberty, pH changes in the cervical region lead to replacement of columnar epithelium of the endocervix to squamous epithelium of ectocervix to “resist” the new acidic environment¹¹². In early 1900, German scientists observed differentiated cells able to stop their specialized function to go back to a less differentiated stage. They called this phenomenon dedifferentiation (**Figure 16**)^{113,114}.

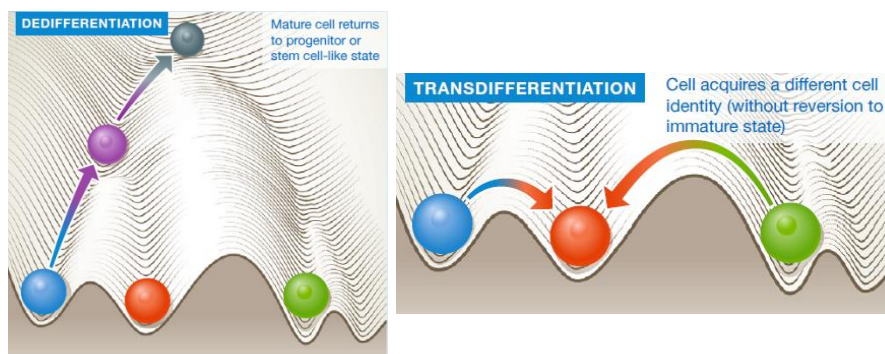


Figure 16: Cellular plasticity. Dedifferentiation and transdifferentiation

In the late 60s and 70s emerged a novel notion of plasticity. Okada isolated eye tissues from embryonic chick in order to grow them in 2D culture. He observed that neural and pigmented cells were able to turn into lens-type cells highlighting their transdifferentiation ability¹¹⁵. Few years before this study, Hadorn showed what he called “transdetermination” in vivo in *Drosophila*.

Van es et al. showed in 2012 that differentiated intestinal cells Dll1^{high}, direct daughters of Lgr5⁺ stem cells were able to revert back to Lgr5⁺ stem cells after sublethal irradiation of the intestine that decreases drastically Lgr5⁺ stem cell pool¹¹⁶. Rompolas et al. showed that, upon hair follicle laser ablation, epithelial cells which normally do not participate in hair follicle regeneration, are able to repopulate the hair follicle stem cell pool¹¹⁷. Inversely, Ito et al. showed hair follicle stem cells contribution to epidermis repair only in wounded condition¹¹⁸. Another group showed, in 2018, that after manual removal of the limbus, it will be restored in less than 30 days. They identified committed corneal cells able to dedifferentiate and give rise to a new limbus⁶⁵. Another important notion in stem cell field is the existence of reserve stem cells. In the intestine epithelium, intestinal stem cells are located at the base of the crypt as showed in **Figure 6A**. These stem cells are actively proliferative and are involved in the normal homeostatic turnover of the intestinal epithelium. However, LRC experiments showed the presence of slowly or non-proliferative cells located 4 positions from the base of the intestinal crypt, called +4 cells¹¹⁹. These cells were able to generate self-renewing organoids possessing all cell lineages of intestinal crypt¹²⁰.

Plasticity cannot be addressed without mentioning Induced Pluripotent Stem cells (IPSc). In 2006, Pr. Shinya Yamanaka's team published the world famous paper where induction of only 4 transcription factors (Oct3/4, Sox2, KLF4 and cMyc) in murine fibroblasts was sufficient for these fibroblasts to dedifferentiate into embryonic-like pluripotent stem cells¹²¹. This breakthrough earned him the Nobel Prize for Physiology or Medicine in 2012.

Since then, numerous studies aimed to use this technology to cure diseases. One of them aimed to correct sickle cells disease-induced anemia. Indeed, Hanna and colleagues performed a very clever experiment in which they harvested adult fibroblasts from mice, reprogrammed those into IPSc using Yamanaka 4 factors and differentiated IPSc into hematopoietic progenitors. Mutation causing sickle cell disease was corrected in those progenitors that were, *in fine*, transplanted back into the same mice subjected to irradiation in the meantime¹²² and see "human IPS cell-based therapy" ¹²³

To be or not to be; Stem cell identity is not binary. It is a complex state depending on various signals received by cell in homeostatic or stressed conditions. Now, we rather use the term "stemness" as cells can go through plasticity. Stem cell is no longer seen as an identity but rather as a state, a state being determined by the surrounding environment of the cell.

V. Epithelial transition zone: a stem cell niche associated with pathogenesis

TZ express the keratin 17, a member of cytokeratin family type I (**Figure 7A**). Keratin 17 is expressed at many places in the body, for example, in nails, hair follicles and in injured skin but not in normal skin^{124,125}. Otherwise, it is constitutively expressed at TZ (**Table 1**). As keratin 17, other wound-associated proteins such as TenascinC (TnC) and $\beta 6$ -integrin are naturally expressed in TZ whereas only expressed after an injury in others tissues⁵⁹. Interestingly, these two proteins were shown to be associated with wound healing and tumorigenesis suggesting a pre-lesional state of TZ. TZ are located in particular regions frequently subjected to bacterial, mechanical and chemical aggressions.

V.1. Transition zone: naturally prone to aggressions

V.1.1. Transition zone and bacterial stress

TZ located in the upper part of the gastro-intestinal tract are frequently associated with ulcers development. It is now well established that, *Helicobacter pylori* (*H. pylori*) bacteria in incriminated in ulcers etiology^{126,127}. After the infection, *H. pylori* induce apoptosis, cell proliferation, disruption of cell-cell junctions of epithelial cells leading to disruption of the gastric barrier¹²⁸. It was shown that *H. pylori* is a bacterium that resists in acidic areas. Some research proposed that a gradient of acid levels may exist in the TZ, TZ being the more acidic area explaining *H. pylori* affinity to the zone¹²⁹. Furthermore, some studies showed that acid suppression reduced *H. pylori* colonization in the antrum¹³⁰. Moreover, gastritis induced by *H. pylori* are more severe when occurring at the TZ¹²⁹.

V.1.2. Mechanical and chemical stress: hallmark of transition zones

TZ are naturally located in regions subjected to mechanical stress. Stomach and anorectal TZ represent a place of passages whether it is food bolus traveling the esophagus and the stomach or stool in the anorectal region.

The notion of metaplasia has been mentioned earlier (Chapter IV.2) as a form of cell plasticity often used in pathological context. The squamo-columnar junction located between esophagus and stomach is frequently associated with Barrett's esophagus, a condition where the stratified

squamous epithelium of esophagus is replaced by simple columnar epithelium of the corpus stomach⁶⁰. Several causes were shown to increase risk of developing Barrett's esophagus such as smoking and chronic acid reflux^{60,131}. Barrett's esophagus is known to be the precursor of esophageal adenocarcinoma arising at this site as metaplastic state can evolve into a neoplasia defined by an abnormal and excessive growth of tissue¹³².

To mimic some inflammatory pathologies such as colitis, chemically induced injury models were developed. The administration of a chemical agent Dextran sulfate sodium (DSS) in drinking-water is known to lead to epithelial cell death and compromise the barrier function of epithelium which open the door to bacteria and antigens that can cause inflammation¹³³.

Other injury models of gastric ulcers were developed that do not involve bacteria. Intra-gastric gavage of chemical agents such as ethanol 96% led to ulcer formation within the hour following the ethanol administration¹³⁴. However, with this method all epithelial cells are injured without the ability to injure specific cell types. Other methods based on the local application of acetic acid were developed to overcome this issue. These methods are more invasive and require surgery to expose the stomach. Acetic acid can be administrated by submucosal injection or by direct application on the desired parts of the stomach^{135,136}.

Moreover, some injury models combine chemical and mechanical stress. EDTA wound usually used to induce wounds in colon region is well detailed by Fukuda and colleagues and consists of epithelium exposure to ethylenedinitrilo tetraacetic acid (EDTA) during few minutes followed by epithelial abrasion using an electric brush¹³⁷. This method is particularly efficient in removing entire crypts compared to scraping wounds where the base of crypts may remain untouched.

V.2. Transition zone microenvironment: One of a kind

V.2.1. Transition zone stromal stiffness

During my participation to the international Gordon congress in 2019 in Newry (Maine, USA), I had the chance to talk to limbus-expert scientists on limbus stroma softness. The limbal region was shown to be softer compared to cornea and some *in vitro* studies already showed that cultures on soft substrates retained limbal stem cell markers whereas stiffer

substrates favored differentiation^{63,64}. Furthermore, the notion of stiffness was approached in 2016 by Bongiorno and colleagues at the cellular level. They concluded that limbal stem cells were softer than cells from central cornea and thus proposed cellular stiffness as a stemness marker¹³⁸. This is not surprising considering TZ as the crossroad of distinct epithelia; TZ may need this stromal flexibility to absorb inputs from both sides (**Figure 17**).

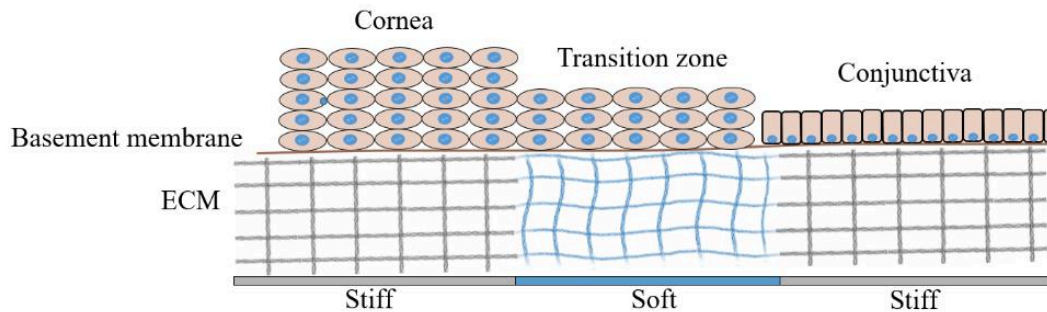


Figure 17: Scheme depicting extracellular matrix (ECM) stiffness in transition zone of the eye. TZ stroma is softer than surrounding epithelia stroma.

V.2.2. The transition zone stroma

Fibroblasts are the main cells composing the connective tissue. Unpublished data from Guasch lab previous studies showed the presence of fibroblasts positive for Vimentin below the anorectal TZ. Among the vimentin positive population, some cells were positive for periostin and α SMA that are markers for myofibroblasts.

In 2014, Ouyang et al investigated Wnt-PAX6 axis in corneal epithelium homeostasis. The corneal epithelium, maintained by limbal stem cells, is a non-keratinized epithelium ensuring corneal transparency. Deficiency of stem cells leads to corneal keratinization and opacification that are associated with blindness. They found that Wnt7a was involved in limbal stem cells specification via PAX6⁷⁴. Earlier this year, a paper on cervical TZ stroma showed that TZ epithelial cells were maintained independently of the Wnt signaling pathway in contrast with the endocervical cells (simple glandular epithelium) that is Wnt-dependent⁵⁵.

V.2.3. Transition zone and immune cells

In both humans and mouse, gut epithelial cells are in tight proximity with bacteria whether commensal or pathogenic. This may explain the presence of immune/inflammation-associated cells along the gut, intestines and anus. Guasch and colleagues already showed the presence

of inflammatory macrophages (Mac1⁺) in the stroma just below the anorectal TZ⁵⁹. Moreover, although several leukocyte populations can be found in the surrounding microenvironment of epithelial cells including lymphoid and myeloid cells, the majority of immune cells found in anorectal TZ are T lymphocytes. In fact, more T lymphocytes reside in the intestinal epithelium than in any other tissues of the body. More precisely, the anorectal TZ is colonized by intraepithelial immune cells called $\gamma\delta$ T. This subpopulation of T lymphocytes is part of both innate and adaptive immunity and, as indicated by their names, is located within the epithelium between the epithelial cells. This T lymphocyte subpopulation was shown to be implicated in epithelial homeostasis, inflammation regulation and tumorigenesis in colorectal cancer¹³⁹. Furthermore, preliminary results from our lab showed the presence of Treg positive for CD3⁺ Foxp3⁺ cells in the anorectal TZ stroma (**Annexe 2**). All these elements (summarized in **Figure 18**) suggest that TZ may represent a stem cell niche in a pre-lesional state prone to malignant transformation⁴⁹.

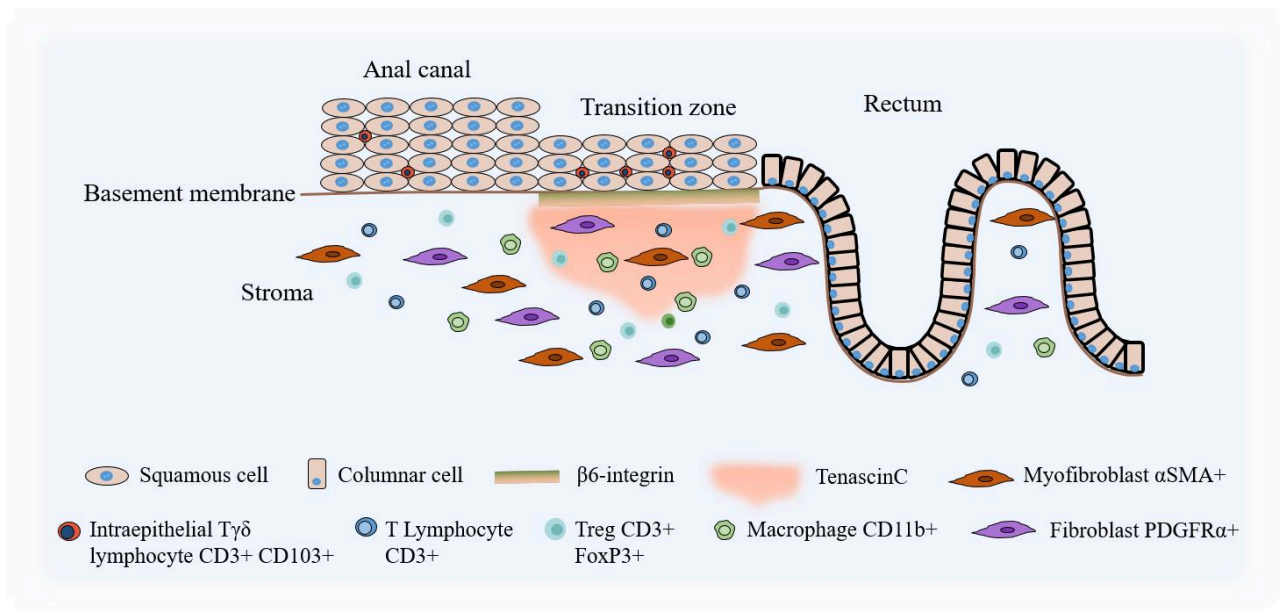


Figure 18: Overview of microenvironment populations present in the anorectal transition zone region during homeostasis. TZ epithelial cells are in close contact with immune cells (mainly T lymphocytes and macrophages) and stromal cells (fibroblasts and myofibroblast)

V.3. Transition zone and cancer susceptibility

It is well known that TZ are associated with poor prognosis cancer susceptibility in humans¹⁴⁰ and in mice^{59,141}. Thus, 86% of esophageal cancers develop at the junction of

esophagus and stomach¹⁴², 99% of cervical cancers develop between the glandular epithelium of endocervix and the stratified epithelium of ectocervix^{143,144} and 85% of highly malignant anorectal cancers develop between the stratified epithelium of the anal canal and the glandular epithelium of the rectum¹⁴⁵⁻⁵⁹. Tumors at the anorectal TZ associated with Squamous Cell Carcinoma (SCC) are three times more common than carcinoma in the anal canal and more aggressive.

Human Papilloma Virus (HPV) infection is associated with anal, cervical and some oropharyngeal cancers. It was shown that HPV was present in greater quantity in esophagus-stomach TZ compared to surrounding epithelia. In order to establish a stable infection, HPV needs to infect basal cells from stratified squamous epithelium of the cervical TZ and squamo-columnar junction between esophagus and stomach¹⁴⁶. Basal cells are not in contact with epithelium lumen and are thus not accessible to the virus. Thereby, epithelial integrity has to break to expose basal cells to the virus. Rajendra and Sharma proposed, in the case of esophageal cancers, that progressive damage occurring in the TZ because of acidic reflux may alter epithelial integrity leading to infection in basal cells. Moreover, HPV was associated with disease severity in case of Barrett's esophagus¹⁴⁷. More globally, in anal, cervical and esophageal cancers, traumas caused by some sexual practices could also affect epithelial integrity promoting basal cells infection⁵³.

Previous studies had shown the presence of cells with cancer stem cell properties within tumors arising at the anorectal TZ¹⁴⁸. These cells were shown to be clonogenic with the ability to unlimitedly self-renew *in vitro* and to be tumorigenic *in vivo* after orthotopic transplantation in anorectal TZ in *Nu/Nu* mice. These cells are also able to self-renew *in vivo* giving rise to differentiated cells thus recapitulating primary tumor hierarchy. Moreover, they can give rise to a new tumor after serial transplantation¹⁴⁹. Furthermore, junctional region between hilum and ovary was showed to be cancer-prone as inactivation of tumor suppressor genes p53 and Rb1 were sufficient for ovarian tumorigenesis^{66,150}.

It had been shown that some mutations in signaling pathways led to tumor development. TGF β signaling pathway is a hallmark of TZ cancers⁴⁹. TGF β is a multifunctional protein that controls proliferation, differentiation, angiogenesis, wound healing and other functions in many cell type¹⁵¹. Effects of TGF β signaling activation on gene expression depend on cell type and cellular context. Indeed, its activation can lead to proliferation in the mammary tissue but have an anti-proliferative effect in human and mouse normal epithelial cells. Mutations in TGF β family drive spontaneous development of squamous cell carcinoma in

various TZ. Deficiency of Smad3 in mice lead to tumor formation at stomach TZ¹⁵². Mutation of TGF β receptor II (TGF β RII) leads to SCC in anorectal TZ⁵⁹. Interestingly, while TGF β pathway mutations alone are sufficient to induce tumor development in TZ; an additional oncogenic event is required in other tissues. TGF β signaling abolishment via TGF β RII or the downstream effector of TGF β , Smad4 deficiency lead to carcinomas in pancreas only when in combination with the activated KRas^{G12D} allele^{153,154}. In colon, bacterial infection such as *Helicobacter* species (e.g. *bilis* and *hepaticus*) combined with the loss of Smad3 are sufficient to induce colonic cancer¹⁵⁵. These data suggest that TZ are more prone to malignant transformation than surrounding epithelia¹⁵⁶.

Moreover, TGF β RII-deficient SCC developed at the anorectal TZ displayed an increase of Ras expression^{59,148}. Ras is a superfamily composed of more than 150 members and implicated in a wide range of functions including cellular differentiation, growth and proliferation. It is divided in 5 main families that are Rho, Ran, Rab, Arf and Ras. The last family, Ras, is further divided into 6 subfamilies including Ras, Ral, Rap, Rad, Rheb, and Rit. Finally, in the Ras subfamily, 3 proteins have been identified as HRas, NRas and KRas¹⁵⁷.

KRas is frequently associated with various cancers including lung, breast, colon and pancreatic cancers where it is found in more than 80% of cases^{158,159}. It is found in different mutated forms such as KRas^{G12D} which is associated with neoplasia in various tissues for example gut, lungs and skin^{160,161}.

Immunity and cancer relationship is now well established. Virchow first hypothesized that cancer was the result of immune system dysfunction/failure back in 1863. Thereafter, Dvorak referred to tumors as “wounds that do not heal”¹⁶². Immunity plays a key role in all steps from tumor initiation to progression and dissemination. During tumor progression, inflammatory cells are present within the tumor microenvironment and their presence was shown to impact cancer prognosis. A T lymphocyte infiltration is correlated with good prognosis in solid cancers whereas macrophages infiltration is associated with worse prognosis⁷⁷.

Transition zone specific Krt17 was showed to have an immunomodulatory role. Jin & Wang proposed a model where Krt17 acts as a stimulator of T cells that can, in response to Krt17 stimulation, upregulate Krt17 expression⁴¹. Furthermore, Depianto et al. showed that genetic ablation of Krt17 in mice delayed tumor initiation and growth. This delay was accompanied with reduced inflammation and immune polarization Th1 to Th2 profile. Among CD4⁺ T lymphocytes, there are T helpers (Th) 1, 2 and 17 with different functions. Th1 is known for its pro-inflammatory function via pro-inflammatory cytokine production in contrast with Th2

that produce anti-inflammatory cytokines. They also showed that Krt17 deletion attenuated hyperplasia and inflammation in acute dermatitis¹⁶³. It is well known that Krt17 promotes keratinocytes proliferation via the Akt/mTOR pathway^{164,165}. This pathway was also shown to promote Th1 differentiation through its mTORC1 complex suggesting a mutual influence between immune cells and keratinocytes.

TGF β pathway has an important role in T cell activation¹⁶⁶. Transcriptional intermediary factor-1 gamma (Tif-1 γ) selectively binds to phosphorylated Smad2/3 in competition with Smad4 to transduce signal in the TGF β pathway. Our collaborator from CRCL, Dr. Julien Marie, found that deletion of Smad4 and Tif-1 γ , specifically in CD4⁺ T lymphocytes using double knock-out (DKO) CD4CrexLSL-Smad4xLSL-Tif1 γ mice induced colonic inflammation and evolve into dysplasia and carcinoma mainly in the anorectal TZ (**Figure 19**). Moreover, these carcinomas have squamous and glandular components suggesting that the transformation may occur in a stem cell giving rise to both components. More interestingly, transplantation of DKO mice bone marrow into irradiated mice led in the same way as before to inflammation with T lymphocytes recruitment, dysplasia and finally carcinoma in the anorectal TZ and further reinforcing the idea of a strong interplay between T lymphocytes and TZ epithelial cells (Manuscript submitted).

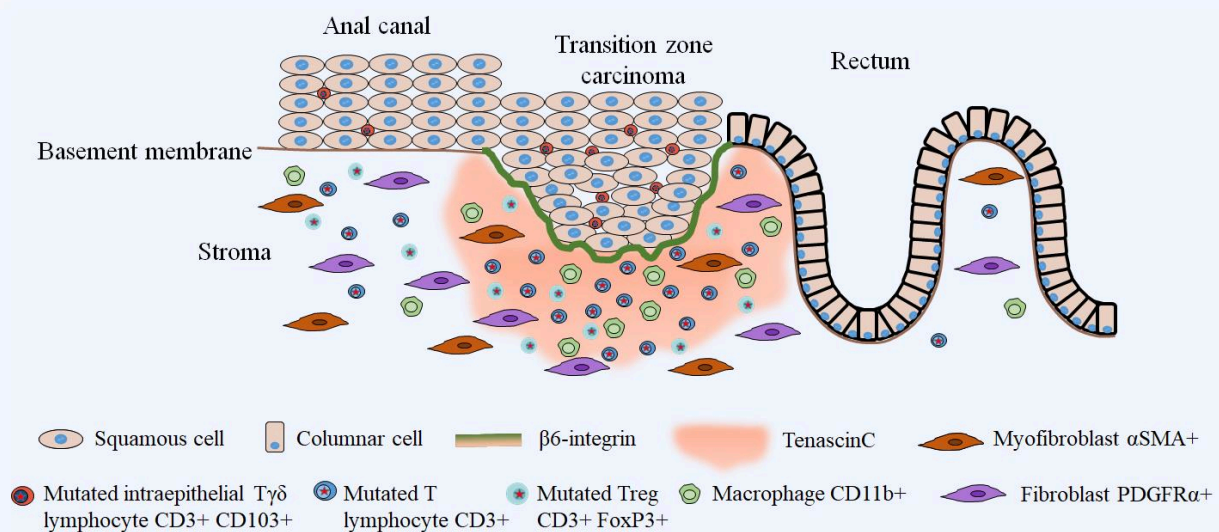


Figure 19: Tumor arise at the anorectal transition zone following mutations in T lymphocytes.

OBJECTIVE

Transition zones are making the link between two different kind of epithelium throughout the body. They are found in the eye, a region called the limbus, in the cervix, between the endo and the ectocervix, between the esophagus and the stomach and between the anal canal and the rectum. These zones are special regions with a cell population displaying stem-cell like properties. Moreover, TZ are frequently associated with congenital disorders and pathologies such as ulcers and aggressive cancers. However, the role of these zones during homeostasis, injury and tumorigenesis remain unsolved. More than 85% of anal and stomach cancers are associated with TZ and almost all cervical cancers are found in the TZ between the endo and the ectocervix. Despite the clinical impact of the TZ cancers, little is known about the initiation events of these cancers. Because TZ unique stroma express constitutively wound-associated proteins, it may represent a pre-lesional state prone to tumor-initiating mutations and malignant transformations. Recent observations from our collaborator indicated a strong interplay between epithelial and immune cells as mutations in T lymphocytes led to tumor development in anorectal TZ.

Based on these observations, **we hypothesized that anorectal TZ cells may maintain surrounding epithelium during homeostasis and injury and may represent a target for malignant transformation.**

The first aim of my Ph.D was to characterize the role of anorectal TZ during homeostasis and after an injury. We used a mouse model of lineage tracing to follow TZ Krt17⁺ cells behavior during homeostasis and injury. We then combined confocal imaging, organoid cultures and single-cell RNA sequencing to decipher anorectal TZ heterogeneity and role during homeostasis and following epithelial injury.

Secondly, we developed a unique mouse model of early neoplasia in the anorectal TZ involving KRas mutation G12D specifically in TZ Krt17⁺ cells. This model will help elucidate the early molecular changes occurring in the epithelial cells and stromal cells to identify tumor susceptibility regulators and target cells that lead to malignant transformation.

This project will allow us to determine which populations are permissive to oncogenes able to lead to abnormal proliferation and to cancer and to identify new therapeutic approaches by proposing more efficient treatments.

RESULTS

I. A stem cell population at the anorectal junction maintains homeostasis and participates in tissue regeneration after injury

Article published on May 12 2021 in *Nature Communications*

Transition zones are special regions located between two different types of epithelia and frequently associated with cancer. Their role in maintaining surrounding epithelia during homeostasis and injury is poorly known. In this paper, for the first time, we developed an *in vivo* mouse model K17CreER-LSL-GFP to lineage trace Krt17⁺ cells of anorectal TZ. During homeostasis, we showed that Krt17⁺ TZ cells were unipotent as they maintained anal canal epithelium only and no GFP cells were found in the glandular epithelium of rectum. We also used single-cell RNA sequencing and pseudo-time analysis to confirm our lineage tracing experiments and the unipotency of TZ during homeostasis. We further found that anorectal TZ cells are heterogeneous and express genes differentially depending on their positioning within the TZ. We also set up a 3D model of anorectal TZ cell culture that successfully recapitulate the heterogeneity and specific markers of TZ. We showed the self-renewal and differentiation ability of sorted Krt17⁺ TZ cells.

In contrast to other stem cell niches, TZ are naturally subjected to mechanical stress. When we challenged it with a wound, TZ cells showed an unexpected plasticity that allows them to switch fate and participate in the regeneration of rectum epithelium, providing fully differentiated crypts. Single-cell RNA sequencing data helped us to identify a new population of TZ cells after the injury that we named hybrid cells, co-expressing both squamous stratified and simple columnar epithelia markers. Those TZ cells expressed the transcription factor JunB, associated with wound response. By using our powerful 3D culture tool, we showed by shRNA experiments, that JunB was involved in the proper differentiation of TZ epithelium.

Our paper suggests that anorectal TZ cells may be a backup reservoir of stem cells to maintain tissue homeostasis. A part of my unpublished data on stomach TZ also showed that stomach TZ cells participate in the first gland, a multilayered stomach gland involved in maintaining homeostatic condition under acidic changes.





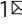
ARTICLE



<https://doi.org/10.1038/s41467-021-23034-x>

OPEN

A stem cell population at the anorectal junction maintains homeostasis and participates in tissue regeneration

Louciné Mitoyan¹, Véronique Chevrier¹, Hector Hernandez-Vargas ^{2,3}, Alexane Ollivier¹, Zeinab Homayed⁴, Julie Pannequin⁴, Flora Poizat⁵, Cécile De Biasi-Cador⁵, Emmanuelle Charafe-Jauffret ^{1,5}, Christophe Ginestier ¹ & Géraldine Guasch ¹ 

At numerous locations of the body, transition zones are localized at the crossroad between two types of epithelium and are frequently associated with neoplasia involving both type of tissues. These transition zones contain cells expressing markers of adult stem cells that can be the target of early transformation. The mere fact that transition zone cells can merge different architecture with separate functions implies for a unique plasticity that these cells must display in steady state. However, their roles during tissue regeneration in normal and injured state remain unknown. Here, by using in vivo lineage tracing, single-cell transcriptomics, computational modeling and a three-dimensional organoid culture system of transition zone cells, we identify a population of Krt17+ basal cells with multipotent properties at the squamo-columnar anorectal junction that maintain a squamous epithelium during normal homeostasis and can participate in the repair of a glandular epithelium following tissue injury.

¹ Aix-Marseille University, CNRS, INSERM, Institut Paoli-Calmettes, CRCM, Epithelial Stem Cells and Cancer Team, Marseille, France. ² Department of Immunity, Virus and Inflammation, Cancer Research Center of Lyon (CRCL), Inserm U 1052, CNRS UMR 5286, Université de Lyon, Centre Léon Bérard, Lyon Cedex 08, France. ³ Department of Translational Research and Innovation, Centre Léon Bérard, Lyon Cedex 08, France. ⁴ CNRS, UMR5203, Inserm U661, Institut de Génomique Fonctionnelle, Montpellier, France. ⁵ Department of Biopathology, Institut Paoli-Calmettes, Marseille, France.
✉email: geraldine.guasch-grangeon@inserm.fr

Several of our organs have a region called transition zone (TZ) that connects two distinct epithelia such as stratified and glandular epithelia¹. These junction areas can be found throughout the body in the eye, esophagus, stomach, ovary, cervix, and anus and are a site of associated pathology in human and mouse including cancers with poor prognosis^{2–8} and prelesional conditions such as ulcer, Barrett's esophagus⁹, and developmental disorders such as cloaca malformation¹⁰. These TZ are composed of cells expressing markers of adult stem cells^{11–13} that can be the target of early transformation^{14–17}. These junctions between our organs allow us to have a continuous lining of tissues, such as in the digestive tract. When affected, the anorectal region is usually associated with high invalidity of patients including fecal incontinence. It is thus essential to understand how important these TZ are to preserve organ homeostasis. In this work, by studying the properties of the anorectal TZ at the single cell level and by combining technologies such as organoid culture, gene sequencing and the use of mouse models, we have identified a population of Keratin 17 positive (Krt17+) basal cells with multipotent properties that maintain a squamous epithelium during normal homeostasis, and can participate to the repair of a wounded glandular epithelium.

Results

Multilineage potential of Krt17+ TZ cells during homeostasis.

In any species, the abrupt transition from one epithelia to another can be readily detected histologically and molecularly as each epithelium expresses characteristic proteins, such as Krt14/5 for the anal stratified epithelium and Krt8 for the glandular rectal epithelium¹¹ (Supplementary Fig. 1a and Fig. 1a). The hyperproliferative-associated-Krt17¹⁸ marks specifically TZ cells^{1,2} (Fig. 1a) with a low expression level in anal canal cells proximal to the TZ (Supplementary Fig. 1b). Krt17 expression correlates with the active renewal occurring in the anorectal TZ (Supplementary Fig. 1c). The mere fact that TZ cells can merge these different epithelia with separate functions implies for a plasticity, that these cells must display in steady state. However, it is unknown if TZ cells have any role in renewing of the epithelium during normal homeostasis and after an injured condition.

Inducible genetic fate mapping method allows the identification of stem cells in many epithelial tissues¹⁹. To investigate the contribution of the Krt17+ basal TZ cells to the renewing of the stratified and/or glandular epithelium, we performed lineage tracing using *K17CreER*^{T2};*R26R*^{GFP} bigenic mice (Fig. 1b) using one injection of tamoxifen to label permanently few cells at the TZ (Fig. 1c, d). No Krt17+GFP+ cells were detected in non-induced *K17CreER*^{T2};*R26R*^{GFP} mice analyzed short and long chase ($n = 3$) (Fig. 1d and Supplementary Fig. 1d) confirming the tight regulation of *K17CreER* activity in the basal TZ cells. Since lineage tracing is reporting transcriptional activity of the *Krt17* gene, we report the location of *Krt17* transcripts in the anorectal region via high quality in situ hybridization. We showed by RNAscope technology that *Krt17* transcript was exclusively found in the anal TZ region, when compared to the anal canal and the rectum (Supplementary Fig. 2a, b and quantified in Supplementary Fig. 2c). Furthermore, tamoxifen injection itself does not change *Krt17* transcript (Supplementary Fig. 2c), neither Krt17 endogenous protein expression level (Supplementary Fig. 3a) and does not induce proliferation of Krt17+ TZ cells (Supplementary Fig. 3b).

We found that lineage-marked GFP+ TZ cells are found in the stratified epithelium of the anal canal after short and long-term tracing and not in the Krt8+ glandular epithelium (at least three mice for each time point analyzed) (Fig. 1c–e). GFP positive cells are still found in mainly all stratified epithelium of the anal canal

after 1-year lineage tracing (Fig. 1d) strongly indicating that all the Krt17+ TZ cells are long-term, self-renewing adult stem cells. Moreover, GFP+ lineage traced cells colocalized with differentiated epithelial cell type Krt10+ and Loricrin+ (Fig. 1f) showing the multilineage potential of the Krt17+ stem cells.

To analyze the hierarchical organization of the anorectal cells we have performed single-cell RNA sequencing (scRNA-seq) analysis^{20,21} from purified FACS-sorted cells (Supplementary Fig. 4), and we obtained initially eight distinct clusters (Supplementary Fig. 5a). A Gene ontology analysis for molecular pathways illustrated that one cluster was specially enriched in signaling cascades involving lipid and steroid metabolism (Supplementary Fig. 5b). This cluster represents anal glands that are present below the anal TZ. These glands are positive for the Oil red O staining and we confirmed at the protein level that perilipin-2, highly expressed in this cluster by sc-RNA seq, marks indeed the anal glands (Supplementary Fig. 5c). Two other clusters identify fibroblasts (Supplementary Fig. 5d) and hair follicle (Supplementary Fig. 5e) with known genes²², such as *Lhx2* and *Lgr5* expressed in the bulge of the hair follicle but not in the anal TZ (Supplementary Fig. 5f, g). These three clusters were further removed from our analysis to only focus on the epithelial anorectal cells (Fig. 2a). From this new analysis, four clusters were found. One cluster, enriched in *Epcam*, *Krt8* and numerous mucins mRNA, identified the rectum cell population (Fig. 2a, b). Differentiated anal canal cells are found in the cluster enriched in *Krt10* and *Gpc3* genes (Fig. 2c). Anal canal cells, depending on their proximal or distal localization, express low level of mRNA *Krt17* (Fig. 2d). Notably, the anal TZ population can be separated into two *Krt17*+ clusters representing the basal and suprabasal cell layer (Fig. 2d, e). Glandular and stratified basal cells are marked by the epithelial polarized marker $\alpha 6$ -integrin (Fig. 2e, f). Cells localized at the basal layer of the TZ show heterogeneity and can express differential level of Krt6 expression depending on their location. TZ cells closer to the anal canal express Krt6 only in the suprabasal layer (Fig. 2fi), whereas TZ cells closer to the rectum express Krt6 in the basal and suprabasal layers (Fig. 2fii). At this location, closer to the rectum, basal TZ cells also express the stem cell marker CD34¹¹ (Fig. 2g). The adherens junction protein nectin-4²³ marks the suprabasal TZ cells (Fig. 2e, f). The scRNA-seq data also shows that the glycoprotein *Gpc3* seems to be exclusively expressed in the anal canal population compared to the TZ (Fig. 2c, h). Overall, the scRNA-seq data revealed heterogeneity within the anal TZ population (Fig. 2i), and suggest that cells located at different positions in the basal layer have distinct molecular signatures.

Krt17+ TZ cells self-renew and differentiate in 3D organoid.

To test the long-term proliferation potential and the self-renewal ability of the anal Krt17+ TZ cells compared to the anal epithelium, we have used three-dimensional organoid culture system. We have used microdissection technique, mouse genetic and flow cell sorting using the *K17CreER*^{T2};*R26R*^{GFP} mouse model induced with tamoxifen for 2 days to label specifically the TZ with GFP in combination with the cell surface marker *Epcam* expressed in a majority of epithelial cells (Fig. 3a and Supplementary Fig. 4). As a control we verified that tracing was initiated only in K17+ TZ cells; In vitro tamoxifen assay, where culture media was supplemented with tamoxifen for 1 week, confirmed that GFP was only induced in TZ organoids and not in anal canal organoids or with oil control supplementation (Supplementary Fig. 6a). Each sorted cell population, stratified (GFP-*Epcam*^{Low}), TZ (GFP+*Epcam*^{Low}), and glandular (GFP-*Epcam*^{High}) can grow as organoid culture and resemble their tissue of origin by histology (Fig. 3b), where stratified squamous epithelium in the TZ

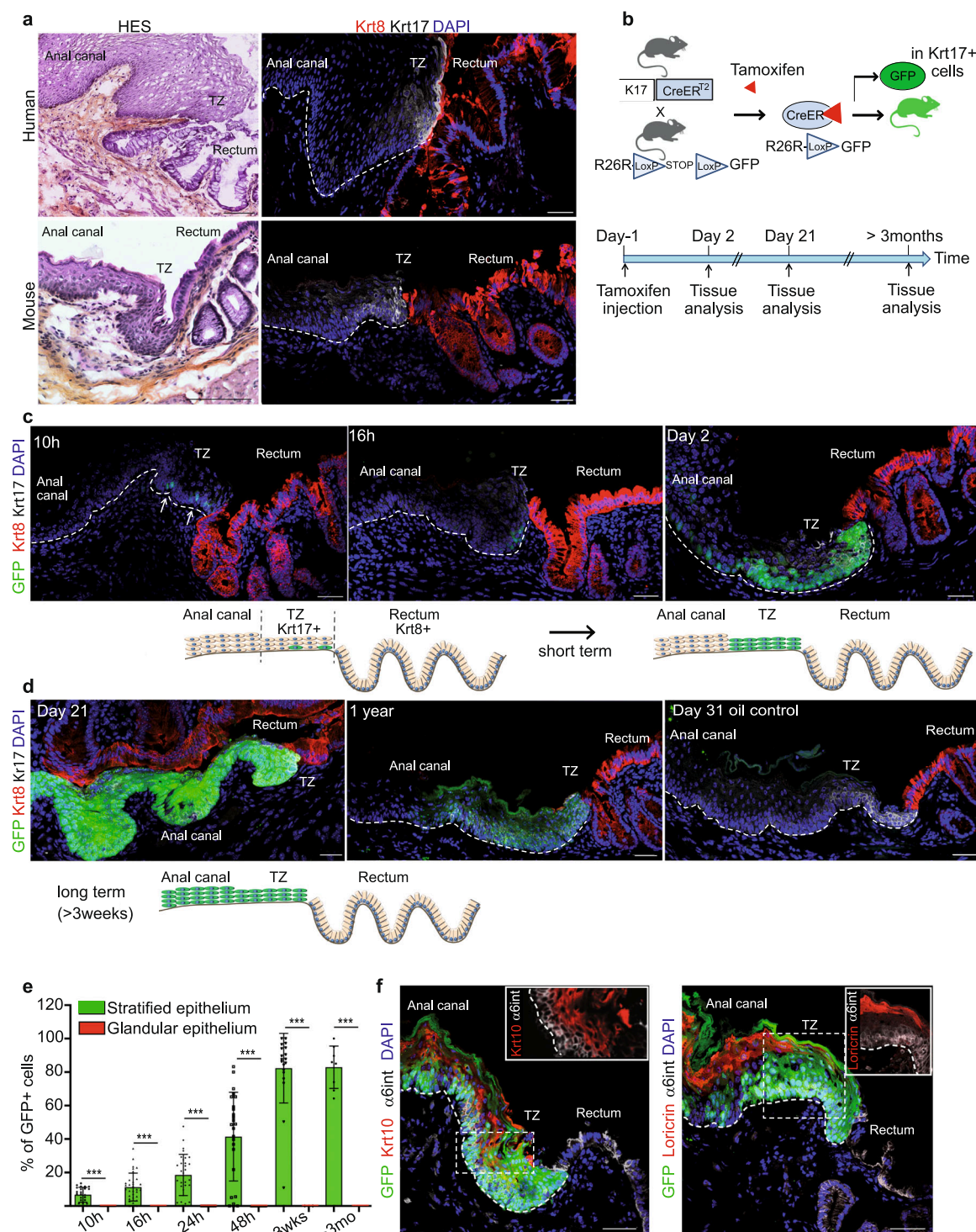


Fig. 1 A population of basal Keratin 17⁺ cells at the anorectal junction contributes to the anal epithelium during normal homeostasis. **a** Human and mouse anorectal TZ are histologically (HES) and molecularly similar. A population of keratin 17 (Krt17) expressing cells (white) shown by immunofluorescence is present at the anorectal TZ ($n = 55$ independent experiments from 58 mice and $n = 3$ independent experiments from two independent human samples). The rectum expresses keratin 8 (Krt8) (red). Scale bars for HES are 100 and 50 μm for immunofluorescence panels. **b** Schematic of the mouse model used and time point analyzed after one injection of 2 mg of tamoxifen to only label few cells at the TZ. **c, d** Unipotency of Krt17⁺ TZ cells (green) during short and long-term lineage tracing. Representative images of $n = 3$ biologically independent samples at each time point are shown. Dashed lines delineate the epithelium from the stroma. Scale bars are 50 μm . **e** Quantification of the % of GFP cells in stratified and glandular tissue ($n = 3$ mice per time point) (Source data are provided as a source data file). Two-tailed paired t -test; error bars, mean \pm SD *** $p < 0.0001$. **f** Krt17⁺ TZ cells give rise to differentiated suprabasal layer cells of the anal canal (4 weeks post-tamoxifen injection) positive for Krt10 (red) and to cornified layer cells positive for Loricrin (red). $\alpha 6$ integrin (in white) marks the basal layer. Scale bars are 50 μm ; Insets for Krt10 and Loricrin are zoom in 1.5-fold and 1.1-fold, respectively.

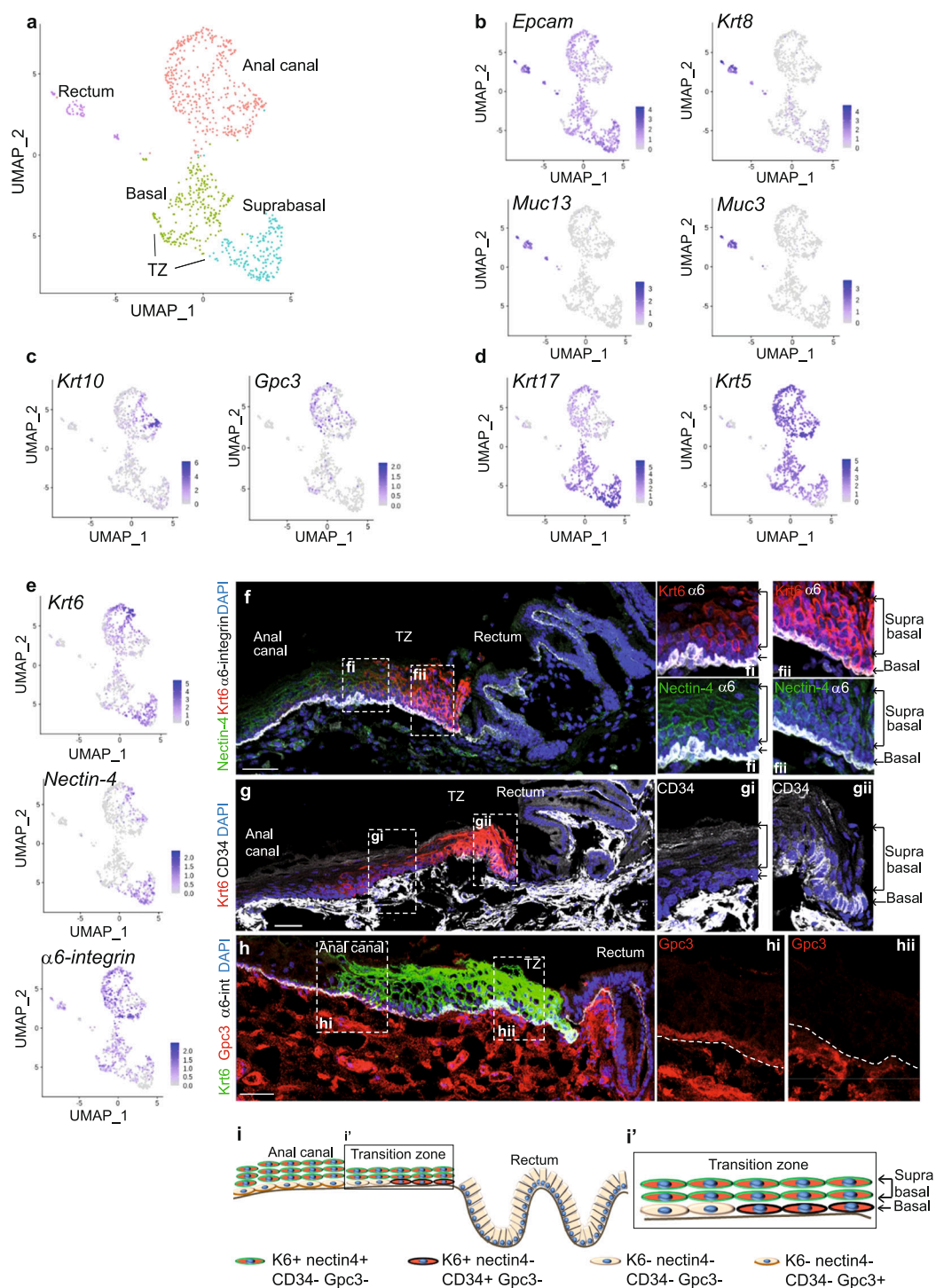


Fig. 2 Single cell analysis reveals hierarchical organization of the anal TZ cells. **a** Main cell populations visualized on Uniform Manifold Approximation and Projection (UMAP) dimensional reduction from scRNA sequencing of anorectal epithelial cells. Nine hundred and thirty-nine cells are visualized and colored by clustering. **b–d** Expression of key genes expressed in rectum, differentiated anal cells and TZ populations respectively. Darker color in the UMAP plot indicates higher expression level of the selected gene. **e** Expression of *Krt6* and *nectin-4* genes defines the suprabasal TZ population. **f** Immunofluorescence with *Krt6* (red), *nectin-4* (green) antibodies confirms that TZ population can be separated into basal (expressing the polarized $\alpha 6$ -integrin in white) and suprabasal clusters ($n = 3$ independent experiments from three mice). Scale bar is 50 μm . **fi, fii** are zoom 2.5-fold into the TZ closed to the anal canal and the rectum respectively. **g** Immunofluorescence with *Krt6* (red), and CD34 (white) shows that TZ basal cells closed to the rectum express the stem cell marker CD34 ($n = 3$ independent experiments from three mice). Scale bar is 50 μm . Boxed areas **gi** and **gii** are shown at higher magnification (2.5-fold). **h** Immunofluorescence with Gpc3 (red), *Krt6* (green) and $\alpha 6$ -integrin (white) shows the specific expression of Gpc3 in basal cells of the anal canal ($n = 3$ independent experiments from three mice). Scale bar is 50 μm . Boxed areas **hi** and **hii** are shown at higher magnification (2.5-fold). **i** Representation of the TZ heterogeneity depending on cell positioning. **i'** Zoom into the TZ.

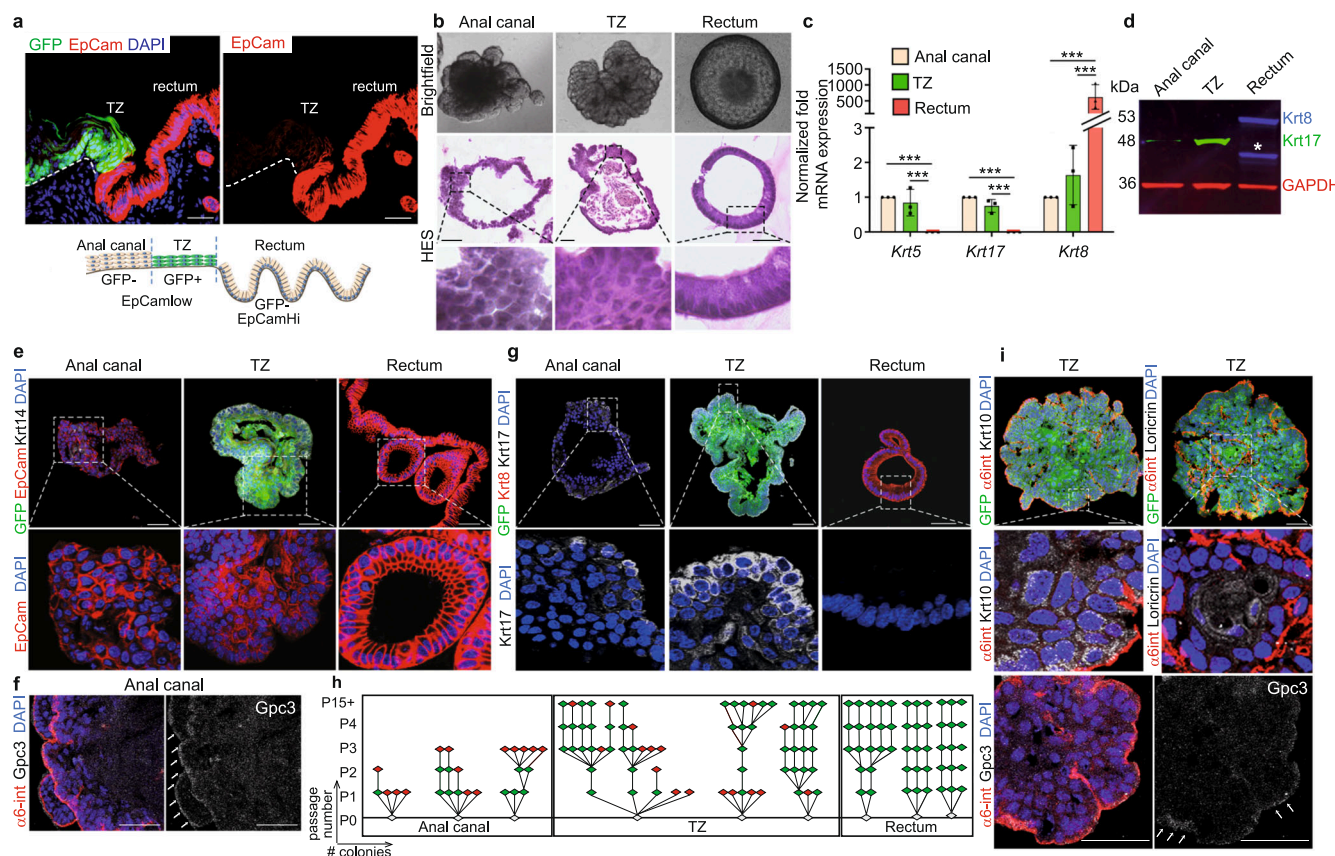


Fig. 3 Keratin 17⁺ basal TZ cells are clonogenic in 3D organoid culture and have long-term self-renewal and differentiation potential. **a** TZ cells are separated based on GFP and EpCam expression (red) ($n = 3$ independent experiments from five mice). See complete FACS strategy in Supplementary Fig. 4. **b** Brightfield and HES images showed the unique characteristics of the anal canal (squamous), anal TZ (squamous) and rectum (columnar) organoids. Representative images of $n = 21$ independent organoid culture experiments derived from $n = 21$ independent FACS sorting isolation after 14, 12, and 11 days of culture without passage for the anal canal, TZ and rectum respectively. **c** Quantitative qPCR analysis of *Krt5*, *Krt17*, and *Krt8* genes on growing organoids at passage 1 show the glandular nature of the rectum organoid expressing higher *Krt8* mRNA expression level than the anal canal and TZ ($n = 3$) (Source data are provided as a source data file). *** $p < 0.001$ calculated using two-way Anova and Bonferroni test; error bars, mean \pm SEM. **d** Western Blot analysis of Krt17 (green) and Krt8 (red) showing higher expression of Krt17 in TZ organoids and Krt8 expression only in rectum organoids ($n = 3$ independent experiments from three independent FACS sorting) (Source data are provided as a source data file). Asterisk (*) denotes degradation of Krt8. GAPDH was used as a loading control. **e-g** immunofluorescences with various antibodies on organoids at passage 1 derived from FACS-sorted anal canal, TZ, and rectum cells showing that the molecular characteristics of the tissue of origin are maintained in culture organoids derived from the three cell populations. Anal canal and TZ organoids express the stratified-specific marker Krt14 (white), lower level of EpCam (red) compared to the rectum ($n = 4$ independent experiments from four biologically independent samples) (**e**), Anal canal organoids express Gpc3 ($n = 3$ independent experiments from three independent organoids) (**f**), whereas TZ organoids express high level of Krt17 expression (white) but no Krt8 (red) ($n = 3$ independent experiments from three independent organoids) (**g**). Images have been taken at the same exposure time and with the same laser intensity for each antibody for comparison. **h** Clonogenicity assay shows that anal canal-derived organoids have limited clonogenic property, whereas TZ and rectum-derived organoids survived 15 or plus passages ($n = 3$). Each triangle represents a single organoid. Red and green triangles respectively mean no growth and growth. PO = No passage, P1 = passage 1. P2 = passage 2 etc... **i** Immunostainings of differentiation markers Krt10 and loricrin (white) (respectively $n = 4$ and $n = 3$ independent experiments from three independent organoids) in TZ-derived organoid. $\alpha 6$ -integrin (red) denotes the basal layer. TZ organoids can give rise to anal canal epithelial cells that express specifically Gpc3 (white) ($n = 3$ independent experiments from three independent organoids). Arrows show positive staining for Gpc3. Scale bars are 50 μ m in **a**, **b**, **e**, **f**, **h**, and **i**. Insets for anal canal and rectum organoids are zoom in 3-fold and TZ organoid is zoom in 2-fold in **b**, 3-fold in **e**, 4-fold in **g**, 6-fold in **i**.

and anal canal organoids can be seen in contrast to a single layer of columnar cells in the glandular rectal organoid, molecularly by qPCR (Fig. 3c), Western blot (Fig. 3d), and immunofluorescence (Fig. 3e–g). The level of protein expression seen in the tissue is maintained in each organoid population such as EpCam^{low}/Krt14⁺ in anal canal and TZ (Fig. 3e), Gpc3 in anal canal (Fig. 3f), EpCam^{High}/Krt8⁺ in rectum (Fig. 3e–g) and Krt17^{high} in TZ organoid only (Fig. 3d, g). However, after subcloning and serial passages (Fig. 3h and Supplementary Fig. 6b), only the TZ organoids and not the anal canal can be maintained unlimited

time in culture (15 passages and plus which correspond to 131 days) demonstrating their ability to self-renew and validate their stem cell potential (Fig. 3h). As expected, rectum organoids can also be maintained unlimited time in culture (five passages and plus) as stem cells may reside in crypt similar than in the colon²⁴. Because not all TZ organoid clones were successfully clonogenic, we tested if we could enrich for a basal TZ subpopulation of cells by FACS-sorting cells based on Nectin4 expression (Supplementary Fig. 6c), as we previously showed their expression specifically in suprabasal layers of TZ (Fig. 2e, f).

Two populations were FACS-sorted; basal Nectin4[−] TZ cells and suprabasal Nectin4⁺ TZ cells (Supplementary Fig. 6c, d). Among these populations, only basal TZ population was able to be maintained for an unlimited time in culture compared to suprabasal TZ cells showing that only a small fraction of basal TZ displays stem cells properties (Supplementary Fig. 6d). The stem cell potential of the anal TZ is further confirmed by the expression of the differentiated markers Krt10 and loricrin expressed in the TZ-derived organoids (Fig. 3i), and the anal canal marker Gpc3 also found in some regions of the TZ organoid (Fig. 3i) showing the multilineage potential of the Krt17⁺ cells as previously demonstrated in vivo (Fig. 1f).

In silico approach reveals anal TZ differentiation path. Next, we have used computational models to predict the hypothetical trajectory or pseudotime²⁵ that could stand from our single cell mRNA sequencing datasets. We have examined the differentiation trajectory that could exist between the anal TZ clusters, the anal canal cluster and the rectum cluster. Differentiation trajectory reconstruction on the four remaining clusters using the slingshot R package^{26,27} suggests three trajectories (Fig. 4a). However, only two trajectories suggest a differentiation trajectory. This is illustrated by pseudotime values, which contain information about ranking and distance of every cell within a given trajectory (Fig. 4b). As shown, Trajectory 1, which suggests a differentiation progression from the anal TZ basal cells to the anal canal (Fig. 4c), displays the longest distribution of pseudotime values, spanning more clusters and cells (Fig. 4b). Trajectory 2, which describes a hierarchical relationship between the anal TZ basal cells and the anal TZ suprabasal (Fig. 4c), shows also a wide range of pseudotime values, in contrast to trajectory 3 (rectum) in which all values are concentrated in a shorter range (Fig. 4b). This result indicates that trajectory 3 is essentially one cluster of relatively homogeneous cells, which doesn't suggest a differentiation trajectory. Altogether, the scRNA seq analysis supports our in vivo lineage tracing data and our in vitro organoid assay showing that, during normal homeostasis, anal TZ cells maintain the stratified squamous epithelium by giving rise to suprabasal TZ cells and anal canal population (Figs. 1 and 3h–i).

Injured Krt17⁺ TZ cells display a phenotypic plasticity. Another essential feature attributed to stem cells in vivo is their ability to repair injured tissue^{28,29}. To test if the anorectal TZ cells were capable of epithelial reconstitution in vivo and investigate their potential plasticity, we lineage-traced TZ Krt17⁺ GFP⁺ cells after removal of adjacent rectal glandular epithelium (Fig. 5a, b). Four weeks is generally sufficient for the glandular epithelium to be repaired³⁰. We therefore analysed the contribution of the GFP⁺-derived anal TZ cells to the repairing glandular epithelium at the beginning, and at the end of the healing phase (1 and 4 weeks of post-wound respectively). Interestingly we found that at 1 week of post-wound, few GFP⁺ derived anal TZ cells, continuous to the TZ, are found in a transition state by co-expressing the Krt17 and the Krt8 proteins (Fig. 5c, d) in three mice over five analysed. In contrast, at 4 weeks of post-wound we detected GFP⁺ rectal crypt derived from anal Krt17⁺ TZ cells in eight mice over 13 analysed (Fig. 5c, d). No GFP⁺ crypts were found in oil injected mice 4 weeks of post-EDTA wound. At least 100 slides with 9 µm-thick sections were screened for each mouse ($n = 4$) (Fig. 5c). These newly formed crypts expressed Krt8 but not Krt17 (Fig. 5c) and contain differentiated cell types, such as enteroendocrine cells (positive for chromogranin A) and alcian-blue positive-goblet cells specifically found in glandular epithelium demonstrating their ability to give rise to cells from multiple lineages (Fig. 5e). Anal Krt17⁺ TZ cells are therefore multipotent

in response to epithelial injury. The GFP⁺ rectal crypts derived from the Krt17⁺ TZ cells are not found continuous to the TZ such as seen, when colonic stem cells are lineage traced after injury³¹. We postulate that the wound activates two stem cell compartments (the rectal stem cell and the anal TZ) and rectal cells are dominantly responsible for the regeneration. Moreover, staining with EdU at shorter time point (48 h) after the wound (Supplementary Fig. 3b) shows that rectal cells are highly proliferative compared to TZ cells. This suggests that residual rectal epithelial cells, closer to TZ, rapidly expand and could contribute to the distance between anal Krt17⁺ TZ cell tracing and TZ over time. To further confirm TZ cells multipotency, we also challenged TZ cells by performing a second type of injury. *K17CreERT²;R26R^{GFP}* mice were injected twice with tamoxifen to mark TZ cells and anal TZ was mechanically wounded the next day (Supplementary Fig. 7a, b). Similar to EDTA wound, at 1 week post-mechanical wound, few GFP⁺ anal TZ cells, continuous to the TZ, co-expressing Krt17 and Krt8 were found (Supplementary Fig. 7c). Furthermore, GFP⁺ cells were also co-localizing with alcian-blue positive goblet cells confirming their multipotent property (Supplementary Fig. 7c). Together, these findings establish that a minority of anal Krt17⁺ TZ cells, when challenged by removing its direct neighbors, can contribute to rectal repair by their ability to change their fate that allow them to give rise to a different epithelium in response to injury.

To investigate dynamics of Krt17⁺ cells in regeneration, we performed single cell analysis upon injury (Fig. 6a and Supplementary Fig. 8). *K17CreERT²;R26R^{GFP}* mice were injected twice with tamoxifen and subjected to EDTA wound the next day (Fig. 5a, b). At 1 week of post-EDTA wound, cells were sorted following the established FACS strategy based on Epcam expression, which was maintained (Supplementary Fig. 8a, b). After single-cell RNA sequencing, we obtained ten clusters (Supplementary Fig. 8c) including hair follicles, fibroblasts, and anal glands clusters, which were further removed as previously done (Supplementary Fig. 5) to focus on anorectal cells. After removal of these three clusters (Supplementary Fig. 8c, d), seven clusters were identified (Fig. 6a). Two clusters with stratified epithelial cells enriched with wound/regeneration genes, such as *IL-33* were found (Supplementary Fig. 8e). One cluster enriched for differentiation markers such as *Krt10* was identified as anal canal/TZ suprabasal cluster (Supplementary Fig. 8e). Two clusters enriched for rectum specific genes were found such as *Muc13* and *Krt8* (Fig. 6). Transition zone cells were identified in one cluster enriched in previously shown markers, such as *Nectin 4* and *Krt6a* (Supplementary Fig. 8e and Fig. 2g). More interestingly, an additional cluster, absent in unwound analysis (Fig. 2), was identified as “TZ hybrid state” cells. This cluster is enriched for TZ marker *Krt17* and glandular markers *Muc13* and *Krt8*.

Then, pseudotime analysis was performed on the post-wound single cell RNAseq dataset (Fig. 6b). We found three major trajectories representing a hierarchical relationship between TZ cells to anal canal/suprabasal cells and wounded epithelial cells. The third trajectory stands for TZ cells transitioning to the “TZ hybrid state” to finally go towards the rectum which support our previous data, where TZ cells displayed multipotency when subjected to injury (Fig. 5). In contrast to the normal condition (Fig. 4), the rectal trajectory in the wounded tissue (pseudotime 3 Fig. 6b) displays a differentiation path. Although pseudotime values are somehow concentrated at the bottom, reflecting the homogeneous rectal cell cluster, their distribution is clearly more elongated than the rectal normal trajectory. This has been confirmed by performing an unsupervised pseudotime analysis on a subset of clusters including the TZ hybrid and rectal cells (Fig. 6c). One trajectory was found suggesting a hierarchical relationship between TZ Krt17⁺ cells and Krt8⁺/Muc13⁺ cells.

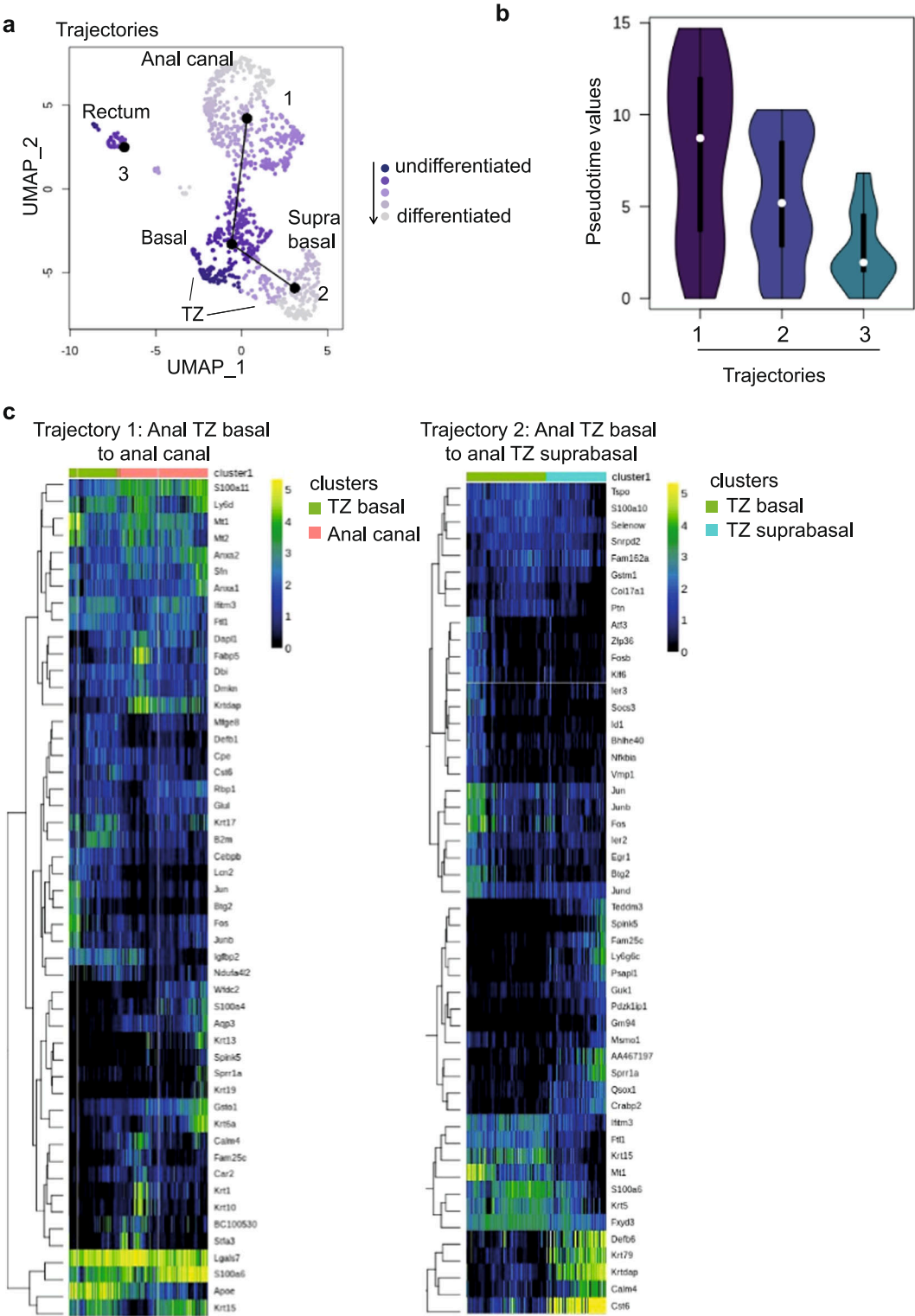
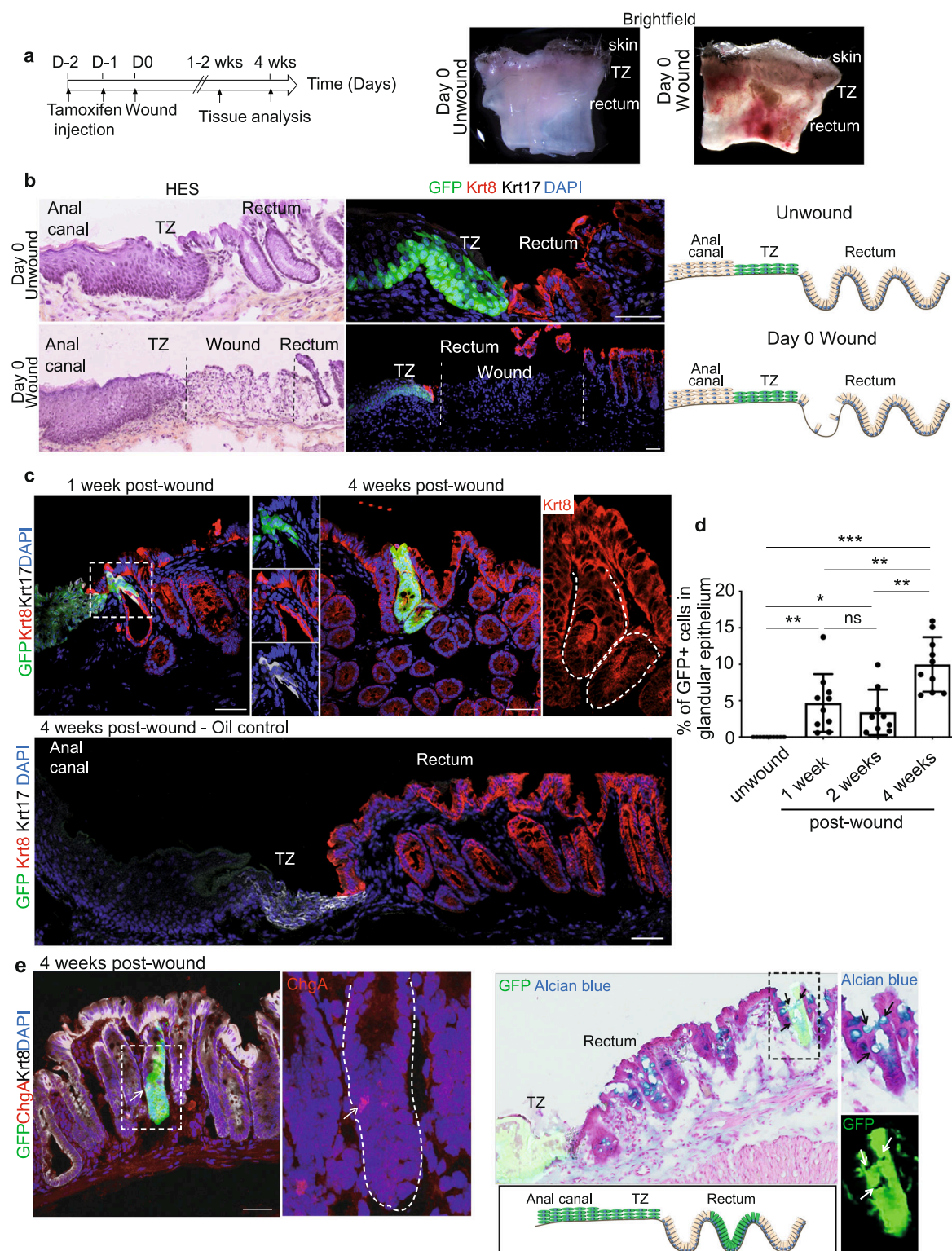


Fig. 4 Pseudotime analysis reveals putative anal TZ differentiation trajectories. **a** Structure of the differentiation trajectory reconstruction using the slingshot R package suggests three trajectories but only two trajectories reflect a differentiation path. Trajectory 1 represents a hierarchical relationship between anal TZ basal cells and anal canal cells and anal TZ basal cells to anal TZ suprabasal cells in trajectory 2. **b** The violin plot shows pseudotime values for all trajectories. The distribution of pseudotime values reflects the heterogeneity of the lineage. If there are more cells, there is a trend to have a longer plot. The round shape of the violin plot from trajectory 3 indicates that this is essentially one cluster and most cells are homogeneous, which do not suggest a differentiation trajectory in contrast to trajectory 1 and 2. **c** Clustering analysis showing the top genes significantly associated with the differentiation paths of trajectories 1 and 2. Heatmaps represent normalized gene expression in logarithmic scale.



JunB is involved in the proper differentiation of anal TZ. We then analyzed pathways enriched in Krt17+ cell clusters and focused on the Jun family as interestingly this pathway has been involved in other epithelial stem cells, such as hair follicle bulge stem cells and is associated with wound response³². First, we have confirmed by immunostaining that the AP-1 transcription factor JunB was enriched at the anal TZ (Fig. 6d, e), but not the anal canal or the rectum confirming the scRNAseq analysis. Moreover,

in a wounded situation we showed that JunB is also expressed in cells participating in both chemical and mechanical wound repair (Fig. 6f and Ext. Data Fig. 7c). We further showed using shRNA in the organoid culture, that JunB is essential for TZ cells ability to differentiate properly. Two shRNA JunB (sh2 and sh3), which have the most efficient JunB downregulation, showed alteration in differentiation markers Krt10 and loricrin by immunofluorescence and western blot analysis on FACS sorted

Fig. 5 Multipotency of anal TZ after a wound injury. **a** Wound strategy in *K17CreER^{T2};R26R^{GFP}* bigenic mice induced with tamoxifen 2 days before injury. Brightfield images at day 0 shows the localization of the wound in the entire tissue. **b** Validation of the removal of the rectal crypt closed to the anal TZ by HES and immunostaining positive for Krt8 (red) ($n = 3$ independent experiments from three mice). **c** At 1 week of post EDTA wound, few TZ-derived GFP+ cells were found in 3/5 mice in the rectum area in a transition state co-expressing the epithelial glandular marker Krt8 (red) and the epithelial TZ marker Krt17 (white). Insets are zoom in 4-fold (left panel) and 2.5-fold (right panel). At 4 weeks post EDTA wound, GFP+ crypt derived from basal Krt17+ anal TZ cells were found in 8/13 mice showing their multipotency. Krt17+ anal TZ cells give rise to Krt8+ glandular cells (inset 2.5-fold zoom). Representative images of $n = 4$ biologically independent samples of oil control injected mice analyzed 4 weeks of post-EDTA wound and stained with Krt17 in white and Krt8 in red. At least 100 slides with 9 μm -thick sections were screened for each mouse and no GFP+ crypts were found. **d** Quantification of the percentage of GFP positive cells, representing the anal TZ Krt17+ derived cells, found in the glandular epithelium at 1week, 2 weeks and 4 weeks post-wound ($n = 3$ mice quantified for each time point). (Source data are provided as a source data file). Two-tailed paired *t*-test; error bars, mean \pm SEM $^*p = 0.0115$, $^{**}p \leq 0.0100$, $^{***}p < 0.0001$. **e** Krt17+ anal TZ cells give rise to differentiated enteroendocrine cells (Chromogranine A+, inset 3-fold zoom) and goblet cells (alcian blue+, inset 2.5-fold zoom) ($n = 3$ independent experiments from three mice). Scale bars are 50 μm .

RFP+ organoids (Fig. 6i, j). These data suggest that JunB may participate into the wound repair by promoting differentiation of the anal TZ cells, which may undergo further plasticity program to give rise to a fully functional glandular cell type.

Discussion

These results of in vivo lineage tracing, 3D organoid culture and in vivo regeneration assays using mouse TZ samples, identified a reservoir of multipotent stem cells for surrounding epithelia that participate to the maintenance of both tissue type. This study has global relevance to stem cell function in many other regenerative tissues. We showed that anorectal TZ cells, which are locally restricted between the stratified squamous epithelium of the anal canal and the simple glandular epithelium of the rectum, contributes to tissue renewal of the anal canal only upon normal homeostasis. Upon injury a minority of anal Krt17+ TZ cells can contribute to rectal repair and give rise to a fully differentiated rectal crypt. This cell fate change during their response to wounding is a common property of many epithelial stem cells in their tissue of origin³³. In contrast to other stem cell niches, transition zones are naturally subjected to mechanical stress and microbiota exposition¹. Thus wounding and healing mechanisms are often activated in the TZ. Here, anal TZ, which have initially squamous-like properties, are able to repair and become a fully differentiated glandular cell-type. This plasticity induced by injury of the surrounding epithelium, may also exist in the progeny of the anal TZ as reported in hair follicle bulge stem cells³⁴ and in the eye limbus TZ following ablation of the stem cell compartment³⁵. One of the existing theories is that different epithelial tissues have their own unique tissue specific stem cells to maintain homeostasis of the tissue from which they are derived³⁶. Instead, here we propose that TZ cells could represent a backup reservoir of stem cells for surrounding epithelium and their phenotypic plasticity seen during wound healing could represent an hallmark of tumor initiation³⁷. In human and mouse, TZ are cancer-prone stem cell niches. Therefore, understanding how these TZ cells participate in driving cancer will be highly relevant for cancer prevention and regression.

Methods

Mice. Mice are housed in a sterile barrier facility as previously described³⁸. The housing conditions of all the mice followed strictly the ethical regulation. Mice are housed in individually ventilated cages (IVC, sealsafe plus TECHNIPLAST) according to SPF FELASA standards and food and water were given at libitum. For social enrichment, six mice per cages are generally housed with sterile nesting materials such as cotton or compressed wood chips for nidification. The room temperature ranged from 20 and 25 °C. The relative ambient humidity was 55% \pm 15. Semi-natural light cycle of 12:12 was used. All experiments were approved by the European and national regulation (ethical committee C2EA14, protocols # 4572, #8287, and #2244) and carried out using standard procedures. Transgenic mouse lines have been previously described: *K17CreER^{T2}*³⁹, *Rosa26-lsl-ZsGreen1* (Jackson laboratories, stock no.007906). We have backcrossed our double

transgenic mouse lines into the C57/BL6J background for six generations. Females and males have been used in all experiments.

Lineage tracing analysis. *K17CreER^{T2}* mice were crossed with *Rosa26-lsl-ZsGreen1* reporter mice, which express the Green Fluorescent protein following Cre excision of a loxP-flanked cassette, to generate *K17CreER^{T2};R26R^{GFP}* bigenic mice (Fig. 1b). To induce GFP expression, *K17CreER^{T2};R26R^{GFP}* mice received daily intraperitoneal injections of 2 mg of tamoxifen (Sigma) or sunflower oil alone (vehicle) for 2 days. Anorectal specimens ($n = 3$ mice per time point) were harvested at the following time after tamoxifen administration: 10 h, 48 h, 3 weeks, and 1 year (Fig. 1c, d). Percentage of GFP+ cells was quantified by analyzing at least ten different areas of anorectal TZ from 19 mice. Total number of cells was counted using DAPI staining in stratified and glandular epithelia. The number of GFP+ cells was counted using Zen software and photoshop CC2019 and the percentage of GFP cells was calculated according to total number of cells (reported as 100%).

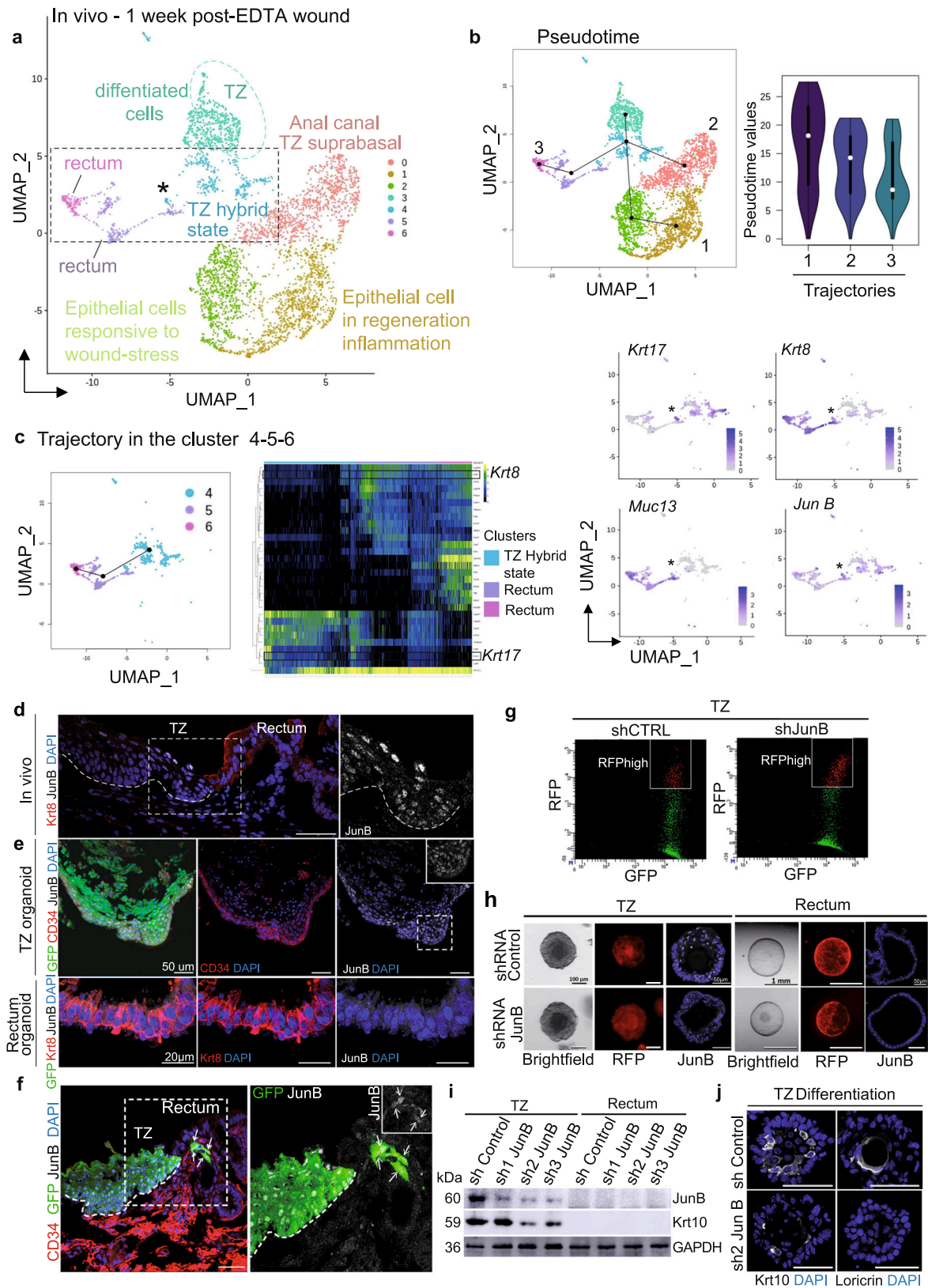
Immunostaining and histology. The anorectal tissue was fixed in 4% paraformaldehyde overnight at 4 °C. The sample was then washed three times in PBS 1 \times and put in sucrose 30% overnight at 4 °C. Lastly, the tissue was put in two volumes of sucrose 30% and one volume of OCT (Tissue-Tek, Sakura, Torrance, CA) for few hours and embedded in OCT compound. For some antibodies, such as Krt6 and nectin-4, the anorectal tissue was fixed in methanol for 30 min at -20 °C instead of the paraformaldehyde and process in 30% sucrose, as previously described. Ten micrometer frozen sections were used to performed immunofluorescence. Briefly, sections were permeabilized in 0.1% Triton X-100 (Euro-medex 2000-B) in PBS 1 \times for 10 min at room temperature and blocked in 2.5% normal goat serum, 2.5% normal donkey serum, 2% gelatin (Sigma G7765), 1% bovine serum albumin, 0.1% Triton X-100 in PBS 1 \times for at least 30 min at room temperature. Whenever mouse antibodies were required, the MOM kit (vector Lab) was used. Primary antibodies were incubated in the blocking solution overnight at 4 °C. After three washes for 10 min in 0.1% Triton X-100 PBS 1 \times , secondary antibodies diluted in the blocking solution containing DAPI (1 $\mu\text{g}/\text{ml}$ Thermo-Scientific 62248) was added for 45 min at room temperature. After three washes for 10 min in 0.1% Triton X-100 PBS 1 \times , slides were mounted in prolong Gold antifade (Invitrogen, P36934). The list of primary and secondary antibodies is in the Supplementary Table 1. Fluorescent images were acquired using a Confocal microscope ZEISS LSM 880. All images were analyzed using ZEN software and Photoshop. Histologies were performed by the IPC/CRCM Experimental Pathology platform (ICEP), and analyzed by two independent pathologists at the Paoli Calmettes Institute.

EdU staining. Mice were injected intraperitoneally with 0.25 mg EdU (Abcam, ab146186) for 4 h and tissue was processed as described in the previous sections. The Click-iT EdU AlexaFluor 647 Imaging kit, (Invitrogen C10640) was used to detect proliferative cells according to the manufacturer instructions.

Oil Red O staining. Slides were dip in 60% isopropanol one time quickly then stained in working Oil Red O solution (30 ml of stock solution mixed with 20 ml of distilled water) for 15 min at RT. Slides were dip in 60% isopropanol one time quickly followed by one quick dip in distilled water. Slides were counterstained with EnVision™ Hematoxylin (SM806 Dako K8008) for 5 min and washed ten times in distilled water. Slides were mounted with Aqueous mounting gel (Aquatex Merck Milipore 1.08532.0050).

Alcian blue staining. OCT sections (9 μm) were stained with Alcian Blue (Biognost AB2-OT-100) according to the manufacturer's instructions and counterstained with nuclear fast red (Merck).

RNAscope fluorescent assays. To detect *Lgr5* and *Krt17* at the mRNA level, OCT sections (9 μm) were prepared on superfrost plus slides and RNAscope highly sensitive probes against *Lgr5* (Cat # 311021-C2; ACD Inc.), and *Krt17* (Cat #479911;



ACD Inc.) were used in the RNAscope fluorescent assay according to the manufacturer's protocol (Catalog Number 320293). Briefly, fixed frozen sections were baked at 60 °C and then post-fixed using 4% paraformaldehyde. Gradient dehydration using 50%, 70 and 100% ethanol was performed and slides were then processed for antigen retrieval followed by pretreatment with protease III, and then incubated with targeting probes for 2 h at 40 °C in a humidity-controlled chamber. Finally, AMP signal amplification followed by RNAscope Amp4-AltB(550) was carried out for

fluorescent visualization. A housekeeping gene *POLR2A* was used as a positive control to ensure the RNA quality of the tissue, in addition, a negative control probe targeting bacterial *DapB* was used to assess nonspecific background labeling.

Human samples. Anorectal tissue samples from adult patients were approved by the Paoli-Calmettes Institute Strategic Orientation Committee (authorization

Fig. 6 Post-wound single cell RNA sequencing reveals a TZ population enriched in the transcription factor JunB. **a** Main cell populations visualized on UMAP from scRNA-seq of anal epithelial cells 1 week of post-EDTA wound **b** Structure of the differentiation trajectory reconstruction using the slingshot R package suggests three trajectories. Pseudotime values show an elongated distribution on each trajectory suggesting that there are more intermediate phenotypes and therefore a differentiation process. **c** Hierarchical relationship between clusters 4, 5, and 6 and expression of key genes expressed in TZ hybrid state cells. **d** In tissue, JunB (white) is specifically expressed by transition zone cells and is absent in Krt8 (red) glandular epithelium ($n = 3$ independent experiments from three mice). **e** Similar to in vivo, CD34 (red) and JunB (white) expressions are specific to TZ-derived organoids but not organoids from the rectum ($n = 3$ independent experiments from three TZ and rectum organoids). **f** One week of post-EDTA wound, few GFP+ (green) cells participating in the regenerative crypt are JunB+ (white) ($n = 3$ independent experiments from three mice). Insets are zoom in 1.7-fold. **g** TZ organoids infected with control shRNA-RFP and shJunB-RFP were FACS-sorted based on double expression of GFP and RFP ($n = 3$ independent FACS from three independent samples). **h** Brightfield and RFP images of TZ and rectum organoids infected with control shRNA or shJunB (red). JunB staining (white) revealed downregulation in TZ organoids infected with shJunB compared to control shRNA. Rectum organoids were used as negative control ($n = 4$ independent experiments from four independent samples). **i, j** JunB knockdown impairs TZ cells differentiation properties. **i** Western Blot analysis showing JunB downregulation in TZ organoids infected with sh2 and sh3 JunB compared to control shRNA and sh1JunB infections ($n = 6$ independent experiments from six biologically independent samples). Differentiation marker Krt10 expression is decreased following JunB downregulation in organoids infected with sh2 and sh3 JunB ($n = 2$ independent experiments from two biologically independent samples). GAPDH was used as a loading control. (Source data are provided as a source data file). **j** Immunofluorescence confirms the downregulation of Krt10 in sh2 and sh3 JunB organoids ($n = 5$ independent experiments from 5 independent samples). The defect in differentiation is also detected using antibody against Loricrin ($n = 5$ independent experiments from five independent samples). Scale bars are 50 μm (**d, e**) (TZ organoid) (**f, j**), and 20 μm (**e**) (TZ rectum).

TZ-cancers-IPC 2015-021). Informed written consent was given by the patients. Samples came from discarded tissues after surgery.

Isolation and purification of anorectal epithelial cells by flow cytometry. The anorectal regions of at least five *K17CreER^{T2};R26R^{GFP}* mice induced with tamoxifen for 2 days were microdissected under a dissecting scope (Leica MZ6), and pooled in epithelial cell culture medium⁴⁰ containing 10% fetal bovine serum (FBS) for further dissociation. Tissues were cut in small pieces using scissor and scalpel in 4 ml HBSS 1 \times + 50 μl collagenase 20% from *Clostridium histolyticum* (Sigma C2674) and were incubated with high agitation 45 min at 37 °C. Then, 4.2 μl of DNase I (10 mg/ml Sigma DN25) were added followed by 10 min incubation at 37 °C under agitation. Samples were then resuspended with 12 ml cold PBS 1 \times and placed in a 50 ml conical tube filled until 50 ml with PBS 1 \times and centrifuged for 10 min at 4 °C at 200 \times g. Pellets were resuspended with 20 ml cold PBS 1 \times and filtered through 70 μm filter. To avoid cell death, 200 μl of FBS was added. To dissociate left over tissues on the filter, 1 ml of TrypLE express enzyme (GibcoTM, 12605010) was added followed by 5 min incubation at 37 °C. Trypsin activity was then stopped by adding 3 ml of epithelial cell culture medium +10% FBS and the mix was filtered through 40 μm filter and centrifuged 10 min at 4 °C at 300 \times g. Pellets were resuspended in PBS 1 \times +2%FBS. Primary antibody was added to samples 30–45 min on ice and covered with foil. Samples were then washed with PBS 1 \times +2% FBS and centrifuged 5 min at 4 °C at 300 \times g. After discarding the supernatant, secondary antibody was added for 20 min at 4 °C and then washed again with PBS 2% FBS. Finally, FVD780 (1/1000, Thermofisher) was added to stain dying cells. Cell sorting was performed using a FACS Aria II equipment (BD Bioscience) and FACS diva software.

Organoid culture. After FACS isolation, 4000–10,000 cells were cultured in 25 μl Matrigel (Corning, 356231) on 48-well plate. Three hundred microliter of medium (Supplemental Table 2) supplemented with 10 μM Y-27632 (only first 5 days to avoid anoikis) were added to wells and the plate was incubated at 37 °C, 5% CO₂. The medium was changed every 3–4 days. Upon outgrowth, organoids were passaged every 10–15 days either by mechanical dissociation by gentle pipetting or by enzymatic dissociation with TrypLE express enzyme (GibcoTM, 12605010). Medium was supplemented with 10 μM Y-27632 the first 3 days.

Imaging organoids. Brightfield images, GFP and RFP expressions were monitored using the Leica M205 FA stereomicroscope.

Embedding for histology. Organoids were washed with PBS and incubated for 30 min at 37 °C with 300 μl of low melting agarose 2% (Promega, V2111). Polymerized agarose was transferred to a 1.5 ml Eppendorf and fixed in 4% paraformaldehyde overnight at 4 °C under agitation. The sample was then washed three times in PBS 1 \times and put in PBS sucrose 30% overnight at 4 °C. Finally, organoids were incubated with gelatin 7.5%/sucrose 15% in PBS at 37 °C for at least 30 min and put in mold to freeze at –80 °C.

Clonogenicity assay. Organoids were washed with PBS and incubated for 5 min at 37 °C with 200 μl of medium (Supplemental Table 2) + 1 μl collagenase 20% from *Clostridium histolyticum* (Sigma C2674) to dissociate matrigel. Under the stereomicroscope (Leica M205 FA), for each passage, at least three organoids of around 150 μm were isolated for anal canal and TZ and 540 μm for rectum. The size difference corresponds to the fact that stratified organoids (anal canal and TZ)

contain more cells overall than simple glandular epithelium organoids (rectum). Each organoid was dissociated for 5 min at 37 °C with 20 μl of TrypLE express enzyme (GibcoTM, 12605010) and after washing, replated in 25 μl of matrigel. Three hundred microliter of medium (Supplemental Table 2) supplemented with 10 μM Y-27632 (only the first 5 days to avoid anoikis) were added to wells and the plate was incubated at 37 °C, 5% CO₂.

In vitro tamoxifen assay. Anal canal cells were sorted by previously established FACS strategy, cultured in 25 μl Matrigel (Corning, 356231) on 48-well plate and incubated at 37 °C, 5% CO₂. At passage 1, culture media was supplemented with oil control or tamoxifen (0.1 μM) in culture media during 7 days and the medium was changed three times every 2 days. As a positive control, we sorted TZ cells based on Epcam expression from *K17CreER^{T2};R26R^{GFP}* bigenic mice non-induced with tamoxifen, and we added the tamoxifen in culture media similarly to the anal canal.

Lentiviral infection of organoids with ShRNA JunB. Vector control (SMARTvector Non-Targeting Mcmv-TurboRFP control particles #S08-005000-01) and sh JunB 1,2,3 vectors (sh1 JunB #V3SM7592-234927818, Sh2 JunB #V3SM7592-236055786 and sh3 JunB #V3SM7592-237743179) were produced by Horizon. 2.5×10^6 viral particles were combined with 2 μg of polybrene (Sigma TR1003-G) and incubated 10 min at room temperature in organoid culture medium. 2×10^4 dissociated organoids cells were then added to virus and polybrene solution and incubated 10 min at room temperature. Twenty-five microliter of Matrigel (Corning ref 356231) were added to the mix and 25 μl of the suspension were dispensed into the center of each well of a 48-well plate. After 10 min, 300 μl of medium containing Y-27632 was added. Twenty-four hours after infection organoids were washed by adding 10 ml of basal medium and centrifuged as previously described. The pellet was suspended with Matrigel and suspension was dispensed in wells as previously described. Y-27632 was added to the medium the first 3 days.

Western blot. Organoids were lysed with lysis buffer (50 mM Tris, pH7.2; 350 mM NaCl; 1% Triton X-100; 0.5% Na deoxycholate; 0.1% SDS; 20 mM MgCl₂ and Inhibitor Cocktail) and proteins were separated by NuPAGE 4–12% Bis-Tris 1.0 mm mini protein gel, transferred to nitrocellulose membranes and blocked for 1 h with 5% non-fat milk or 5% BSA in TBS 1 \times (Tris Buffer Saline: 1 M Tris pH 7.4–7.5; 5 M NaCl) depending of the primary antibody. Membranes were subjected to immunoblotting using antibodies against the following proteins at the indicated dilutions: GAPDH (1/5000), Krt17 (1/20000), Krt8 (1/4000), Krt10 (1/500) in 5% non-fat milk and Jun B (1/2000) in 5% BSA. See Supplemental Table 1 for complete reference list of the antibodies used. Full scan blots are provided in the Supplementary information. Membranes were then washed three times with TBS 0.1% Tween for 10 min. Fluorescent secondary antibodies or HRP-coupled secondary antibodies listed in the supplementary Table 1 were used at 1/1000 in 5% non-fat milk or 5% BSA. Fluorescent images were acquired using Biorad Chemidoc imager and HRP immunoblots were developed using standard ECL Prime (Amersham, RPN 2236).

Real-time PCR. Total RNA was isolated, using a Qiagen Rneasy Micro Kit, and used to produce cDNA using the Maxima first strand cDNA synthesis kit. Reverse transcription reactions were diluted to 10 ng/ μl and 1–2 μl of cDNA was used to perform Real time PCR using the CFX96 real-time PCR System, CFX Manager Software and the Ssofast EvaGreen Supermix reagent. All reactions were run in triplicate and analyzed using the $\Delta\Delta\text{CT}$ method with relative expression normalized to *GAPDH*. (See Supplemental Table 3 for all primer sequences).

Single cells RNA sequencing. After tissue dissection and dissociation, FACS purified suspended cells were partitioned into nanoliter-scale Gel Bead-In-Emulsions (GEMs) with the Chromium Single Cell Controller (10× Genomics) (performed by HailioDx company and TGMML Marseille Luminy platform). After cell encapsulation and barcoding, library preparation followed the standard scRNAseq protocol comprising reverse transcription, amplification, and indexing (10× Genomics). Sequencing was performed using a NextSeq Illumina device (Illumina). Illumina bcl files were basecalled, demultiplexed and aligned to the mouse mm10 genome using the cellranger software (version 3.1.0, 10× Genomics). All downstream analyses were done with R/Bioconductor packages, R version 4.0.3 (2020-10-10) [<https://cran.r-project.org/>; <http://www.bioconductor.org/>]. Raw counts were imported into R and single cell data was analyzed with the ‘Seurat’ package v.3.2.2²¹. After filtering for library size (between 200 and 5000 features per cell) and mitochondrial gene expression (less than 25%), pre-processing was performed using Seurat functions for counts normalization (NormalizeData using the LogNormalize method), scaling (ScaleData using the 2000 most variable features), dimension reduction with principal component analysis (PCA) (RunPCA with default parameters), construction of a shared nearest neighbor (SNN) graph (FindNeighbors using ten dimensions of reduction as input) and clustering (FindClusters with a resolution of 0.2). Data was adjusted for cell cycle using the CellCycleScoring function and regressing for S and G2/M phases scores. After visualization with Uniform Manifold Approximation and Projection (UMAP) dimensional reduction technique [<https://arxiv.org/abs/1802.03426>], contaminating cell types were filtered out (i.e., anal glands, hair follicle, and fibroblasts) followed by re-scaling of each dataset. An additional filtering based on the expression of *Lgr5*, *Lhx2*, *Tbx1*, was necessary in the normal sample to remove hair follicle cells that were contaminating the basal cluster. After filtering of bad quality and contaminating cells, 939 cells from the normal sample and 4147 cells from the wounded sample were used for all downstream analyses. Markers of each cluster were identified using the wilcox test option of the FindAllMarkers function, with a bonferroni *p* value adjustment. The same criteria for filtering, dimension reduction, clustering, visualization, adjusting for cell cycle, and pseudotime were used to analyze the normal and the wounded sample. Cell-filtering parameters are nFeature_RNA > 200, nFeature_RNA < 5000, percent.mt < 25%. Other parameters included ScaleData (x, vars.to.regress = c(“S.Score”, “G2M.Score”)), RunPCA(x) # default parameters, FindNeighbors(dims = 1:10), FindClusters(resolution = 0.2), RunUMAP(dims = 1:10).

Pseudotime analysis. We used the dynverse R package to compare across pseudotime algorithms and choose the one best suited for our dataset²⁷. Final trajectory (pseudotime) analyses were performed using the slingshot R package²⁶. To this end, clustering information was extracted from Seurat objects and passed directly to slingshot’s main function, using the “Basal” cell cluster as the starting cluster. The same “granularity” parameters (i.e., Omega = 20) were used for both conditions, normal and wounded, to assure comparability. Once pseudotime trajectories were identified, a general additive model (GAM) was fitted to identify genes, whose expression was significantly associated to each trajectory.

Rectal wound

Chemical wound. To remove rectal crypts close to the anorectal TZ we treated the anorectal region with hot EDTA followed by a mechanical wound as previously described⁴¹ using 2–4 months old *K17CreERT2*; *R26R^{GFP}* bigenic mice injected with tamoxifen 2 days before the wound (for lineage tracing experiments). Briefly, under isoflurane anesthesia, a thin catheter equipped with a small balloon, was inserted into the anus and 200 µl of hot (50 °C) fresh 0.25 M EDTA/PBS was added using a syringe and a thin catheter. After 2 min of exposure, one wash with PBS was done and the balloon was deflated and catheters removed. Epithelial wound was performed using an electric brush closed to the anorectal TZ for approximately 1 min, and removal of the rectum crypts confirmed under a dissecting microscope. Mice were monitored carefully after the injury and analyzed 2 weeks and 4 weeks of post-wound.

Mechanical wound. Under isoflurane anesthesia, 2–4-months-old *K17CreERT2*; *R26R^{GFP}* bigenic mice injected with tamoxifen 2 days before the wound, were subjected to a mechanical wound using a sterile scalpel (InterFocus #10073-14) inserted into the anus. The glandular region close to the anal transition zone was scraped with the scalpel to create the wound. Mice were monitored carefully after the injury and analyzed 1 week of post-wound.

All mice were injected subcutaneously with 50 µl of METACAM (1 mg/kg) before every wounding experiment.

Quantifications. Krt17 protein expression was evaluated for each region (anal canal, TZ, and rectum). At least eight areas have been quantified per regions and per mice (*n* = 3 mice per condition). Immunostainings were performed the same day with the same antibody solution and identical imaging settings were applied, when comparing different conditions. Images were acquired with a Confocal microscope ZEISS LSM 880 and were analyzed with ImageJ. A threshold was applied to all images to remove the background before measuring the integrated density, while keeping the same ROI for each images (see Supplemental methods

for details). For EdU quantification, eight areas per mice and per region were manually counted using Zen software and photoshop CC2019. Krt17 expression was used to separate TZ from anal canal and rectum. At least eight different areas of TZ and anal canal and 16 different crypts from nine mice were quantified (*n* = 3 per condition). Percentage of EdU+ cells was calculated according to total number of DAPI cells (reported as 100%). CD34 fraction was quantified manually and the percentage of CD34 was calculated according to total number of DAPI cells (reported as 100%). Quantification on EdU+ cells within the CD34+ population was quantified manually, and the percentage of EdU was calculated according to total number of CD34+ cells (reported as 100%).

Reporting summary. Further information on research design is available in the Nature Research Reporting Summary linked to this article.

Data availability

All the raw scRNA sequencing data have been deposited in the Gene Expression Omnibus under Series GSE163394 (Accession # GSM4982239 and GSM4982240) Source data are provided with this paper.

Received: 9 March 2020; Accepted: 11 April 2021;

Published online: 12 May 2021

References

- McNairn, A. & Guasch, G. Epithelial transition zones: merging microenvironments, niches, and cellular transformation. *Eur. J. Derm.* **21**, 21–28 (2011).
- Guasch, G. et al. Loss of TGFβ signaling destabilizes homeostasis and promotes squamous cell carcinomas in stratified epithelia. *Cancer Cell* **12**, 313–327 (2007).
- Fluhmann, C. F. Carcinoma in situ and the transitional zone of the cervix uteri. *Obstet. Gynecol.* **16**, 424–437 (1960).
- Deans, G. T., McAleer, J. J. & Spence, R. A. Malignant anal tumours. *Br. J. Surg.* **81**, 500–508 (1994).
- Waring, G. O. 3rd, Roth, A. M. & Ekins, M. B. Clinical and pathologic description of 17 cases of corneal intraepithelial neoplasia. *Am. J. Ophthalmol.* **97**, 547–559 (1984).
- Shannon, B. A., McNeal, J. E. & Cohen, R. J. Transition zone carcinoma of the prostate gland: a common indolent tumour type that occasionally manifests aggressive behaviour. *Pathology* **35**, 467–471 (2003).
- Bleuming, S. A. et al. Bone morphogenetic protein signaling suppresses tumorigenesis at gastric epithelial transition zones in mice. *Cancer Res.* **67**, 8149–8155 (2007).
- Nam, K. T. et al. Gastric tumor development in Smad3-deficient mice initiates from forestomach/glandular transition zone along the lesser curvature. *Lab Invest.* **92**, 883–895 (2012).
- Wang, X. et al. Residual embryonic cells as precursors of a Barrett’s-like metaplasia. *Cell* **145**, 1023–1035 (2011).
- Runk, L. A. et al. Defining the molecular pathologies in cloaca malformation: similarities between mouse and human. *Dis. Model Mech.* **7**, 483–493 (2014).
- Runk, L. A., Kramer, M., Ciralo, G., Lewis, A. G. & Guasch, G. Identification of epithelial label-retaining cells at the transition between the anal canal and the rectum in mice. *Cell Cycle* **9**, 3039–3045 (2010).
- Cotsarelis, G., Cheng, S. Z., Dong, G., Sun, T. T. & Lavker, R. M. Existence of slow-cycling limbal epithelial basal cells that can be preferentially stimulated to proliferate: implications on epithelial stem cells. *Cell* **57**, 201–209 (1989).
- Flesken-Nikitin, A. et al. Ovarian surface epithelium at the junction area contains a cancer-prone stem cell niche. *Nature* **495**, 241–245 (2013).
- Jiang, M. et al. Transitional basal cells at the squamous-columnar junction generate Barrett’s oesophagus. *Nature* **550**, 529–533 (2017).
- Moon, H., Zhu, J., Donahue, L. R., Choi, E. & White, A. C. Krt5+ / Krt15+ foregut basal progenitors give rise to cyclooxygenase-2-dependent tumours in response to gastric acid stress. *Nat. Commun.* **10**, 2225 (2019).
- Herfs, M. et al. A discrete population of squamocolumnar junction cells implicated in the pathogenesis of cervical cancer. *PNAS* **109**, 10516–10521 (2012).
- Yamamoto, Y. et al. Mutational spectrum of Barrett’s stem cells suggests paths to initiation of a precancerous lesion. *Nat. Commun.* **7**, 10380 (2016).
- Depianto, D., Kerns, M. L., Dlugosz, A. A. & Coulombe, P. A. Keratin 17 promotes epithelial proliferation and tumor growth by polarizing the immune response in skin. *Nat. Genet.* **42**, 910–914 (2010).
- Blanpain, C. & Simons, B. D. Unravelling stem cell dynamics by lineage tracing. *Nat. Rev. Mol. Cell Biol.* **14**, 489–502 (2013).
- Wagner, A., Regev, A. & Yosef, N. Revealing the vectors of cellular identity with single-cell genomics. *Nat. Biotechnol.* **34**, 1145–1160 (2016).

21. Stuart, T. et al. Integration of single-cell data. *Cell* **177**, 1888–1902 (2019).
22. Tudorita Tumber, G. G. et al. Defining the epithelial stem cell niche in skin. *Science* **303**, 5 (2004).
23. Fabre, S. et al. Prominent role of the Ig-like V domain in trans-interactions of nectins. Nectin3 and nectin 4 bind to the predicted C'-C"-D beta-strands of the nectin1 V domain. *J. Biol. Chem.* **277**, 27006–27013 (2002).
24. Barker, N. et al. Identification of stem cells in small intestine and colon by marker gene Lgr5. *Nature* **449**, 1003–1008 (2007).
25. Chloé, S. & Baron, A. v. O. Unravelling cellular relationships during development and regeneration using genetic lineage tracing. *Nat. Rev. Mol. Cell Biol.* **20**, 753–765 (2019).
26. Street, K. et al. Slingshot: cell lineage and pseudotime inference for single-cell transcriptomics. *BMC Genomics* **19**, 477 (2018).
27. Saelens, W., Cannoodt, R., Todorov, H. & Saeys, Y. A comparison of single-cell trajectory inference methods. *Nat. Biotechnol.* **37**, 547–554 (2019).
28. Lu, C. P. et al. Identification of stem cell populations in sweat glands and ducts reveals roles in homeostasis and wound repair. *Cell* **150**, 136–150 (2012).
29. Blanpain, C. & Fuchs, E. Stem cell plasticity. Plasticity of epithelial stem cells in tissue regeneration. *Science* **344**, 1242281 (2014).
30. Fukuda, M. et al. Small intestinal stem cell identity is maintained with functional Paneth cells in heterotopically grafted epithelium onto the colon. *Genes Dev.* **28**, 1752–1757 (2014).
31. Ishibashi, F. et al. Contribution of ATOH1+ cells to the homeostasis, repair, and tumorigenesis of the colonic epithelium. *Stem Cell Rep.* **10**, 27–42 (2018).
32. Singh, K. & Camera, E. JunB defines functional and structural integrity of the epidermo-pilosebaceous unit in the skin. *Nat. Commun.* **9**, 3425 (2018).
33. Watt, G. Da. F. M. Stem cell heterogeneity and plasticity in epithelia. *Cell Stem Cell* **16**, 465–476 (2015).
34. Rompolas, P., Mesa, K. R. & Greco, V. Spatial organization within a niche as a determinant of stem-cell fate. *Nature* **502**, 513–518 (2013).
35. Nasser, W. et al. Corneal-committed cells restore the stem cell pool and tissue boundary following injury. *Cell Rep.* **22**, 323–331 (2018).
36. Visvader, J. E. & Clevers, H. Tissue-specific designs of stem cell hierarchies. *Nat. Cell Biol.* **18**, 349–355 (2016).
37. Gupta, P. B. et al. Phenotypic plasticity: driver of cancer initiation, progression, and therapy resistance *Cell Stem Cell* **24**, 65–78 (2019).
38. McCauley, H., Chevrier, V., Birnbaum, D. & Guasch, G. De-repression of ELMO1 in cancer stem cells drives progression of TGFβ-deficient squamous cell carcinoma from transition zones. *ELife* **6**, e22914 (2017).
39. Doucet, Y., Woo, S. H., Ruiz, M. E. & Owens, D. M. The Touch Dome defines an epidermal niche specialized for mechanosensory signaling. *Cell Rep.* **6**, 1759–1765 (2013).
40. Nowak, J. & Fuchs, E. Isolation and culture of epithelial stem cells. *Methods Mol. Bio* **482**, 215–232 (2009).
41. Sugimoto, S. et al. Reconstruction of the human colon epithelium in vivo. *Cell Stem Cell* **22**, 171–176 (2018).

Acknowledgements

Processing of the slides for histology was performed by Emilie Agavvian in the experimental histopathology (ICEP) core facility at the Institut Paoli Calmettes. All organoid cultures were done in the 3D-Hub-O platform at CRCM. We thank Manon Richaud and Françoise Mallet in the Flow cytometry facility, Daniel Isnardon and Magda Rodriguez (especially for the RNAscope quantification) in the microscopic core facility at the CRCM, Charlyne Gard for the scRNA seq experiment at Aix Marseille Univ, INSERM, TAGC, TGML, Marseille, France. Ghislain Bidaut in the Cibi platform for the initial

scRNAseq analysis, David Owens for the K17CreERT2 mouse lines and Marc Lopez for the anti-nectin-4 monoclonal antibody. Jean-Christophe Orsoni and Arnaud Capel in the mouse facility at the CRCM. Samuel Granjeaud for helping with statistics. This study was supported by ANR grant #ANR20-CE13-0009-01 (G.G.) and ANR-10-INBS-0009-10 (platform TAGC), partly supported by research funding from the Canceropôle Provence-Alpes-Côte d'Azur, Institut National du Cancer and Région Sud, grants from the Excellence Initiative of Aix-Marseille University A*Midex, "Investissement d'avenir" (CapoStromEx) and Inserm Plan Cancer AAP single cell (G.G. and H.H.V.). L.M. is a recipient of the French ministerial research fellowship and the Ligue National Contre le Cancer fellowship.

Author contributions

L.M. designed and performed all the experiments, analyzed the data, did all the quantifications and wrote the manuscript. V.C. performed some cryosectioning, immunostainings, wounding, shRNA experiments, western blot and analyzed the data. G.G. designed experiments, analyzed the data and wrote the manuscript. H.H.V. performed all the bioinformatics single cell analysis. A.O. performed cryosectioning, immunostainings and mouse genetics. Z.H. and J.P. performed all RNAscope experiments. F.P. and C.B.-C. provided human anal samples and histological analysis. E.C.J. provided histological analysis. C.G. assisted with gene ontology analysis and analyzed the data.

Competing interests

The authors declare no competing interests.

Additional information

Supplementary information The online version contains supplementary material available at <https://doi.org/10.1038/s41467-021-23034-x>.

Correspondence and requests for materials should be addressed to G.G.

Peer review information *Nature Communications* thanks Nick Barker and the other, anonymous, reviewer(s) for their contribution to the peer review of this work. Peer reviewer reports are available.

Reprints and permission information is available at <http://www.nature.com/reprints>

Publisher's note Springer Nature remains neutral with regard to jurisdictional claims in published maps and institutional affiliations.



Open Access This article is licensed under a Creative Commons Attribution 4.0 International License, which permits use, sharing, adaptation, distribution and reproduction in any medium or format, as long as you give appropriate credit to the original author(s) and the source, provide a link to the Creative Commons license, and indicate if changes were made. The images or other third party material in this article are included in the article's Creative Commons license, unless indicated otherwise in a credit line to the material. If material is not included in the article's Creative Commons license and your intended use is not permitted by statutory regulation or exceeds the permitted use, you will need to obtain permission directly from the copyright holder. To view a copy of this license, visit <http://creativecommons.org/licenses/by/4.0/>.

© The Author(s) 2021

Supplementary information

A stem cell population at the anorectal junction maintains homeostasis and participates in tissue regeneration

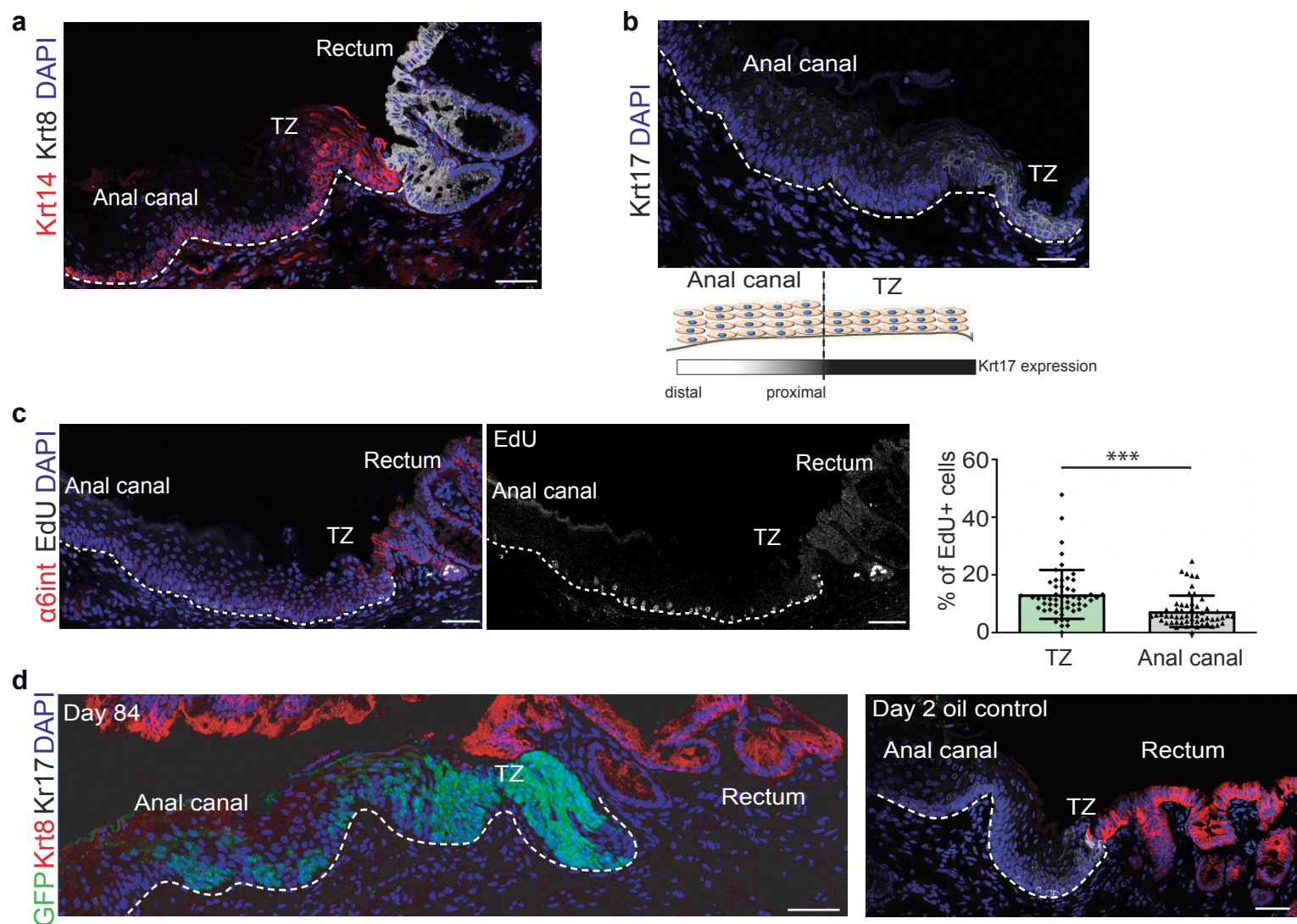
Louciné Mitoyan¹, Véronique Chevrier¹, Hector Hernandez-Vargas^{2,3}, Alexane Ollivier¹, Zeinab Homayed⁴, Julie Pannequin⁴, Flora Poizat⁵, Cécile De Biasi-Cador⁵, Emmanuelle Charafe-Jauffret^{1,5}, Christophe Ginestier¹, and Géraldine Guasch^{1*}

Supplementary Figure 1. Active renewal occurring in the anorectal transition zone.

a. Immunofluorescence staining shows the squamous nature of the anal canal and the TZ expressing the Krt14 (red) and the glandular nature of the rectum expressing the Krt8 (white) (n=4 independent experiments from 4 mice). **b.** Krt17 (white) is strongly expressed at the TZ and weakly in anal canal cells proximal to the TZ. Section is from mouse anorectal day 31 oil control (n=22 independent experiments from 25 mice). **c.** Proliferative cells are detected at the TZ at a higher rate compared to the anal canal. Quantification of the % of Edu positive cells in TZ and anal canal area (Source data are provided as a source data file). Edu+ cells were quantified based on differential CD34 expression found in the TZ compared to the anal canal as previously described^{11,38}. At least 9 different areas were analyzed for TZ and anal canal for each mouse (n=5). Total number of cells was counted using DAPI staining (reported as 100%) in TZ and anal canal. Paired t test two-tailed; error bars, mean \pm SEM ***p<0.0001. Representative image of Edu positive cells (nuclear white staining) at the TZ and in the anal canal area. Source data for the Edu quantification is provided as a Source Data file. **d.** Unipotency of Krt17+ TZ cells (green) during long-term lineage tracing (n=3 mice) (left image) and representative images of n=3 biologically independent samples of oil control injected mice

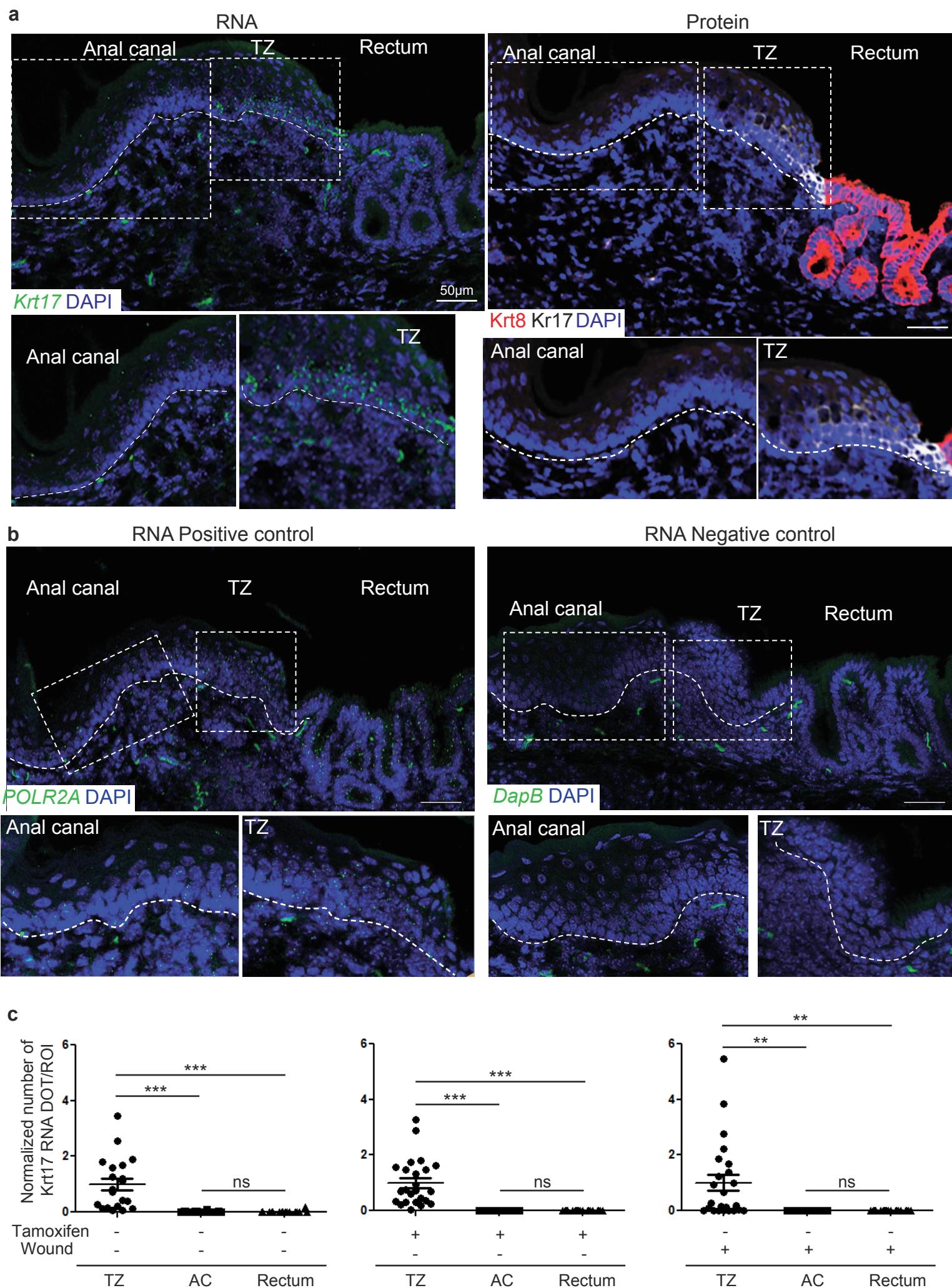
analyzed after two days of chase and stained with Krt17 in white and Krt8 in red. Dashed lines delineate the epithelium from the stroma. Scale bars are 50 μm .

Mitoyan et al., Supplementary Figure 1



Supplementary Figure 2. Expression of *Krt17* transcript in the anorectal region.

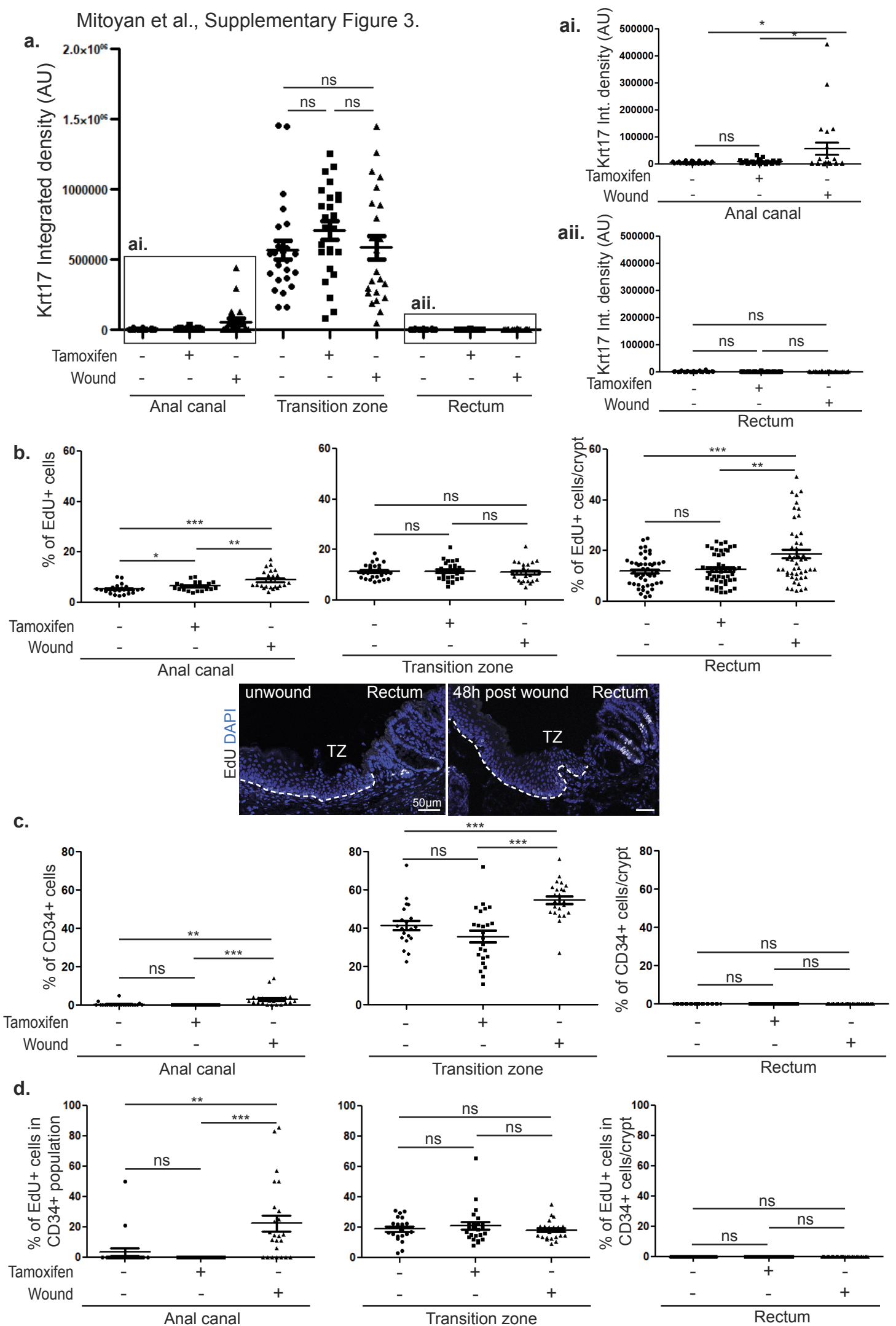
a,b. high quality in-situ hybridization (RNAScope) shows expression of *Krt17* in the anal TZ. Representative images of n=3 biologically independent samples in which fluorescence has been quantified in the absence or presence of 2 days tamoxifen injection. Insets are zoom in 1.2 fold (AC RNA), 1.4 fold (TZ RNA), 1.3 fold (AC protein), 1.25 fold (TZ protein). **b.** Positive control shows expression of *Actin* transcript in all tissue and **c.** negative control shows background level. Insets are zoom in 1.42 fold (AC and TZ RNA positive control) and 1.6 fold (AC and TZ RNA negative control) **c.** Normalized dot/ROI *Krt17* RNA expression visualized by RNAScope technology (see supplemental methods for details and source data are provided as a source data file). (n=3 mice were analyzed per condition). Unpaired t test two-tailed error bars, mean \pm SEM **p=0.0011 ***p<0.0001. At least 6 areas of each region (anal canal, TZ and rectum) were quantified per mice (n=3 mice were quantified per condition). Source data for the *Krt17* RNA quantification is provided as a Source Data file. Scale bars are 50 μ m.



Supplementary Figure 3. Tamoxifen injection does not induce a wound response. a.

Tamoxifen does not induce Krt17 expression in the anal canal and in rectum. Krt17 protein integrated density was measured by ImageJ in unwound conditions in the presence and absence of tamoxifen injected twice and 48h post-wound without tamoxifen in transition zone, anal canal (**ai**) and rectum (**aii**). Unpaired t test two-tailed $*p \leq 0.0376$ **b.** Quantification of EdU expression shows that tamoxifen injection does not change the proliferation status of Krt17+ TZ cells. At 48h post-wound, rectal cells are highly proliferative compared to TZ. Representative images of Edu positive cells (nuclear white staining at the TZ and rectum) **c-d.** Quantification of CD34 and EdU expression shows that tamoxifen injection does not change either the proliferation status of CD34+ TZ cells or the CD34 expression. Note that upon wounding, CD34 is expressed in the anal canal cells. Unpaired t test two-tailed $*p = 0.0256$ $**p \leq 0.0039$ $***p \leq 0.0006$. Quantifications for **a**, **b**, **c** and **d** were done using at least 8 areas of each region (anal canal, TZ and rectum) per mice (n=3 mice were quantified per condition). (Source data are provided as a source data file).

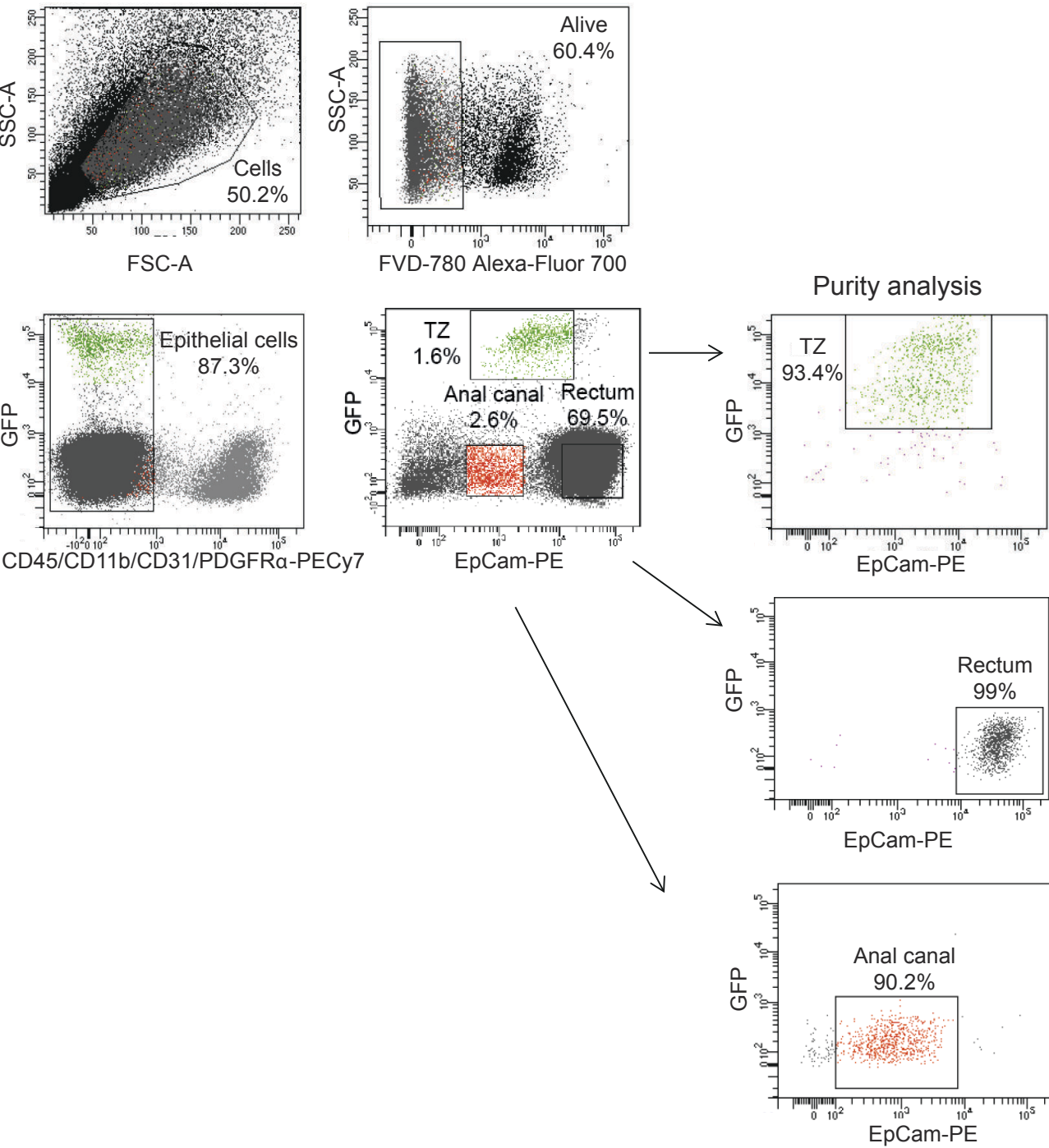
Mitoyan et al., Supplementary Figure 3.



Supplementary Figure 4. Strategy to isolate the anorectal region

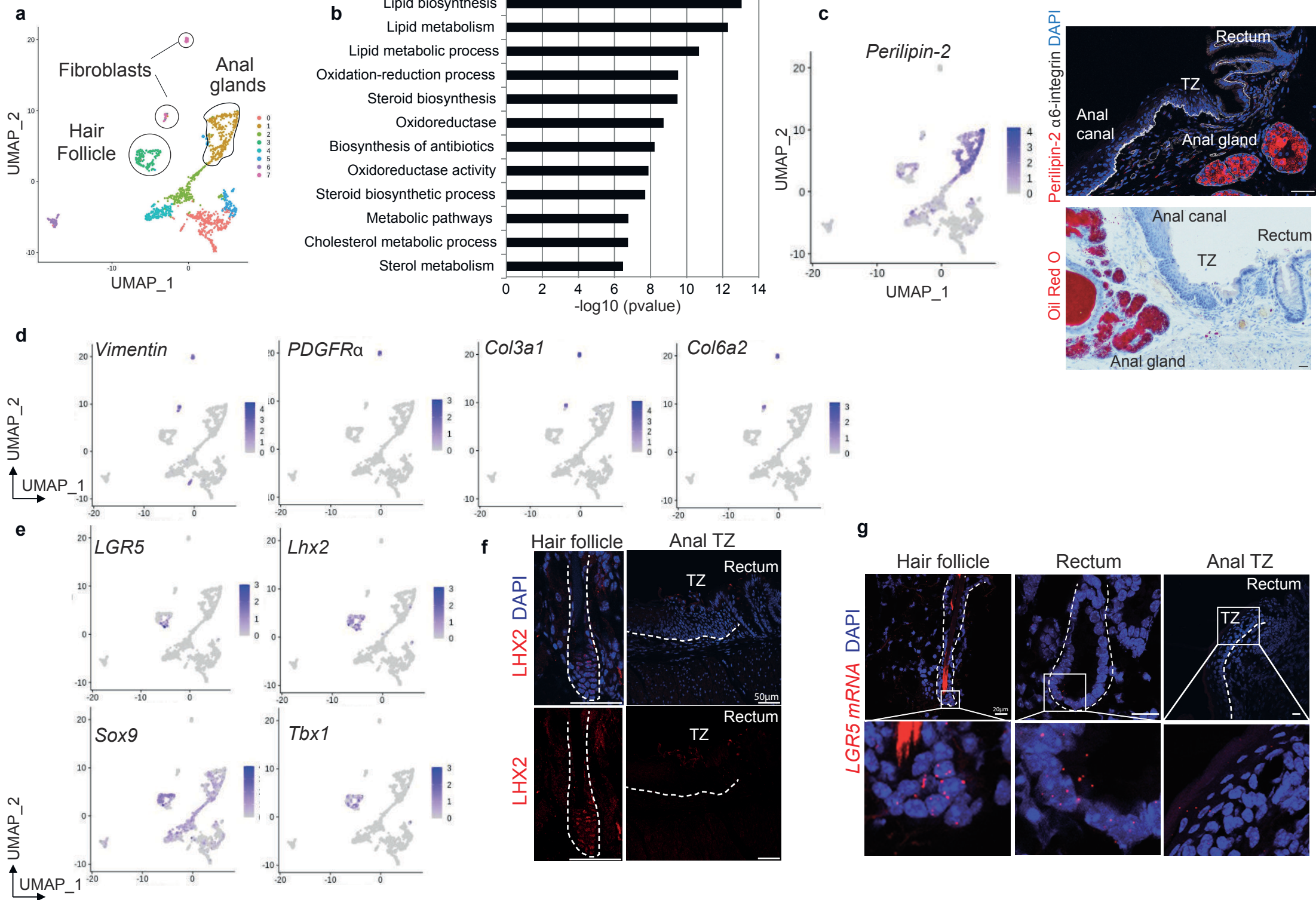
Representative example of the FACS strategy to isolate TZ cells, anal canal and rectum from *K17CreER^{T2};R26R^{GFP}* mice induced with tamoxifen for 2 days (n=20). CD45⁺ blood cells, CD11b⁺ macrophages, CD31⁺ endothelial cells and PDGFR α ⁺ fibroblasts were excluded from the live (FVD-780-), K17⁺GFP⁺ population. These epithelial cells were further purified by gating for EpCam⁺ cells. Anal canal cells are EpCam⁺GFP⁻ and rectum cells are EpCam^{High}GFP⁻. An example of the purity of each population is described.

Mitoyan et al., Supplementary Figure 4



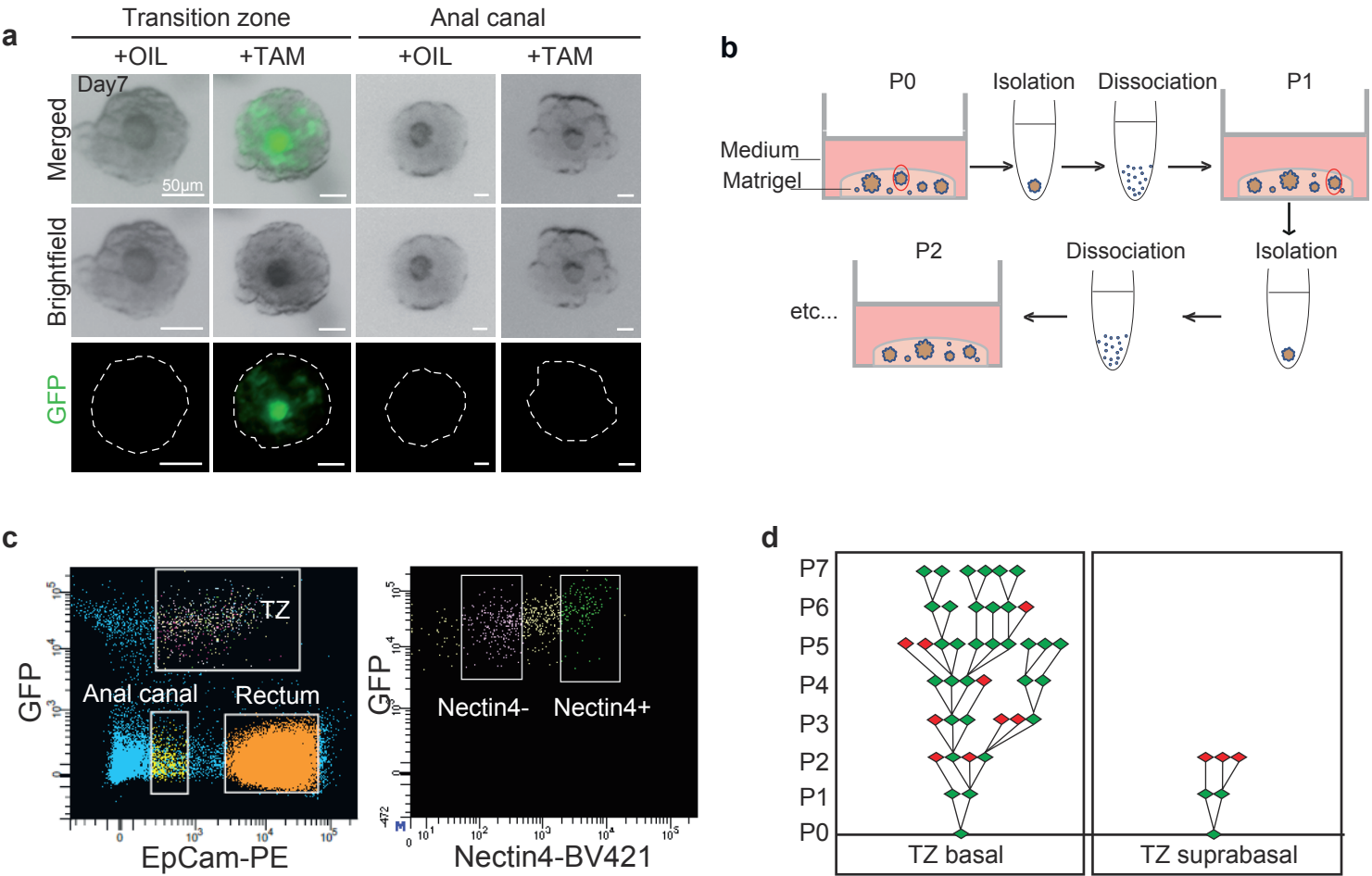
Supplementary Figure 5. Single-Cell RNA seq of FACS-sorted anorectal cells

a. Main cell populations visualized on Uniform Manifold Approximation and Projection (UMAP) dimensional reduction from scRNA sequencing of anorectal epithelial cells. **b.** To determine the pathways associated with the cluster 1, we perform a gene functional classification using DAVID algorithm. Bar plot represents enrichment for each of the pathway identified, where the strength of the association is represented by the log₁₀ (p-value). A majority of genes defining cluster 1 appears to be involved in lipid synthesis, a characteristic of the anal gland (Source data are provided as a source data file). A two-sided Fisher's exact test was used for data analysis. **c.** Immunofluorescence with perilipin-2 antibody (red), found in cluster 1, confirms that it represents the anal gland populations positive for oil Red O (n=3 independent experiments from n=3 mice). Scale bars are 50 μ m for the immunofluorescence and 20 μ m for the oil Red O staining. **d-e.** Expression of key genes expressed in the cluster 7 representing the fibroblast (**d**) and the cluster 3 representing the hair follicle (**e**). Source data for the genes in clusters 1, 3 and 7 is provided as a Source Data file. Darker color in the UMAP plot indicates higher expression level of the selected gene. **f.** Immunofluorescence of Lhx2 that specifically marks the hair follicle but is absent in TZ (n=4 independent experiments from n=3 mice), confirms the hair follicle nature of cluster 3. **g.** RNAscope shows expression of *Lgr5* in the hair follicle bulge and at the base of the rectal crypt but not in the anal TZ (n=3 independent experiments from n=3 mice).



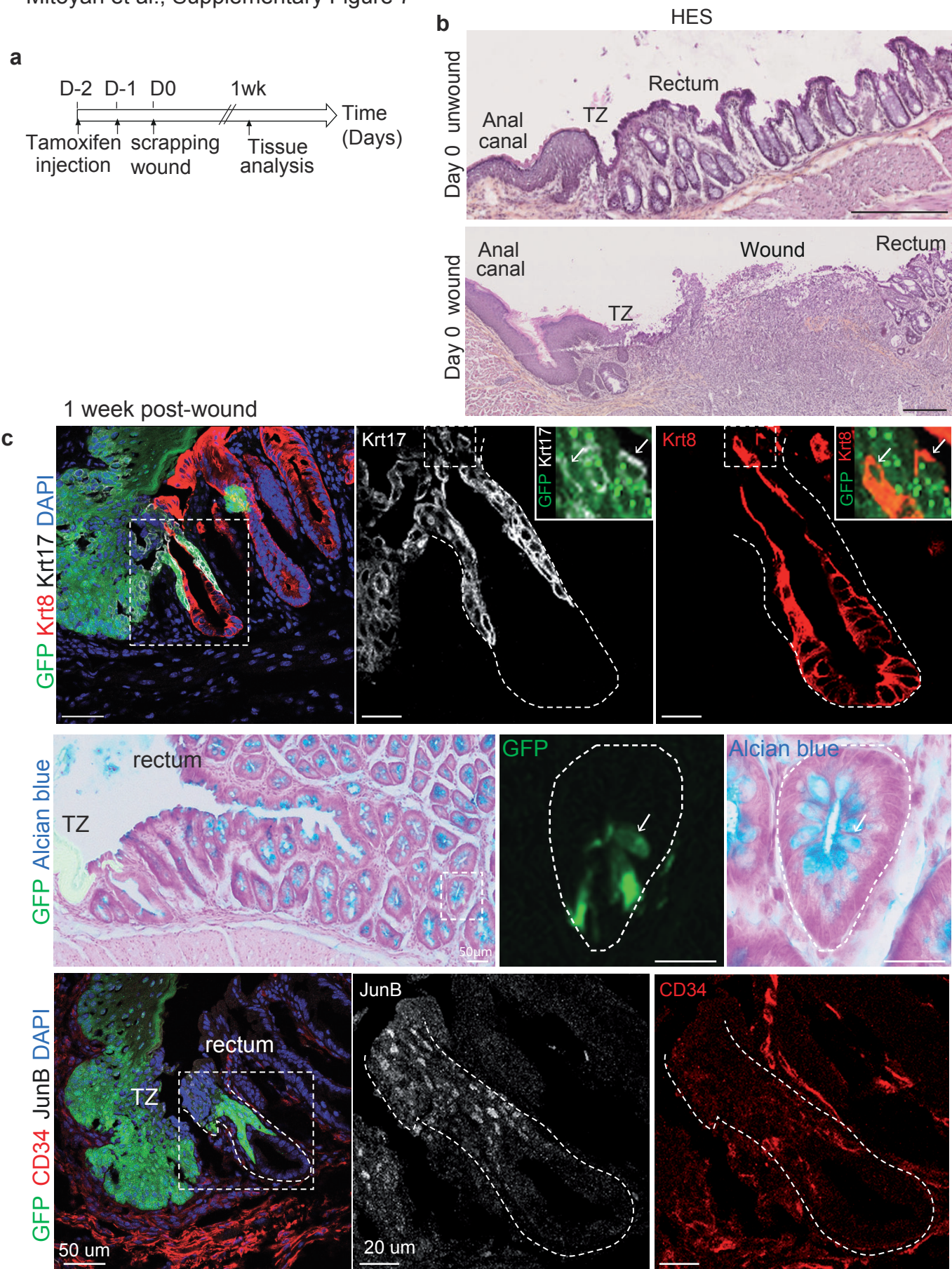
Supplementary Figure 6. Markers of the anal canal and TZ.

a. Tamoxifen induces GFP expression specifically in transition zone-derived organoids. Anal canal cells were sorted by previously established FACS strategy. As a positive control, Epcam^{low} cells from non-induced *K17CreER^{T2};R26R^{GFP}* mice were sorted. At passage 1, culture media was supplemented with tamoxifen or oil control during 7 days. Brightfield and GFP images were acquired at day 7 with the Leica M205FA stereomicroscope and showed the specific induction of GFP expression in transition zone organoids in the presence of Tamoxifen compared to oil control condition and anal canal-derived organoids (n=3 independent experiments from 3 independent FACS sortings). **b.** Subcloning strategy to test the self-renewal potential of anal TZ cells compared to the anal canal and rectal cells. At passage 0, organoids were individually isolated under a Leica stereomicroscope M205FA, dissociated into single cells and replated in new matrigel (P1). This process was repeated as long as organoids grew. **c.** Cells were sorted according to previous established FACS strategy but adding Nectin antibody here. After stroma exclusion, epithelial cells were purified by gating for EpCam^{low}GFP⁺ cells. These epithelial cells were further purified by gating for Nectin4⁺ and Nectin4⁻ cells. **d.** Clonogenicity assay shows that TZ basal organoids have unlimited clonogenic property whereas TZ suprabasal organoids cannot survive passage 2 (n=2).



Supplementary Figure 7. Mechanical wound at the anal TZ shows multipotency of anal TZ

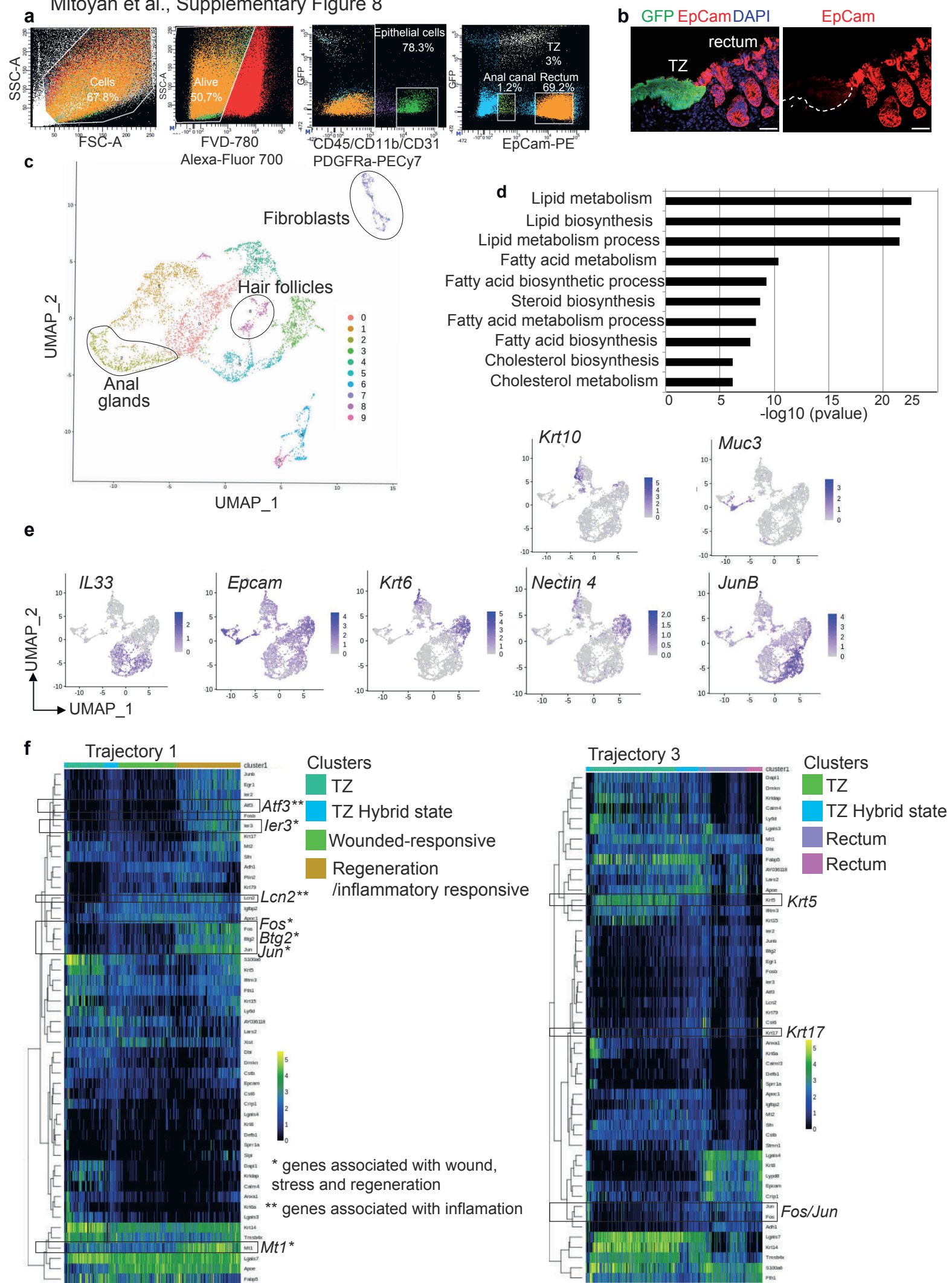
a. Wound strategy in *K17CreER^{T2};R26R^{GFP}* bigenic mice induced with tamoxifen 2 days before injury. **b.** HES at day 0 shows wounded region in the rectum epithelium close to the TZ (n=3 mice analyzed). **c.** Similar to the EDTA wound, Few TZ-derived GFP⁺ cells were found in the rectum epithelium in a transition state co-expressing the glandular marker Krt8 (red) and the TZ marker Krt17 (white) (n=5/13 mice analyzed) Insets are zoom in 4 fold (left panel) and 2.5 fold (right panel). TZ cells give rise to differentiated goblet cells (alcian blue⁺) (n=3 independent experiments). GFP⁺ TZ cells participating in the regenerative crypt after a mechanical wound are JunB⁺ (white) and CD34⁺ (red) (n=3 independent experiments). Scale bars are 250 μ m for **b** and 50 μ m for **c**.



Supplementary Figure 8. Analysis of the single-Cell RNA seq of FACS-sorted anorectal cells 1 week post-EDTA wound

a-b. Representative example of the FACS strategy to isolate TZ cells, anal canal and rectum from *K17CreER^{T2};R26R^{GFP}* mice induced with tamoxifen for 2 days, wounded with EDTA and analyzed 1 week later. **b.** Epcam expression profile is maintained at 1 week post EDTA wound in stratified and glandular epithelia (n=3 independent experiments from n=3 mice). **c.** Main cell populations visualized on Uniform Manifold Approximation and Projection (UMAP) dimensional reduction from scRNA sequencing of anorectal wounded epithelial cells. (Source data are provided as a source data file). **d.** Gene functional classification using DAVID algorithm was used to reveal lipid synthesis-associated pathways in cluster 2 which characterizes anal gland cluster. A two-sided Fisher's exact test was used for data analysis. Source data for the genes in clusters 2, 7 and 8 is provided as a Source Data file. **e.** Expression of key genes expressed in the different populations of wounded epithelial anorectal cells. Darker color in the UMAP plot indicates higher expression level of the selected gene. **f.** Clustering analysis showing the top genes significantly associated with the differentiation paths of trajectories 2 and 3. Heatmaps represent normalized gene expression in logarithmic scale.

Mitoyan et al., Supplementary Figure 8



Supplementary Table 1 – Antibodies

Primary Antibody	Host Species	Supplier	Catalogue number	Dilution
α 6-integrin	Rat	BD Biosciences	555734	1/100
SP-1 Chromogranin A	Rabbit	Euromedex	20086-IMMUNO	1/200
PE-EpCam CD326	Rat	Biolegend	118206	1/100
Biotin-CD34	Rat	eBioscience	13-0341	1/50
Gpc3	Mouse	ThermoFischer	MA5-17083	1/1000
JunB	Rabbit	Cell Signaling	3753	1/500
Keratin8	Rat	Developmental Studies Hybridoma Bank (DSHB)	AB_531826	1/50
Keratin8	Rat	Millipore	MABT329-25UG	1/400
Keratin10	Rabbit	OZYME BIOLEGEND	905401	1/1000
Keratin10	Rabbit	OZYME BIOLEGEND	905404	1/500
Keratin14	Mouse	Millipore	MAB3232	1/400
Keratin17	Rabbit	Abcam	Ab53707	1/20000
Keratin 6	Rabbit	Biolegend	905701	1/500
Lhx2	Rabbit	Millipore	ABE1402	1/2000
Loricrin	Rabbit	OZYME BIOLEGEND	905101	1/500

Lysozyme	Rabbit	DAKO	A0099	1/500
Nectin-4 clone N4.mu1	Mouse	Dr. Marc Lopez's gift	NA	1/200
PE-Cy7-CD11b	Rat	BD Pharmingen	561098	1/200
PE-Cy7-CD31	Rat	BD Pharmingen	561410	1/100
PE-Cy7-CD45	Rat	eBioscience	25-0451	1/200
PE-Cy7-PDGFRa (CD140a)	Mouse	Biolegend (Ozyme)	BLE323507	1/50
eFLUOR780 (Fixable Viability Dye)		Thermofisher	65-0865	1/1000
Perilipin-2	Rabbit	Novus	NB110-40877SS	1/1000
GAPDH	Mouse	Santa Cruz	sc-32233	1/5000

Secondary Antibody	Host	Coupled with	Supplier	Reference	Dilution
Anti-rat IgG	Donkey	Cy3	Jackson ImmunoResearch	712-166-153	1/1000
		Alexa 647		712-606-153	
Anti-rabbit IgG	Donkey	Cy3	Jackson ImmunoResearch	711-606-152	1/1000
		Alexa 647		711-606-152	
Dapi 1mg/ml			Thermo Scientific	62248	1/2000
APC-Streptavidin			BD Pharmingen	554067	1/200
Anti-mouse BV-421	Rat		BD Biosciences	562580	1/100
Anti-mouse IgG	Donkey	Peroxidase	Jackson ImmunoResearch	715-036-151	1/10000
Anti-rabbit IgG	Donkey	Peroxidase	Jackson ImmunoResearch	711-036-152	1/10000

Supplementary Table 2 – Organoid cell culture media

Medium component	Supplier	Catalogue number	Final concentration
Advanced DMEM/F12	Gibco™	12634010	1x
Glutamax 100x	Gibco™	35050061	1x
Hepes 100x	Gibco™	15630056	1x
Penicillin/Streptomycin 100x	Gibco™	15070063	1x
Wnt3A conditioned medium	Hubrecht Institute	MTA	50% home made
R-spondin conditioned medium	Millipore	SCC111	20% home made
Noggin conditioned medium	Hubrecht Institute	MTA	10% home made
B27 supplement without vitamin A 50x	Gibco™	12587010	1x

N2 supplement 100x	Gibco™	17502048	1x
n-Acetyl Cysteine	Sigma	A9165	1,25 mM
Nicotinamide	Sigma	N0636	10 mM
EGF	Gibco™	PMG8043	50 ng/mL
FGF2	Sigma	SRP4037	50 ng/mL
IGF-1	Biolegend	590906	100 ng/mL
Prostaglandine E2	Tocris	2296	10 nM
Gastrin 1	Sigma	G9145	100 nM
A83-01	Tocris	2939	500 nM
SB202190	Sigma	S7067	3 µM
Primocin 500x	Invivogen	ant-pm-1	1x
LY27632	Sigma	Y0503	10 µM

Supplementary Table 3 – qPCR primer sequences

Gene	Primer sequence
<i>GAPDH</i>	Forward CGTAGACAAAATGGTGAAGGTCGG Reverse AAGCAGTTGGTGGTGCAGGATG
<i>Krt5</i>	Forward GGCCCACAGAGACTGCTTCTTT Reverse AACATTTTGGGGTCTGGGTCAC
<i>Krt17</i>	Forward CTTCCGTACCAAGTTTGAGAC Reverse CGGTTCTTCTCCGCCATCTTC
<i>Krt8</i>	Forward GGACATCGAGATCACCACCT Reverse TGAAGCCAGGGCTAGTGAGT

SUPPLEMENTAL METHODS

A stem cell population at the anorectal junction maintains homeostasis and participates in tissue regeneration

Louciné Mitoyan¹, Véronique Chevrier¹, Hector Hernandez-Vargas^{2,3}, Alexane Ollivier¹, Zeinab Homayed⁴, Julie Pannequin⁴, Flora Poizat⁵, Cécile De Biasi-Cador⁵, Emmanuelle Charafe-Jauffret^{1,5}, Christophe Ginestier¹, and Géraldine Guasch^{1*}

RNAscope quantification was done following the “Guideline on how to quantify RNAscope Fluorescent Assay Results”. All images were acquired using a confocal microscope ZEISS LSM 880 with exact same parameters and analyzed with ImageJ.

Analysis:

All channels were projected over the z axis. DAPI and *Krt17* were then split. DAPI channel was segmented to create a Mask of the nuclear area. It is in this area that the intensity of the *Krt17* was measured to ensure that the measurement is done within the nuclear area.

To ensure the selection of the DAPI only contained in the epithelium, we used the “Particule analysis”. Size of selected objects was set to 200-infinity. With the “Image Calculator” the Mask DAPI was ADDED to mask *Krt17*. ROI (Region Of Interest) of 500 pixels per 500 pixels was created (the same ROI was used for all images), placed and then duplicated. Images were binarized creating a mask of the *Krt17* staining contained in the DAPI Area. The plugin “Extended Particle Analyzer” of the Biovoxxel tool box was used. To ensure the selection of the dots, the analysis parameters were set as 0.01-Infinity for Area (micron²). This value was established by experimental trials. Segmented particules corresponding to the

dots were created and then this particles were overlayed on the native *Krt17* z projection for parameters measurement in each particles.

Measurement:

We reported measured Area and IntDen (Integrated density) and calculated total Dot number in ROI according to the following formula:

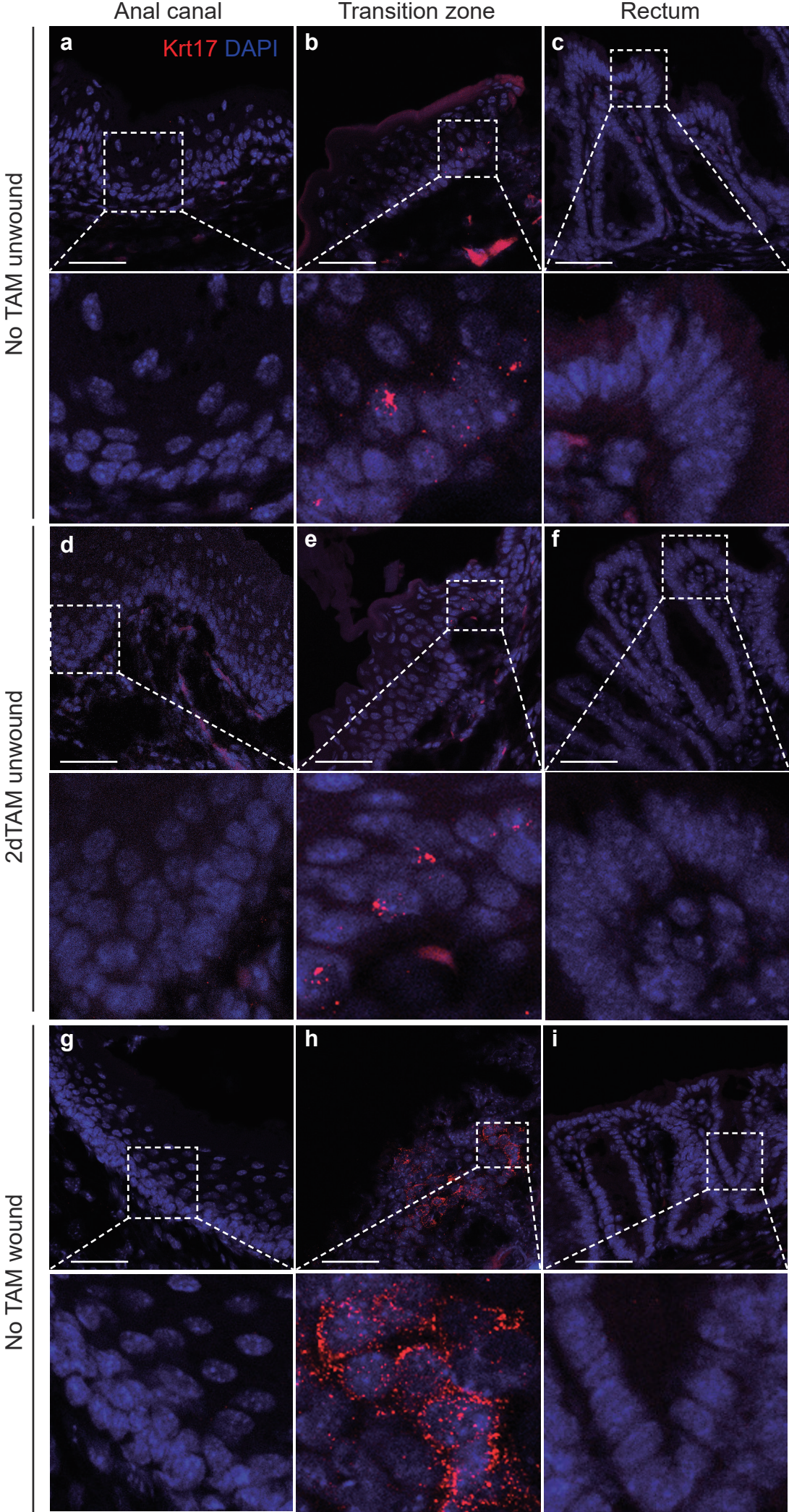
$$\text{Total dot number in ROI} = \frac{\text{Total Integrated density of selected dots} \times \text{Total Area}}{\text{Average Intensity per Single Dot}}$$

Data were then normalized on TZ for each condition (see Source Data File).

N.B: The average intensity per single dot was calculated based on the expression of few single dots from 3 different mice and following this formula:

$$\text{Average Intensity per single dot} = \frac{\sum \text{Integrated density of selected dots} \times \sum \text{Area of selected dots}}{\text{Number of selected dots}}$$

Legend of supplementary method figure. A representative example of the *Krt17* (red) quantification in different regions (AC, TZ and rectum) quantified in absence (**a**, **b** and **c**) and presence (**d**, **e** and **f**) of tamoxifen (TAM) injected twice and 48h post-wound without TAM (**g**, **h** and **i**). A least 6 areas of each region (anal canal, TZ and rectum) were quantified per mice (n=3 mice per condition). Scale bars are 50µm. Insets for **a**, **b**, **c**, **d**, **e**, **f**, **g**, **h** and **i** are respectively zoom in 2.8 fold, 4.4 fold, 3.4 fold, 1 fold, 5.3 fold, 3.3 fold, 3.6 fold, 4.7 fold and 4.8 fold.



II. SUPPLEMENTARY RESULTS 1

TZ in stomach region is located between esophagus and corpus stomach in human and between the forestomach and stomach in mouse (**Figure 9**). In both cases, TZ is found between a stratified squamous epithelium and a simple columnar epithelium. Pathologies such as ulcers, Barrett's esophagus and cancer are frequently associated with stomach TZ as mentioned in Introduction (Chapter V.1.1 and V.1.2). However, the role of Krt17⁺ TZ cells during homeostasis and injury has not been investigated yet in stomach.

Stomach TZ during homeostasis

Stomach TZ cells maintain stratified squamous epithelium of esophagus

Using our mouse model and strategy of lineage tracing K17Cre-EGFP to track TZ Krt17⁺ cells previously described⁵¹, we showed that, shortly after tamoxifen injection, in homeostatic condition, stomach TZ cells maintain stratified epithelium of forestomach. GFP⁺ cells were restricted to the TZ and no GFP cells were found in the glandular epithelium of the corpus stomach (**Fig. S1a**). At longer time points (>3 weeks) post tamoxifen, GFP⁺ TZ cells are found all along the stratified epithelium of the forestomach and are absent from the columnar epithelium of the corpus stomach (**Fig. S1b**). These results are consistent with our previous lineage tracing data of the anorectal TZ.

Stomach TZ cells colonize the First Gland

A unique structure residing between the stratified epithelium of esophagus and the glandular epithelium of stomach has been described in both human and mouse called respectively cobelli's gland and first gland^{70,167}. This structure is a gland composed of a multilayered epithelium with squamous cells surrounding columnar cells (**Fig. S1a**). The function of the first gland is not fully understood but it may play a protective role in response to acidification that may occur in the esophageal-gastric junction. Indeed, the first gland may neutralize acids in stomach by producing electrolytes like bicarbonate ions (HCO₃⁻)¹⁶⁷.

First gland is composed of different cell types such as tuft cells that are chemosensory terminally differentiated cells expressing doublecortin-like kinase 1 (DCLK1) as reported by O'Neil and colleagues in 2016⁷⁰. We hypothesized that stomach TZ stem cells may be a reservoir for tuft cells in order to maintain tissue integrity in case of an increase of acidity in the stomach.

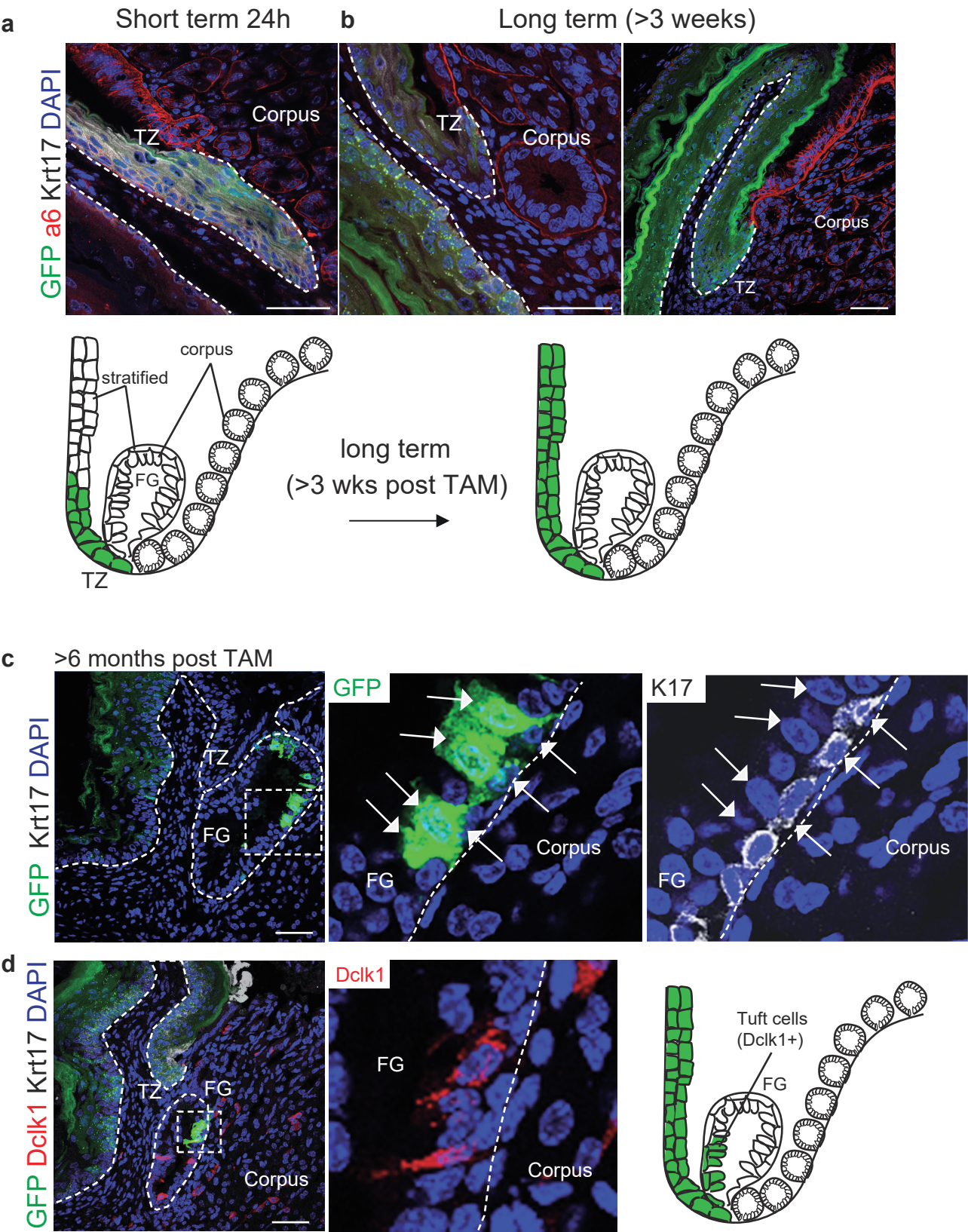
Long time point analyses (6 months post-tamoxifen), we found GFP⁺ TZ cells in the first gland (**Fig. S1c**). Krt17⁺ GFP⁺ cells, which are squamous cells, gave rise to GFP⁺ Krt17⁻ columnar cells. Among GFP⁺Krt17⁻ cells, we found differentiated cells positive for DCLK1⁺ cells that correspond to tuft cells. (**Fig.S1d**). These data show the multipotency potential of stomach TZ cells.

Stomach TZ and injury

To further investigate the role of tuft cells in tissue integrity maintenance in case of an increase of acidity in the stomach, we developed a collaboration with Dr. Philippe Jay (IGF, Montpellier), expert in tuft cells. His team developed a mouse model of tuft cell deletion (Pou2f3 knock-out mice)¹⁶⁸ to study the role of tuft cells. Deletion of tuft cells combined with acid-induced irritation (low-pH acidified drinking water) for 1 week to mimic chronic irritation offer a unique model to investigate tuft cells role during injury in stomach. We will compare the efficiency to repair acid-induced injuries in WT and Pou2f3 knock-out mice at early and late time points after injury (24h, 1 week and 3 weeks) by quantifying proliferation rate. Regeneration of the epithelium and TZ will be monitored by the expression of known molecular TZ markers (Krt17, Krt6, Krt10).

Figure S1: *In vivo* potency of stomach Krt17⁺ TZ cells. a-b. Lineage tracing of stomach Krt17⁺ cells at short (**a**) and long (**b**) time-points following tamoxifen injection (2mg). Krt17⁺ cells (green) maintain stratified squamous epithelium during homeostasis. Basement membrane is highlighted with α 6-integrin (red). **c.** At longer time-points post tamoxifen (>6 months) TZ-derived GFP⁺ cells are found in the first gland (FG). **d.** Progeny of Krt17⁺ TZ cells are tuft cells positive for Dclk1 (red) and negative for Krt17 (white). Scale bars for **a-d** are 50 μ m.

Figure Supplementary 1 stomach TZ



III. SUPPLEMENTARY RESULTS 2

In preparation

Characterization of the immune niche in a model of pre-cancerous anorectal
development

INTRODUCTION

Transition zones are frequently associated with cancers in humans¹⁴⁰ and in mice^{59,141}. Indeed, 86% of esophageal cancers develop at the junction of esophagus and stomach¹⁴² and 85% of highly malignant anorectal cancers develop between the stratified epithelium of the anal canal and the glandular epithelium of the rectum¹⁴⁵⁻⁵⁹. Tumors at the anorectal TZ associated with Squamous Cell Carcinoma (SCC) are three times more common than carcinoma in the anal canal.

We previously showed that TZ display wound-associated proteins such as TnC and Krt17 suggesting a pre-lesional state of TZ that may be more permissive to malignant transformations. Along with these data, TZ microenvironment is infiltrated by immune cells, which comfort the idea of a permissive TZ state. Moreover, recent observations of our collaborator Dr. J. Marie (CRCL Lyon), that TGF β signaling mutations in Smad4 and Tif1 specifically in T lymphocytes lead to spontaneous tumor development in anorectal TZ, suggests an important interplay between immune and epithelial cells. Out of 5 tumors arising at the anorectal TZ following T lymphocytes mutations, 2 tumors had mutations in KRas. Interestingly, it was shown in a previous study that TGF β RII-deficiency Krt14⁺ cells (expressed in TZ; see **Table 1**), led spontaneously to SCC in anorectal TZ and RNAsequencing of these SCC showed an upregulation of Ras pathway¹⁴⁸. These data show the important role of Ras in the pathogenesis of TZ cancer.

In parallel with the characteriazation of anorectal TZ cells during homeostasis and in injured state, I started a project to understand the role of anorectal TZ cells in tumorigenesis. **We hypothesized that TZ cells may be target of early transformation associated with microenvironment remodeling.**

I have developed an inducible mouse model of pre-neoplasia using K17CreERxLSL-GFPxLSL-KRas^{G12D} mice where KRas in its active form KRas^{G12D} is expressed specifically in Krt17⁺ TZ cells. To mimic human physiopathology and chronic inflammation, we combined KRas^{G12D} activation with mechanical chronic wounds. We used this model to explore molecular changes occurring before tumor development and progression.

This project combining cancer and immunology fields aims to unveil key regulators of tumor susceptibility.

RESULTS

Establishment of a mouse model to study tumor initiation and progression

KRas^{G12D} expression induces hyperplasia in TZ

K17CreERxLSL-GFPxLSL-KRas^{G12D} mice were injected twice with 2mg tamoxifen as previously described⁵¹ to label all TZ cells and induce KRas expression in its mutated form G12D (**Fig.1a**). Different strategies were performed following tamoxifen injections; tamoxifen injections alone or followed by mechanical wounds twice a week for 2 weeks or 4 weeks. We observed different phenotypes depending on the strategy applied. At least 6 weeks post tamoxifen injections, anorectal TZ showed hyperplasia compared to WT mice. Interestingly, this phenotype was also found in the stomach TZ of these mice (**Fig.1B and S1**).

KRas^{G12D} expression and chronic wounds are sufficient to induce dysplasia in anorectal TZ

TZ are naturally prone to mechanical stress. In order to reproduce that event *in vivo*, we established a protocol to subject chronically mechanical wounds in the anorectal TZ (ethical committee C2EA14, protocols #4572 and #2308). When subjected to chronic mechanical wounds in addition with KRas^{G12D} mutation, we observed dysplasia whose phenotype depended on the number of wounds performed. After 4weeks of mechanical wounds, we observed an *in situ* carcinoma while 2 weeks of wounds induce low-grade dysplasia (**Fig.1b**). In both hyperplasia and *in situ* carcinoma conditions, 4 mice were analyzed for each condition and all mice developed described phenotypes. Histologies have been analyzed by 2 independent anatomo-pathologists at the Paoli Calmettes Institute, Dr. Coslet and Pr. Charafe Jauffret.

In situ carcinoma hallmarks include keratin switch, alteration in differentiation and proliferation. All three characteristics were found in our model of carcinoma as shown in **Figure 1d-g**. We assessed the proliferation status in these conditions, we confirmed the hyperproliferation occurring in the hyperplastic condition by quantification (**Fig.1d-e**), and we showed EdU+ cells in suprabasal layers of the carcinoma epithelium. During homeostasis TZ cells are Krt17⁺ and negative for glandular marker Krt8. In pathologic condition such as carcinoma, we observe a “switch” in those keratins. Parts of GFP⁺ carcinoma downregulate Krt17 expression and express Krt8 (**Fig.1f**). In the meantime, the differentiation marker Krt10 that is normally expressed in suprabasal layers of stratified squamous epithelia is

downregulated in TZ carcinoma when completely normal in anal canal. Control and hyperplastic conditions do not display these phenotypes (**Fig.1f**).

T cells: key player of TZ tumor susceptibility?

Transition zone is a special zone that expresses wound-associated markers such as Krt17, TenascinC and β -integrin. Associated with wound markers, TZ stroma is infiltrated with T lymphocytes CD3⁺ (**Fig.2a**).

To study further T cells interplay with epithelial TZ cells, we sorted CD8⁺ and CD4⁺ cells among CD3⁺ T lymphocytes in order to culture them with KRas-derived organoids. First, we isolated CD4⁺ and CD8⁺ lymphocytes from mice mesenterium (**Fig.2b**). We then co-cultured CD3⁺ T cells with TZ organoids from WT mice as previously established (**Fig.2c**). We successfully co-cultured both cell compartments for up to 9 days and T cells were visible near the TZ organoid (**Fig.2c**). Further optimizations need to be done to investigate more deeply the effect of lymphocytes on KRas mice-derived organoids.

In order to highlight key regulators of tumor initiation and to understand better the interplay between microenvironment and epithelial cells, we performed single-cell RNA sequencing. We used the previously well-established strategy to isolate and sort epithelial cells from the anorectal region which are EpCam^{high} glandular cells and EpCam^{low} stratified squamous cells⁵¹. Because 100% of K17CreERxLSL-GFPxLSL-KRas^{G12D} mice subjected to chronic wounds for 4 weeks developed an *in situ* carcinoma, we pooled at least 4 of these mice and successfully sorted by FACS the anorectal TZ cells and their microenvironment. Immune cells were sorted based on the expression of CD45 and CD11b; fibroblasts were sorted using the PDGFR α marker and endothelial cells were sorted based on the expression of CD31 (**Fig.3a**). Next, cells were sequenced using 10X genomics. After filtration of mitochondrial genes and adjustment on cell cycle genes, 5527 were analyzed and 13 clusters were identified (**Fig.3b**). Stratified and glandular epithelia were identified based on their respective specific markers Krt5 and Krt8 (**Fig.3c**). Immune populations were identified with the pan-immune CD45 marker. More precisely, B cells were identified based on CD74, T cells with CD3 and granulocytes with s100a9 gene (**Fig.3c**).

This project is ongoing in the lab, and future single cell RNAsequencing are planned in WT, hyperplasia and low-grade dysplasia conditions. We will use these data to establish gene signatures of different KRas-induced phenotypes. We will investigate changes occurring in

epithelial and microenvironment of anorectal TZ cells from hyperplasia and dysplasia and we will identify candidates implicated in tumor susceptibility and development. We will further investigate the role of selected candidates using our 3D culture model

CONCLUSION

In this project, we first established a unique inducible mouse model of early neoplasia in anorectal TZ. We showed that KRas in its active form KRas^{G12D} induced hyperplasia in anorectal TZ cells. Combining KRas mutation with 2 or 4 weeks of chronic wounds led to low and high-grade dysplasia. We successfully isolated and performed single cell RNAsequencing on epithelial and microenvironment cells from mice that developed an *in situ* carcinoma.

Many studies using germ-free and/or antibiotic-treated mice have showed the influence of microbiota on intestinal epithelium caused by the lack of bacteria. In some parts of the intestine such as jejunum and ileum villus height and crypt depth was decreased¹⁶⁹. Gavage of neonatal mice with *Lactobacillus reuteri* probiotic increases enterocyte migration, proliferation and crypt height. This altered intestinal microbiota composition suggests that microbial diversity can directly influence intestinal epithelial homeostasis¹⁷⁰. Since, bacteria either commensal or pathogenic colonize anorectal transition zone, our lab aims to target microbiota as it was shown to be involved in numerous pathologies including cancers. Treatment with broad-spectrum antibiotics (Vancomycin, ampicillin, metronidazole and neomycin) along the dysplasia protocol previously established was used (KRas + 4 weeks of chronic wounds). Preliminary results showed that reduced inflammation attenuated KRas-induced *in situ* carcinoma suggesting one more time the crucial role of immune cells in tumor initiation and the need to understand all interplays.

Legends

Figure 1: KRas mutation in addition with chronic wounds induces an *in situ* carcinoma at the anorectal transition zone. **a.** Schematic of the mouse model used, KRas^{G12D} mutation and EGFP were induced in Krt17⁺ TZ cells following tamoxifen injections. **b.** Hematoxylin and Eosin staining show hyperplasia of TZ following KRas^{G12D} mutation alone and low grade dysplasia and *in situ* carcinoma development when chronic wounds were performed. 4/4 mice analyzed for hyperplasia and *in situ* carcinoma conditions developed these phenotypes. Low-grade dysplasia developed in 2/2 analyzed. **c.** mice injected with oil control n=X **d.** Proliferative cells EdU⁺ are found in carcinoma suprabasal layers of cells compared to ctrl and hyperplasia conditions. **e.** Increase of EdU⁺ cells in hyperplastic mice compared to WT condition. At least 5 sections from 3 different mice were quantified for each condition. Two-tailed unpaired t-test; error bars, mean ± SEM ***p=0.0003. **f.** Glandular and stratified specific markers respectively Krt8 and Krt17 are shown by immunofluorescence in WT condition and with KRas in its active form as well as differentiation alteration in carcinoma showed by differentiation marker Krt10 (red) in all four conditions. Basement membrane is highlighted with α6-integrin (white). Scale bars are 50µm. **g.** Scheme summarizing the kinetic of KRas^{G12D} phenotypes from hyperplasia to *in situ* carcinoma.

Figure 2: Increase of Tγδ intra-epithelial lymphocytes following KRas^{G12D} activation. **a.** Expression of T lymphocytes marker CD3⁺ (red) in control, hyperplastic, low grade dysplasia and mice bearing an *in situ* carcinoma. Arrows highlight CD3⁺ cells **b.** Cell sorting strategy used to sort immune CD8⁺ and CD4⁺ T cells a. **c.** After isolation, TZ cells and immune cells were cultured together for 7 days. TZ organoid surrounded by T cells shown in brightfield and by immunofluorescence using CD3 T cell marker. Scale bars are 100µm and 50µm respectively for brightfield and immunofluorescence images.

Figure 3: Overview of epithelial and microenvironment landscape during different stages. **a.** Isolation of KRas mutated cells stromal and epithelial cells by FACS. Stromal cells were sorted according to specific markers CD31 (endothelial cells), CD45 (lymphocytes), CD11b (macrophages) and PDGFRα (fibroblasts) and epithelial cells were sorted according to EpCam expression and GFP (specific for TZ). **b.** Main cell populations visualized on Uniform Manifold Approximation and Projection (UMAP) dimensional reduction from scRNA

sequencing of anorectal epithelial and stromal cells from mice that developed an *in situ* carcinoma 4 weeks post chronic wound. **c.** Expression of key genes expressed in rectum, stratified epithelium, T cells, B cells, macrophages, granulocytes and fibroblasts. Darker color in the UMAP plot indicates higher expression level of the selected gene.

Supplemental Figure 1: a. KRas^{G12D} induces different phenotypes depending on used strategy. Macroscopic and brightfield pictures of anal regions from WT, hyperplasic and carcinoma-bearing mice **b.** Stomach tissues from WT and KRas^{G12D} mutated mice have been harvested 6 weeks post-tamoxifen injections. **c.** Hematoxylin & Eosin staining of stomachs from WT and mutated mice. KRas^{G12D} induction alone induced hyperplasia in stomach TZ. Scale bars are 100µm.

Figure 1_KRas

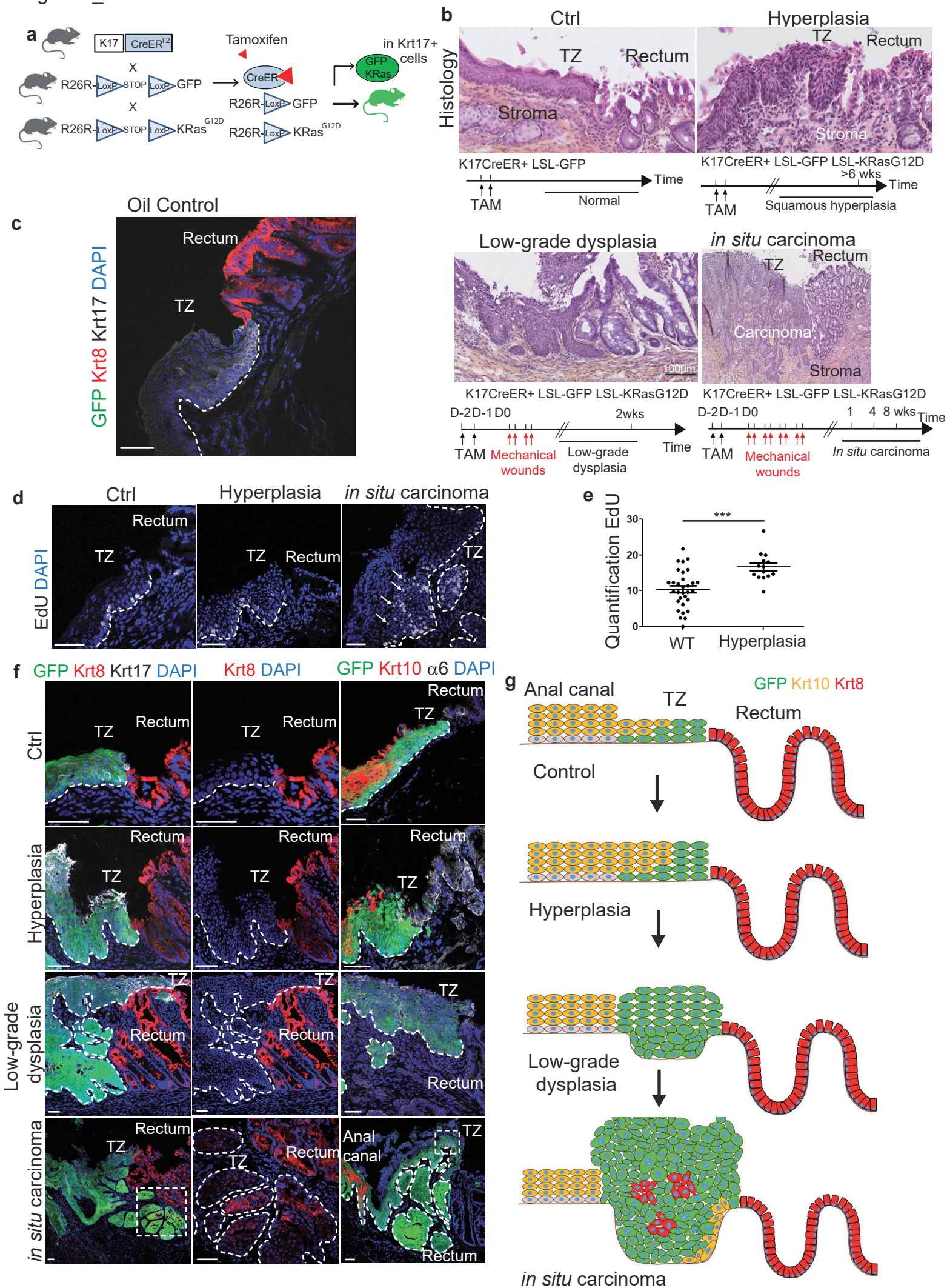
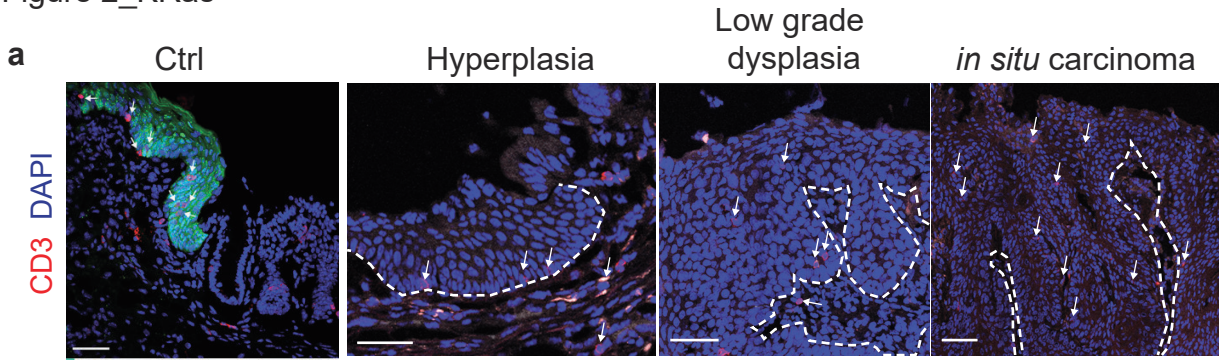


Figure 2_KRas



b LT isolation from mesenterium

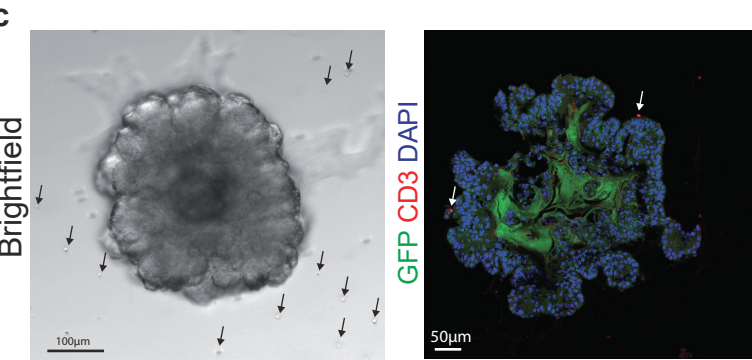
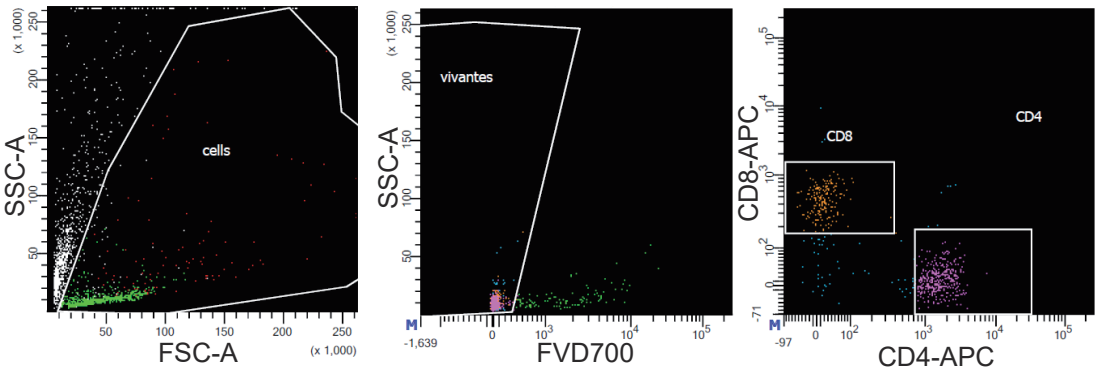
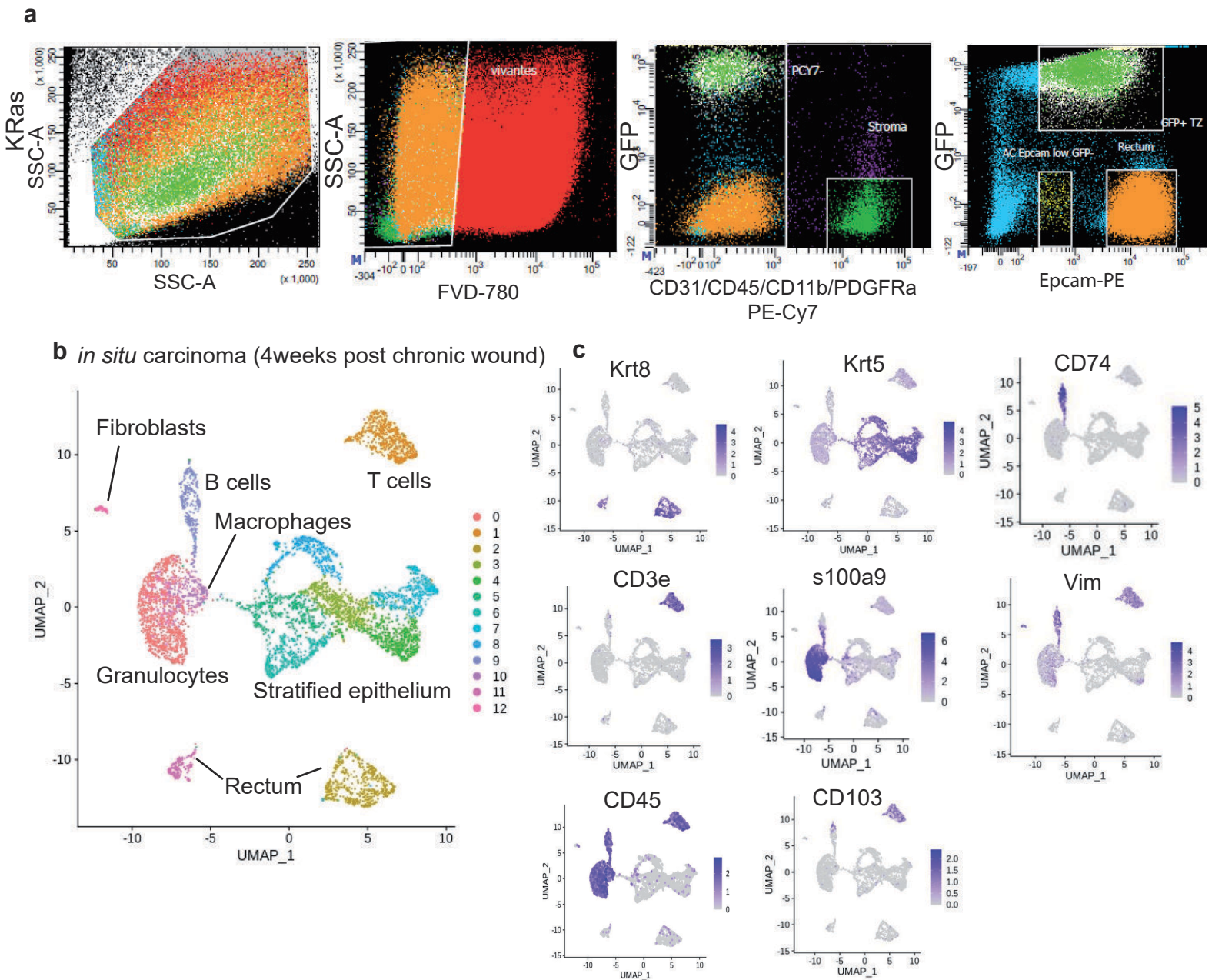
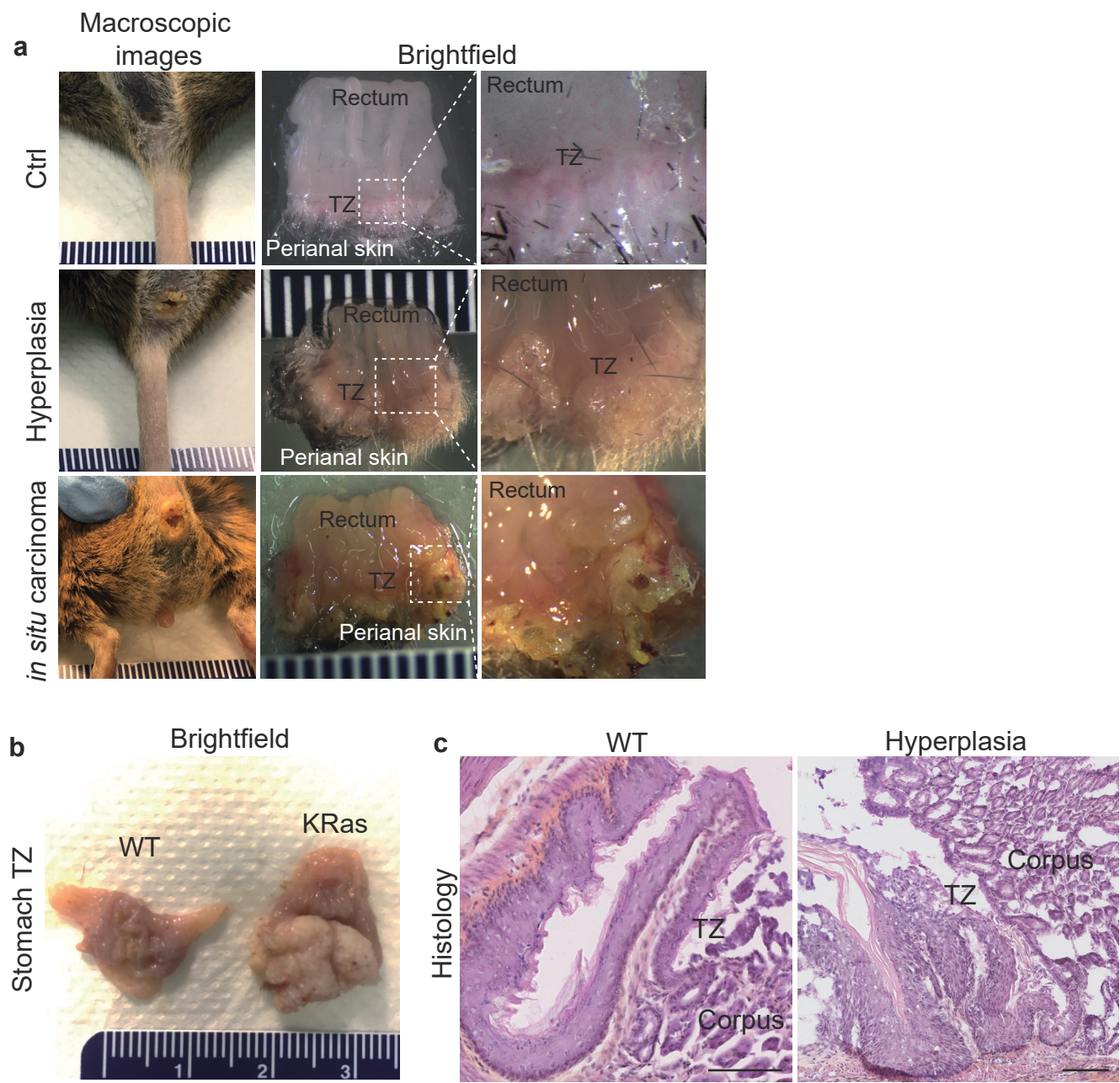


Figure 3_KRas



Supplemental Figure 1



CONCLUSION

Although TZ research has intensified the last few years providing new insights on TZ role in epithelial maintenance, contribution to wound repair and its implication in tumorigenesis, numerous unanswered questions stand still.

During my PhD, I developed a mouse model of lineage tracing using K17CreER-LSL-GFP mice to trace TZ Krt17⁺ cells between the anal canal and the rectum. The model allowed us to show the unipotent property of TZ cells during homeostasis as they maintained only the stratified squamous epithelium of the anal canal. We also successfully developed a 3D organoid culture of anorectal TZ cells that recapitulated the heterogeneity and specific markers of TZ.

Next, we challenged those cells with a wounding method called EDTA wound to remove specifically crypt of the rectum. When challenged, a minority of Krt17⁺ TZ cells were able to change their properties to become multipotent and participate in repair of the simple columnar epithelium constituting the rectum. Using single-cell RNAsequencing and pseudo time analysis, we confirmed our lineage tracing data that is the unipotency of TZ cells during homeostasis and allowed us to define the heterogeneous anorectal TZ cells. We also showed by bioinformatics analysis the emergence of a cell type identified as “hybrid cell” when wounding the region. Hybrid cells showed specific markers at the mRNA and protein level from both squamous stratified and simple columnar cells. Moreover, single-cell RNA sequencing allowed us to highlight the expression of the wound-associated JunB gene present in hybrid cells that we further confirmed is involved in proper differentiation of TZ cells.

During homeostatic conditions, TZ display a particular stroma expressing wound-associated proteins and immune cells infiltration representing a pre-lesional state prone to transformations. TZ are frequently associated with aggressive tumors and recent observations of tumor development at the anorectal TZ following mutations in T lymphocytes suggest a strong interplay between immune and epithelial cells that may lead to tumor initiation. We developed a unique mouse model expressing KRas in its active form G12D to access those questionings. We showed that KRas mutation alone induced hyperplasia in anorectal TZ. However, combining KRas mutation with chronic mechanical wounds that mimic a chronic inflammation that exists in human anorectal carcinoma, led to the development of low and high-grade dysplasia. This model combined with 3D organoid cultures and single-cell RNA sequencing will unveil pre-neoplastic molecular changes occurring in stromal and epithelial compartments leading to carcinoma. It is possible that discovered candidates would represent master regulators of tumor susceptibility of the TZ that can be blocked in order to prevent cancer progression.

DISCUSSION/PERSPECTIVE

I. Cellular plasticity and transition zone heterogeneity

I.1. Heterogeneity of anorectal transition zone

In intestine, stem cells are located at the base of the crypts. In this particular location, intestinal stem cells are in close relationship with niche components that participate in stemness. In anorectal TZ, we identified different cells displaying different markers depending on their location in the TZ. TZ cells close to the rectum and located at the basal layer of the epithelium co-express CD34 and Krt6. Their upstairs neighbors lose CD34 stem cell marker and gain Nectin4 marker. Basal cells located at the other extremity of TZ, close to anal canal express neither CD34 nor Krt6 (**Figure 20**).

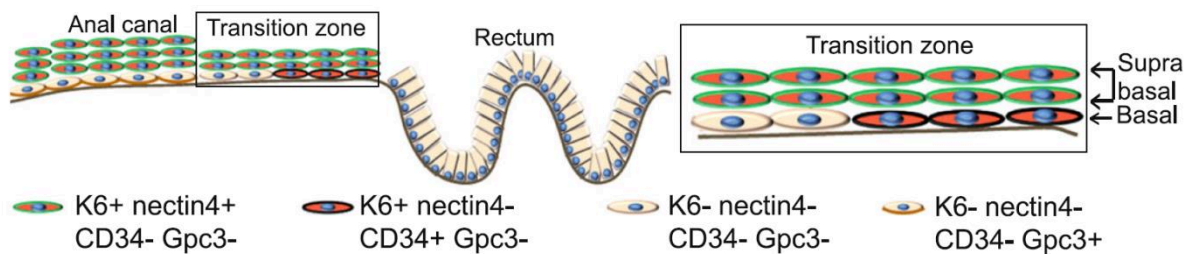


Figure 20: Anorectal TZ heterogeneity. Three different populations were identified in anorectal TZ using CD34, Krt6 and Nectin4 markers.

After FACS sorting these different populations, we showed that basal CD34⁺ Krt6⁺ cells were the ones able to self-renew and differentiated in 3D cultures showing their stemness properties. Their location, in contact with basement membrane and thus close to stromal and immune compartments may explain their stemness.

In our study we used inducible transgenic K17CreER mice which allowed us to track Keratin17⁺ cells with the specific expression of GFP. We have used low dose of tamoxifen to label single cells and follow clone of cells during time. However, we showed heterogeneity within the Krt17 TZ population (**Figure 20**). Another mouse model can be interesting to use for lineage tracing experiments, it is multi-color fluorescent Reporter Mice also called Confetti mice (see Introduction Chapter I.2.3). Confetti mice express 4 different reporter

genes and tamoxifen injection induce clonal labeling of a given cell type population with the expression of one of these 4 fluorescent genes in a random manner⁵⁸. This system has the advantage to follow the fate of individual clone and its progeny and allows analyzing potential cell population heterogeneity and would highlight more precisely which TZ cell is recruited for rectum tissue repair.

We showed in the paper, a plasticity of TZ cells that participate in rectum tissue repairing after an injury. TZ cells migrate and give rise to fully differentiated and functional crypts positive for columnar epithelium specific Krt8. This point is particularly interesting as during esophageal development (that is squamous stratified epithelium), esophagus consists of a single layer of cuboidal cells expressing Krt8. As this single layer of cells progressively turns into a stratified epithelium, Krt8 expression is lost and cells express Krt14, a marker of adult squamous stratified epithelium³⁸. This is particularly interesting that in TZ, Krt14 population encompass and co-localize with Krt17 population and the novel “hybrid cells” we published earlier this year express both Krt17 and Krt8.

I.2. Genetic ablation of transition zone

The study focusing on the removal of the limbal region showed plasticity of corneal cells able to give rise to a new limbus⁶⁵. This observation raises questions whether genetic ablation of the anorectal TZ will lead to the same observation. Anorectal TZ is composed of basal Krt17⁺ cells divided into CD34⁺ and CD34⁻ cells, stem cells being positive for CD34. When CD34⁻ cells from TZ and anal canal were sorted and cultured into organoids, we observed CD34⁺ cells in these organoids suggesting plasticity of non-stem cells populations (data not shown). This data let us consider high probability of anal canal cells plasticity to replace the anorectal TZ. To elucidate this point, we are currently crossing our mouse model of lineage tracing Krt17CreER with Rosa^{iDTR} mice in which the diphtheria toxin receptor (DTR) is induced specifically in Krt17⁺ cells in order to delete genetically TZ upon diphtheria toxin administration (protocol according to Doucet et al.¹⁷¹). However, this DTR model was reported to have some issues to access sites of interest; we could consider using another model of genetic ablation with diphtheria toxin fragment (DTA). In this case, DTA will be synthesized by Krt17⁺ TZ cells and will consequently die (**Figure 21**).

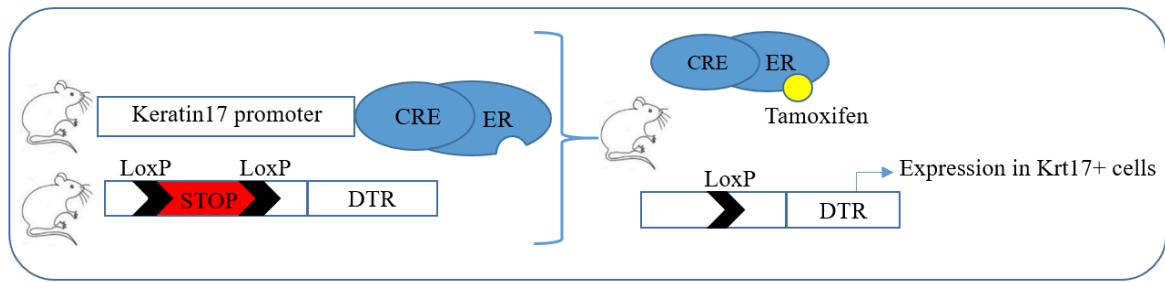


Figure 21: Mouse genetic to specifically delete TZ Krt17⁺ cells

In the intestinal epithelium, stem cells located at the base of the crypt (**Figure 6A**) are actively proliferative for normal homeostatic turnover. However, LRC experiments revealed slow-cycling (or non-proliferative) cells at position 4 from the base of the crypt¹²⁰. Those potential stem cells were positive for BMI1 and were able to generate self-renewing organoids¹¹⁹. *In vivo*, using a DTR mouse model to ablate LGR5⁺ crypt stem cells, BMI1⁺ cells were able to compensate this loss by giving rise to LGR5⁺ cells ensuring intestinal epithelial homeostasis suggesting their role of “reserve stem cells”¹⁷². In anorectal TZ, we showed a minority of TZ cells participating in rectum regeneration⁵¹. Anorectal TZ multipotent cells may constitute a backup stem cell reservoir for rectum epithelium.

II. Regulation of transition zone cells by external stimuli

II.1. Niche signaling in TZ

In the cervix TZ, between the ecto and the endocervix, Chumduri and colleagues reported an opposing signal in Wnt pathway. In an organoid model, they showed that endocervix cell-derived organoid were dependent on Wnt signaling in contrast with ectocervix cell-derived organoids that were not. In addition to this result, in absence of Wnt in culture medium, they observed that endocervix organoids “gave rise” to ectocervix-like organoids expressing p63 and Krt5 that they interpreted as a form of transdifferentiation induced by the absence of Wnt⁵⁵. However, few months after this article, a paper from Clevers lab contradicted those results. Using also an organoid model, they first showed that, indeed, ectocervix cell-derived organoids were not dependent on Wnt signaling. However, they showed that deprivation of Wnt in endocervical organoids culture medium did not induce transdifferentiation into ectocervix-like organoids¹⁷³. To my knowledge, such investigations have not been carried out

regarding the anorectal TZ. However, using our single-cell RNAsequencing data, we did not found Wnt-associated genes in stratified squamous epithelium of anorectal TZ that is consistent with other groups findings.

However, TnC, expressed straight at the anorectal TZ, can be activated by TGF β signaling pathway¹⁷⁴. Moreover, *in vivo* deletion of TGF β RII in Krt14⁺ TZ cells led to spontaneous development of SCC at the anorectal TZ⁵⁹ implying for a role of TGF β signaling in the homeostasis of TZ.

After an injury, we showed that a minority of TZ cells were able to participate in glandular epithelium repair with the ability to give rise to a fully differentiated new rectal crypt. It will be particularly interesting to identify changes and outputs received by TZ stem cells during homeostasis and injuries that prompted TZ cells to show their multipotency. In my hypothesis, during homeostasis, TZ reserve stem cells may receive inhibitory signals from rectum cells/environment. During an injury, inhibitory signals coming from rectum may be abolished and TZ cells, not inhibited anymore, may be allowed to help the injured rectum.

II.2. Transition zone and epigenetics

In addition to factors already cited in the introduction, epigenetic changes are an essential determinant of cell fate. Epigenetic focus on the influence of environment on cells. Cell fate is determined by extrinsic and intrinsic changes. One fascinating example is the determinism demonstrated in ants and honey bees colonies. In both realms, there is only one queen and “social” castes are tightly regulated and determined way before insects are operational. Larvae exposed to specific environmental stimuli, pheromones, temperature and specific nutrition become completely different individuals morphologically and functionally while sharing the same genomes. In some ant species, a worker will never be a queen and vice versa¹⁷⁵.

In mammals, molecule addition on DNA can modulate gene expression by activating or repressing genes. These DNA modifications include methylation and acetylation that are catalyzed by several enzymes. DNA methylation is ensured by DNA methyltransferase family (DNMT), enzymes that catalyze transfer of methyl groups to DNA. Histone deacetylase (HDAC) are responsible for DNA acetylation. Deletion of DNMT1 or HDAC1/2 in mice led both to alopecia and abnormal thickening of the epidermis^{176,177}. After an excisional wound of

mouse skin, topical inhibition of HDAC1,2 and 3 with SiRNA accelerates wound healing whereas knock-down of histone H3K27 demethylase delayed wound healing^{178,179}.

In this project, we did not investigate the epigenetic changes occurring at the anorectal TZ. To my knowledge, epigenetic changes have not been investigated yet in epithelial TZ.

Epigenetic differences were shown between differentiated and stem cell compartments. Indeed, DNMT1 is upregulated in basal layer of adult human epidermis and is lost during differentiation in the upper layers¹⁸⁰. It will be interesting to investigate epigenetic profiles in the heterogeneous populations of TZ and their impact on cell behavior in our mouse models during homeostasis, injury and tumorigenesis. Hybrid TZ cells that we previously identified, could have particular epigenetic changes that favored their plasticity. Furthermore, we could use our mouse model of neoplasia to identify epigenetic changes that may be important in tumor initiation and development. These modifications may later be targeted by specific molecules¹⁸¹.

III. Immunity and KRas mutation in anorectal transition zone

III.1. Immune infiltration of anorectal transition zone

The presence of immune cells in the gastrointestinal tract is a fact but we may wonder why there are naturally more immune cells below the anorectal TZ compared to anal canal and rectum? This is probably the result of multifactorial events and secretions. ECM was proven to influence stem cells within their niche. Some studies have also showed the role of ECM members in immune cell recruitment. TenascinC which is present in TZ stroma is known to play a pro-inflammatory role during wound healing and affects adhesion properties of monocytes, B cells and T cells^{182,183}. ECM-immune cells interplay is not one-sided. Immune cells are true regulators of ECM; they secrete cytokines that stimulate the synthesis of ECM components but also enzymes called metalloproteinases (MMP) able to degrade ECM components. Interestingly, Th1 cells are a source of MMP¹⁸³. Since TZ microenvironment is abundant in immune cells, we can hypothesize that they produce MMP that degrade TZ stroma and explain the stromal softness of TZ compared to surrounding epithelia. Moreover, MMP7 was reported as a marker of squamo-columnar junction in cervix⁵⁴. Physical properties of stroma and epithelial cells need to be investigated further.

It was showed that in Barrett's esophagus, stomach TZ was remodeled in association with immune cells and inflammatory factors infiltration such as IL1B, IL4 and IL6. Interestingly, those factors are upregulated during gastro-esophageal reflux that represents a risk factor for Barrett's esophagus. The majority of immune cells of TZ microenvironment are T lymphocytes. However, during Barrett's esophagus, the T lymphocyte profile change to a B lymphocytes profile accompanied with an upregulation of the immunosuppressive CD3⁺ FoxP3⁺ Treg population¹⁸⁴. Moreover, Barrett's esophagus is a precursor of esophageal cancer and the microenvironment remodeling occurring during this pathological state suggests the importance of immune cells in pathology progression.

III.2. KRas-induced carcinoma

We have previously showed the existence of anorectal TZ cells able to display multipotency after an injury to participate in glandular epithelium repair. The fact that tumors arising in the anorectal TZ after mutations in T lymphocytes are bi-component (squamous and glandular) suggests that these tumors may arise from these TZ cells possessing multipotential property.

Similarly to anorectal TZ, it is interesting to note that we observed hyperplasia in stomach TZ with KRas mutation alone. We could imagine performing adapted chronic injuries in this region (for example acid-induced injuries) to see if the combination of both KRas mutation and chronic wounds induces cancer initiation comparable to what we observed in the anorectal TZ. Moreover, if indeed tumors are initiated in stomach TZ, it will be interesting to compare mechanisms that lead to tumor development in both tissues.

III.3. Epithelial and immune cells interplay

The second part of my Ph.D focused on T lymphocytes and their interplay with epithelial cells. However, TZ stroma is a complex and heterogeneous environment with different cell types. Understanding the contribution of the other stromal compartments such as macrophages, fibroblasts or neutrophils may help to further new insights into how homeostasis is maintained and how stromal disturbance may lead to disease states.

The impact of microbiota on disease progression is now well established. It was particularly studied in chronic disease such as diabetes and inflammatory bowel disease. Healthy

individuals have a balanced microbiome with microbial heterogeneity. Balance disturbance leads to diseases for example in diabetic patients that have less microbial diversity or the expansion of a particular species of bacteria negatively associated with diabetes¹⁸⁵. Crohn's disease, an inflammatory bowel disease, is also associated with a microbial population shift¹⁸⁶. Interestingly, a bacterium called *Debaryomyces hansenii* identified in non-healed and chronically inflamed intestinal tissues was found in Crohn's disease patients and mice. Moreover, it was shown that antibiotic treatment, that represents an dysregulation of microbiota balance, led to impaired wound healing in the intestine¹⁸⁷. It will be, therefore, interesting to investigate TZ microbiota as TZ constitutively express wound-associated proteins. Otherwise, microbiome was shown to be implicated in cancer progression. Studies on colorectal cancers showed that colorectal cancer patients had an altered microbiome compared to healthy individuals. More precisely, *Fusobacterium* species in colorectal cancer was shown to promote tumor growth. Moreover, patients with inflammatory bowel disease have an increased cancer incidence¹⁸⁸. Based on these observations, the lab is currently developing a project to study the impact of microbiota in neoplasia progression. Using the KRas mouse model I developed during my Ph.D, the aim is to give a cocktail of antibiotics to decrease inflammation all along the neoplasia development. Preliminary results of the lab show that the neoplastic phenotype is reduced following antibiotic treatment.

Tumors are often referred to as wounds that do not heal. Our findings in homeostasis and injury conditions combined with the current ongoing project aiming to identify tumor susceptibility will ultimately help establish molecular signatures of mechanisms governing those special regions of our body called transition zones.

REFERENCES

1. Fortier, L. A. Stem Cells: Classifications, Controversies, and Clinical Applications. *Vet. Surg.* **34**, 415–423 (2005).
2. Wobus, A. M. & Boheler, K. R. Embryonic Stem Cells: Prospects for Developmental Biology and Cell Therapy. *Physiol. Rev.* **85**, 635–678 (2005).
3. Eaves, C. J. Hematopoietic stem cells: concepts, definitions, and the new reality. *Blood* **125**, 2605–2613 (2015).
4. Little, M.-T. & Storb, R. History of haematopoietic stem-cell transplantation. *Nat. Rev. Cancer* **2**, 231–238 (2002).
5. Weissman, I. L. & Shizuru, J. A. The origins of the identification and isolation of hematopoietic stem cells, and their capability to induce donor-specific transplantation tolerance and treat autoimmune diseases. *Blood* **112**, 3543–3553 (2008).
6. Wu, A. M., Till, J. E., Siminovitch, L. & McCulloch, E. A. CYTOLOGICAL EVIDENCE FOR A RELATIONSHIP BETWEEN NORMAL HEMATOPOIETIC COLONY-FORMING CELLS AND CELLS OF THE LYMPHOID SYSTEM. *J. Exp. Med.* **127**, 455–464 (1968).
7. Wu, A. M., Till, J. E., Siminovitch, L. & McCulloch, E. A. A cytological study of the capacity for differentiation of normal hemopoietic colony-forming cells. *J. Cell. Physiol.* **69**, 177–184 (1967).
8. Akashi, K., Traver, D., Miyamoto, T. & Weissman, I. L. A clonogenic common myeloid progenitor that gives rise to all myeloid lineages. *Nature* **404**, 193–197 (2000).
9. Blanpain, C. & Fuchs, E. Epidermal Stem Cells of the Skin. *Annu. Rev. Cell Dev. Biol.* **22**, 339–373 (2006).
10. Levy, V., Lindon, C., Harfe, B. D. & Morgan, B. A. Distinct Stem Cell Populations Regenerate the Follicle and Interfollicular Epidermis. *Dev. Cell* **9**, 855–861 (2005).

11. Lu, C. P. *et al.* Identification of Stem Cell Populations in Sweat Glands and Ducts Reveals Roles in Homeostasis and Wound Repair. *Cell* **150**, 136–150 (2012).
12. Van Keymeulen, A. *et al.* Distinct stem cells contribute to mammary gland development and maintenance. *Nature* **479**, 189–193 (2011).
13. Clayton, E. *et al.* A single type of progenitor cell maintains normal epidermis. *Nature* **446**, 185–189 (2007).
14. Tumber, T. Defining the Epithelial Stem Cell Niche in Skin. *Science* **303**, 359–363 (2004).
15. Sartaj, R. Characterization of slow cycling corneal limbal epithelial cells identifies putative stem cell markers. *Sci. Rep.* 14.
16. dos Santos, C. O. *et al.* Molecular hierarchy of mammary differentiation yields refined markers of mammary stem cells. *Proc. Natl. Acad. Sci.* **110**, 7123–7130 (2013).
17. Zhang, D. *et al.* Histone 2B-GFP Label-Retaining Prostate Luminal Cells Possess Progenitor Cell Properties and Are Intrinsically Resistant to Castration. *Stem Cell Rep.* **10**, 228–242 (2018).
18. Blanpain, C., Lowry, W. E., Geoghegan, A., Polak, L. & Fuchs, E. Self-Renewal, Multipotency, and the Existence of Two Cell Populations within an Epithelial Stem Cell Niche. *Cell* **118**, 635–648 (2004).
19. Kretzschmar, K. & Watt, F. M. Lineage Tracing. *Cell* **148**, 33–45 (2012).
20. Snippert, H. J. *et al.* Intestinal Crypt Homeostasis Results from Neutral Competition between Symmetrically Dividing Lgr5 Stem Cells. *Cell* **143**, 134–144 (2010).
21. Barker, N. *et al.* Identification of stem cells in small intestine and colon by marker gene Lgr5. *Nature* **449**, 1003–1007 (2007).
22. Ginestier, C. *et al.* ALDH1 Is a Marker of Normal and Malignant Human Mammary Stem Cells and a Predictor of Poor Clinical Outcome. *Cell Stem Cell* **1**, 555–567 (2007).

23. Rochat, A., Kobayashi, K. & Barrandon, Y. Location of stem cells of human hair follicles by clonal analysis. *Cell* **76**, 1063–1073 (1994).
24. Macara, I. G., Guyer, R., Richardson, G., Huo, Y. & Ahmed, S. M. Epithelial Homeostasis. *Curr. Biol.* **24**, R815–R825 (2014).
25. Kong, S., Zhang, Y. H. & Zhang, W. Regulation of Intestinal Epithelial Cells Properties and Functions by Amino Acids. *BioMed Res. Int.* **2018**, 1–10 (2018).
26. Snoeck, V., Goddeeris, B. & Cox, E. The role of enterocytes in the intestinal barrier function and antigen uptake. *Microbes Infect.* **7**, 997–1004 (2005).
27. Cheng, H. & Leblond, C. P. Origin, differentiation and renewal of the four main epithelial cell types in the mouse small intestine V. Unitarian theory of the origin of the four epithelial cell types. *Am. J. Anat.* **141**, 537–561 (1974).
28. Blanpain, C., Horsley, V. & Fuchs, E. Epithelial Stem Cells: Turning over New Leaves. *Cell* **128**, 445–458 (2007).
29. Rawlins, E. L. & Hogan, B. L. M. Ciliated epithelial cell lifespan in the mouse trachea and lung. *Am. J. Physiol.-Lung Cell. Mol. Physiol.* **295**, L231–L234 (2008).
30. Wansleben, C., Barkauskas, C. E., Rock, J. R. & Hogan, B. L. M. Stem cells of the adult lung: their development and role in homeostasis, regeneration, and disease: Stem cells of the adult lung. *Wiley Interdiscip. Rev. Dev. Biol.* **2**, 131–148 (2013).
31. Frisan, T., Levitsky, V. & Masucci, M. Limiting Dilution Assay. in *Epstein-Barr Virus Protocols* (eds. Wilson, J. B. & May, G. H. W.) 213–216 (Humana Press, 2001).
doi:10.1385/1-59259-227-9:213.
32. Sieburg, H. B., Cho, R. H. & Müller-Sieburg, C. E. Limiting dilution analysis for estimating the frequency of hematopoietic stem cells. *Exp. Hematol.* **30**, 1436–1443 (2002).

33. Simian, M. & Bissell, M. J. Organoids: A historical perspective of thinking in three dimensions. *J. Cell Biol.* **216**, 31–40 (2017).
34. Clevers, H. Modeling Development and Disease with Organoids. *Cell* **165**, 1586–1597 (2016).
35. Waddington, C. H. *The Strategy of the Genes*. (1957).
36. Noah, T. K., Donahue, B. & Shroyer, N. F. Intestinal development and differentiation. *Exp. Cell Res.* **317**, 2702–2710 (2011).
37. Fuchs, E. Skin stem cells: rising to the surface. *J. Cell Biol.* **180**, 273–284 (2008).
38. Rosekrans, S. L., Baan, B., Muncan, V. & van den Brink, G. R. Esophageal development and epithelial homeostasis. *Am. J. Physiol.-Gastrointest. Liver Physiol.* **309**, G216–G228 (2015).
39. Haines, R. L. & Lane, E. B. Keratins and disease at a glance. *J. Cell Sci.* **125**, 3923–3928 (2012).
40. Kim, S., Wong, P. & Coulombe, P. A. A keratin cytoskeletal protein regulates protein synthesis and epithelial cell growth. *Nature* **441**, 362–365 (2006).
41. Jin, L. & Wang, G. Keratin 17: A Critical Player in the Pathogenesis of Psoriasis: KERATIN 17. *Med. Res. Rev.* **34**, 438–454 (2014).
42. de Réaumur, R.-A. F. Sur les diverses reproductions qui se font dans les ecrevisses, les omars, les crabes, etc. et entr’autres sur celles de leurs jambes et de leurs ecailles. in *Mem Acad Roy* (1712).
43. Campos-Sanchez, E., Sanchez-Garcia, I. & Cobaleda, C. Plasticity and Tumorigenicity. *Atlas Genet. Cytogenet. Oncol. Haematol.* (2012)
doi:10.4267/2042/47289.
44. Spallanzani, L. *Prodromo di un opera da imprimersi sopra la riproduzioni animali* (*An Essay on Animal Reproduction*). (1769).

45. Velnar, T., Bailey, T. & Smrkolj, V. The Wound Healing Process: An Overview of the Cellular and Molecular Mechanisms. *J. Int. Med. Res.* **37**, 1528–1542 (2009).
46. Arwert, E. N. Epithelial stem cells, wound healing and cancer. *C N Ce R* **11** (2012).
47. Plikus, M. V. *et al.* Epithelial stem cells and implications for wound repair. *Semin. Cell Dev. Biol.* **23**, 946–953 (2012).
48. Gurtner, G. C., Werner, S., Barrandon, Y. & Longaker, M. T. Wound repair and regeneration. *Nature* **453**, 314–321 (2008).
49. Mcnairn, A. J. & Guasch, G. Epithelial Transition Zones: merging microenvironments, niches, and cellular transformation. *Eur. J. Dermatol.* **21**, 21–28 (2011).
50. Wurm, P. *et al.* Qualitative and Quantitative DNA- and RNA-Based Analysis of the Bacterial Stomach Microbiota in Humans, Mice, and Gerbils. *mSystems* **3**, (2018).
51. Mitoyan, L. *et al.* A stem cell population at the anorectal junction maintains homeostasis and participates in tissue regeneration. *Nat. Commun.* **12**, 2761 (2021).
52. Schepers, A. & Clevers, H. Wnt Signaling, Stem Cells, and Cancer of the Gastrointestinal Tract. *Cold Spring Harb. Perspect. Biol.* **4**, a007989–a007989 (2012).
53. Wang, X. *et al.* Residual Embryonic Cells as Precursors of a Barrett’s-like Metaplasia. *Cell* **145**, 1023–1035 (2011).
54. Herfs, M. *et al.* A discrete population of squamocolumnar junction cells implicated in the pathogenesis of cervical cancer. *Proc. Natl. Acad. Sci.* **109**, 10516–10521 (2012).
55. Chumduri, C. Opposing Wnt signals regulate cervical squamocolumnar homeostasis and emergence of metaplasia. *Nat. Cell Biol.* **23**, 30 (2021).
56. Runck, L. A., Kramer, M., Ciraolo, G., Lewis, A. G. & Guasch, G. Identification of epithelial label-retaining cells at the transition between the anal canal and the rectum in mice. *Cell Cycle* **9**, 3111–3117 (2010).

57. Byrne, C. & Fuchs, E. Probing keratinocyte and differentiation specificity of the human K5 promoter in vitro and in transgenic mice. *Mol. Cell. Biol.* **13**, 3176–3190 (1993).
58. Amitai-Lange, A. *et al.* Lineage Tracing of Stem and Progenitor Cells of the Murine Corneal Epithelium: Lineage Tracing of Limbal and Corneal Epithelial Cells. *STEM CELLS* **33**, 230–239 (2015).
59. Guasch, G. *et al.* Loss of TGF β Signaling Destabilizes Homeostasis and Promotes Squamous Cell Carcinomas in Stratified Epithelia. *Cancer Cell* **12**, 313–327 (2007).
60. Jiang, M. *et al.* Transitional basal cells at the squamous–columnar junction generate Barrett’s oesophagus. *Nature* **550**, 529–533 (2017).
61. Runck, L. A. *et al.* Defining the molecular pathologies in cloaca malformation: similarities between mouse and human. *Dis. Model. Mech.* **7**, 483–493 (2014).
62. Moon, H., Zhu, J., Donahue, L. R., Choi, E. & White, A. C. Krt5+/Krt15+ foregut basal progenitors give rise to cyclooxygenase-2-dependent tumours in response to gastric acid stress. *Nat. Commun.* **10**, (2019).
63. Smedts, F. *et al.* Keratin Expression in Cervical Cancer. **141**, 15 (1992).
64. Smedts, F., Ramaekers, F. & Leube, R. E. Expression of Keratins 1, 6, 15, 16, and 20 in Normal Cervical Epithelium, Squamous Metaplasia, Cervical Intraepithelial Neoplasia, and Cervical Carcinoma. **10**.
65. Nasser, W. *et al.* Corneal-Committed Cells Restore the Stem Cell Pool and Tissue Boundary following Injury. *Cell Rep.* **22**, 323–331 (2018).
66. Flesken-Nikitin, A. *et al.* Ovarian surface epithelium at the junction area contains a cancer-prone stem cell niche. *Nature* **495**, 241–245 (2013).
67. Fu, D.-J. *et al.* Stem Cell Pathology. *Annu. Rev. Pathol. Mech. Dis.* **13**, 71–92 (2018).
68. Seishima, R. *et al.* Neonatal Wnt-dependent Lgr5 positive stem cells are essential for uterine gland development. *Nat. Commun.* **10**, 5378 (2019).

69. Curcio, C., Lanzini, M., Calienno, R., Mastropasqua, R. & Marchini, G. The expression of LGR5 in healthy human stem cell niches and its. *Mol. Vis.* **5** (2015).
70. O'Neil, A., Petersen, C. P., Choi, E., Engevik, A. C. & Goldenring, J. R. Unique Cellular Lineage Composition of the First Gland of the Mouse Gastric Corpus. *J. Histochem. Cytochem.* **65**, 47–58 (2017).
71. Moshi, J. M. *et al.* Switches of SOX17 and SOX2 expression in the development of squamous metaplasia and squamous intraepithelial lesions of the uterine cervix. *Cancer Med.* **9**, 6330–6343 (2020).
72. Bhattacharya, S. *et al.* SOX2 Regulates P63 and Stem/Progenitor Cell State in the Corneal Epithelium: SOX2 Regulates P63 and Corneal Stem/Progenitor Cells. *STEM CELLS* **37**, 417–429 (2019).
73. Ksander, B. R. *et al.* ABCB5 is a limbal stem cell gene required for corneal development and repair. *Nature* **511**, 353–357 (2014).
74. Ouyang, H. *et al.* WNT7A and PAX6 define corneal epithelium homeostasis and pathogenesis. *Nature* **511**, 358–361 (2014).
75. Lopez, P. P., Gogna, S. & Khorasani-Zadeh, A. Anatomy, Abdomen and Pelvis, Duodenum. *StatPEARLS* (2021).
76. Schofield, R. The relationship between the spleen colony-forming cell and the haemopoietic stem cell. *Blood cells* (1978).
77. Gonzalez, H., Hagerling, C. & Werb, Z. Roles of the immune system in cancer: from tumor initiation to metastatic progression. *Genes Dev.* **32**, 1267–1284 (2018).
78. Hirata, Y. *et al.* CD150^{high} Bone Marrow Tregs Maintain Hematopoietic Stem Cell Quiescence and Immune Privilege via Adenosine. *Cell Stem Cell* **22**, 445–453.e5 (2018).
79. Biton, M. *et al.* T Helper Cell Cytokines Modulate Intestinal Stem Cell Renewal and Differentiation. *Cell* **175**, 1307–1320.e22 (2018).

80. Sehgal, A. *et al.* The role of CSF1R-dependent macrophages in control of the intestinal stem-cell niche. *Nat. Commun.* **9**, 1272 (2018).
81. Gyorki, D. E., Asselin-Labat, M.-L., van Rooijen, N., Lindeman, G. J. & Visvader, J. E. Resident macrophages influence stem cell activity in the mammary gland. *Breast Cancer Res.* **11**, R62 (2009).
82. Koliarakis, V., Prados, A., Armaka, M. & Kollias, G. The mesenchymal context in inflammation, immunity and cancer. *Nat. Immunol.* **21**, 974–982 (2020).
83. Kinchen, J. *et al.* Structural Remodeling of the Human Colonic Mesenchyme in Inflammatory Bowel Disease. *Cell* **175**, 372–386.e17 (2018).
84. Mifflin, R. C., Pinchuk, I. V., Saada, J. I. & Powell, D. W. Intestinal myofibroblasts: targets for stem cell therapy. *Am. J. Physiol.-Gastrointest. Liver Physiol.* **300**, G684–G696 (2011).
85. van Beurden, H. E., Von den Hoff, J. W., Torensma, R., Maltha, J. C. & Kuijpers-Jagtman, A. M. Myofibroblasts in Palatal Wound Healing: Prospects for the Reduction of Wound Contraction after Cleft Palate Repair. *J. Dent. Res.* **84**, 871–880 (2005).
86. Kondo, A. & Kaestner, K. H. Emerging diverse roles of telocytes. *Development* **146**, dev175018 (2019).
87. McCarthy, N. *et al.* Distinct Mesenchymal Cell Populations Generate the Essential Intestinal BMP Signaling Gradient. *Cell Stem Cell* **26**, 391–402.e5 (2020).
88. Rezza, A., Sennett, R. & Rendl, M. Adult Stem Cell Niches. in *Current Topics in Developmental Biology* vol. 107 333–372 (Elsevier, 2014).
89. Reya, T. *et al.* A role for Wnt signalling in self-renewal of haematopoietic stem cells. *Nature* **423**, 409–414 (2003).
90. Brittan, M. & Wright, N. A. Gastrointestinal stem cells. *J. Pathol.* **197**, 492–509 (2002).

91. MacDonald, B. T., Tamai, K. & He, X. Wnt/ β -Catenin Signaling: Components, Mechanisms, and Diseases. *Dev. Cell* **17**, 9–26 (2009).
92. Ota, C., Baarsma, H. A., Wagner, D. E., Hilgendorff, A. & Königshoff, M. Linking bronchopulmonary dysplasia to adult chronic lung diseases: role of WNT signaling. *Mol. Cell. Pediatr.* **3**, 34 (2016).
93. Huelsken, J., Vogel, R., Erdmann, B., Cotsarelis, G. & Birchmeier, W. β -Catenin Controls Hair Follicle Morphogenesis. **13**.
94. Fuchs, E. The Tortoise and the Hair: Slow-Cycling Cells in the Stem Cell Race. *Cell* **137**, 811–819 (2009).
95. Sigal, M. *et al.* Stromal R-spondin orchestrates gastric epithelial stem cells and gland homeostasis. *Nature* **548**, 451–455 (2017).
96. Kim, K.-A. *et al.* Mitogenic Influence of Human R-Spondin1 on the Intestinal Epithelium. *Science* **309**, 1256 (2005).
97. Sato, T. *et al.* Paneth cells constitute the niche for Lgr5 stem cells in intestinal crypts. *Nature* **469**, 415–418 (2011).
98. Demitrack, E. S. & Samuelson, L. C. Notch regulation of gastrointestinal stem cells: Notch regulates GI stem cells. *J. Physiol.* **594**, 4791–4803 (2016).
99. Pellegrinet, L. *et al.* Dll1- and Dll4-Mediated Notch Signaling Are Required for Homeostasis of Intestinal Stem Cells. *Gastroenterology* **140**, 1230-1240.e7 (2011).
100. Sancho, R., Cremona, C. A. & Behrens, A. Stem cell and progenitor fate in the mammalian intestine: Notch and lateral inhibition in homeostasis and disease. *EMBO Rep.* **16**, 571–581 (2015).
101. VanDussen, K. L. *et al.* Notch signaling modulates proliferation and differentiation of intestinal crypt base columnar stem cells. *Development* **139**, 488–497 (2012).

102. Poulos, M. G. *et al.* Endothelial Jagged-1 Is Necessary for Homeostatic and Regenerative Hematopoiesis. *Cell Rep.* **4**, 1022–1034 (2013).
103. Maillard, I. *et al.* Canonical Notch Signaling Is Dispensable for the Maintenance of Adult Hematopoietic Stem Cells. *Cell Stem Cell* **2**, 356–366 (2008).
104. Garside, V. C., Chang, A. C., Karsan, A. & Hoodless, P. A. Co-ordinating Notch, BMP, and TGF- β signaling during heart valve development. *Cell. Mol. Life Sci.* **70**, 2899–2917 (2013).
105. Qi, Z. *et al.* BMP restricts stemness of intestinal Lgr5+ stem cells by directly suppressing their signature genes. *Nat. Commun.* **8**, 13824 (2017).
106. Oshimori, N. & Fuchs, E. Paracrine TGF- β Signaling Counterbalances BMP-Mediated Repression in Hair Follicle Stem Cell Activation. *Cell Stem Cell* **10**, 63–75 (2012).
107. Ollivier, A., Mahe, M. M. & Guasch, G. Modeling Gastrointestinal Diseases Using Organoids to Understand Healing and Regenerative Processes. *Cells* **10**, 1331 (2021).
108. Conboy, I. M. *et al.* Rejuvenation of aged progenitor cells by exposure to a young systemic environment. *Nature* **433**, 760–764 (2005).
109. Wen, Y., Hu, S. & Wu, J. Extracellular Matrix Plays an Important Role in Stem Cell Biology. *J. Stem Cell Res. Ther.* **08**, (2018).
110. Ahmed, M. & French-Constant, C. Extracellular Matrix Regulation of Stem Cell Behavior. *Curr. Stem Cell Rep.* **2**, 197–206 (2016).
111. Gjorevski, N. *et al.* Designer matrices for intestinal stem cell and organoid culture. *Nature* **539**, 560–564 (2016).
112. Park, K. J. & Soslow, R. A. Current Concepts in Cervical Pathology. *Arch. Pathol. Lab. Med.* **133**, 729–738 (2009).
113. Mills, J. C., Stanger, B. Z. & Sander, M. Nomenclature for cellular plasticity: are the terms as plastic as the cells themselves? *EMBO J.* **38**, (2019).

114. Adami, J. G. & Nicholls, A. G. *The principles of pathology*. vol. II (Lea & Febiger, 1908).
115. Okada, T. S. 'TRANSDIFFERENTIATION' OF CELLS FROM CHICK EMBRYONIC EYE TISSUES IN CELL CULTURE. *Dev. Growth Differ.* **17**, 289–290 (1975).
116. van Es, J. H. *et al.* Dll1+ secretory progenitor cells revert to stem cells upon crypt damage. *Nat. Cell Biol.* **14**, 1099–1104 (2012).
117. Rompolas, P., Mesa, K. R. & Greco, V. Spatial organization within a niche as a determinant of stem-cell fate. *Nature* **502**, 513–518 (2013).
118. Ito, M. *et al.* Stem cells in the hair follicle bulge contribute to wound repair but not to homeostasis of the epidermis. *Nat. Med.* **11**, 1351–1354 (2005).
119. Buczacki, S. J. A. *et al.* Intestinal label-retaining cells are secretory precursors expressing Lgr5. *Nature* **495**, 65–69 (2013).
120. Bankaitis, E. D., Ha, A., Kuo, C. J. & Magness, S. T. Reserve Stem Cells in Intestinal Homeostasis and Injury. *Gastroenterology* **155**, 1348–1361 (2018).
121. Takahashi, K. & Yamanaka, S. Induction of Pluripotent Stem Cells from Mouse Embryonic and Adult Fibroblast Cultures by Defined Factors. *Cell* **126**, 663–676 (2006).
122. Hanna, J. *et al.* Treatment of Sickle Cell Anemia Mouse Model with iPS Cells Generated from Autologous Skin. *Science* **318**, 1920–1923 (2007).
123. Sun, N., Longaker, M. T. & Wu, J. C. Human iPS cell-based therapy: Considerations before clinical applications. *Cell Cycle* **9**, 880–885 (2010).
124. Shi, X. *et al.* IL-17A Upregulates Keratin 17 Expression in Keratinocytes through STAT1- and STAT3-Dependent Mechanisms. *J. Invest. Dermatol.* **131**, 2401–2408 (2011).

125. McGowan, K. M. & Coulombe, P. A. Onset of Keratin 17 Expression Coincides with the Definition of Major Epithelial Lineages during Skin Development. *J. Cell Biol.* **143**, 469–486 (1998).
126. Marshall, B. J. *Campylobacter pyloridis* and Gastritis. *J. Infect. Dis.* **153**, 650–657 (1986).
127. Korman, M. G. & Tytgat, G. N. J. *Helicobacter pylori* and Peptic Ulcer. *Scand. J. Gastroenterol.* **30**, 92–96 (1995).
128. Alzahrani, S. Effect of *Helicobacter pylori* on gastric epithelial cells. *World J. Gastroenterol.* **20**, 12767 (2014).
129. Veldhuyzen van Zanten, S. J. O., Dixon, M. F. & Lee, A. The gastric transitional zones: Neglected links between gastroduodenal pathology and *Helicobacter* ecology. *Gastroenterology* **116**, 1217–1229 (1999).
130. Kuipers, E. J., Lee, A., Klinkenberg-Knol, E. C. & Meuwissen, S. G. M. The development of atrophic gastritis-*Helicobacter pylori* and the effects of acid suppressive therapy. *Aliment. Pharmacol. Ther.* **9**, 331–340 (2007).
131. Inadomi, J. *et al.* Recent advances in Barrett’s esophagus. *Ann. N. Y. Acad. Sci.* **1434**, 227–238 (2018).
132. Yamamoto, Y. *et al.* Mutational spectrum of Barrett’s stem cells suggests paths to initiation of a precancerous lesion. *Nat. Commun.* **7**, 10380 (2016).
133. Wirtz, S. *et al.* Chemically induced mouse models of acute and chronic intestinal inflammation. *Nat. Protoc.* **12**, 1295–1309 (2017).
134. Simões, S. *et al.* Animal models of acute gastric mucosal injury: Macroscopic and microscopic evaluation. *Anim. Models Exp. Med.* ame2.12060 (2019)
doi:10.1002/ame2.12060.

135. Wang, J. P., Yamasaki, S., Takeuchi, K. & Okabe, S. Delayed Healing of Acetic Acid-Induced Gastric Ulcers in Rats by Indomethacin. *Gastroenterology* **96**, 393–402 (1989).
136. Okabe, S. & Amagase, K. An Overview of Acetic Acid Ulcer Models—The History and State of the Art of Peptic Ulcer Research—*Biol. Pharm. Bull.* **28**, 1321–1341 (2005).
137. Fukuda, M. *et al.* Small intestinal stem cell identity is maintained with functional Paneth cells in heterotopically grafted epithelium onto the colon. *Genes Dev.* **28**, 1752–1757 (2014).
138. Bongiorno, T., Chojnowski, J. L., Lauderdale, J. D. & Sulchek, T. Cellular Stiffness as a Novel Stemness Marker in the Corneal Limbus. *Biophys. J.* **111**, 1761–1772 (2016).
139. Yang, Y. *et al.* $\gamma\delta$ T Cells: Crosstalk Between Microbiota, Chronic Inflammation, and Colorectal Cancer. *Front. Immunol.* **9**, 1483 (2018).
140. FLUHMANN, C. F. Carcinoma in situ and the transitional zone of the cervix uteri.
141. Smith, M. E. Clinical and Pathologic Description of 17 Cases of Corneal Intraepithelial Neoplasia. *Am. J. Ophthalmol.* **98**, 383 (1984).
142. Trudgill, N. J., Suvarna, S. K., Royds, J. A. & Riley, S. A. Cell cycle regulation in patients with intestinal metaplasia at the gastro–oesophageal junction. 5.
143. Maliekal, T. T., Antony, M.-L., Nair, A., Paulmurugan, R. & Karunagaran, D. Loss of expression, and mutations of Smad 2 and Smad 4 in human cervical cancer. 9.
144. Kloth, J. N. *et al.* Expression of Smad2 and Smad4 in cervical cancer: absent nuclear Smad4 expression correlates with poor survival. *Mod. Pathol.* **21**, 866–875 (2008).
145. Grodsky, L. Transitional Cell Cancer of the Anus and Rectum. *Calif. Med.* 5.
146. Khalili, K. & Jeang, K.-T. Viral Oncology: Basic Science and Clinical Applications. 510.

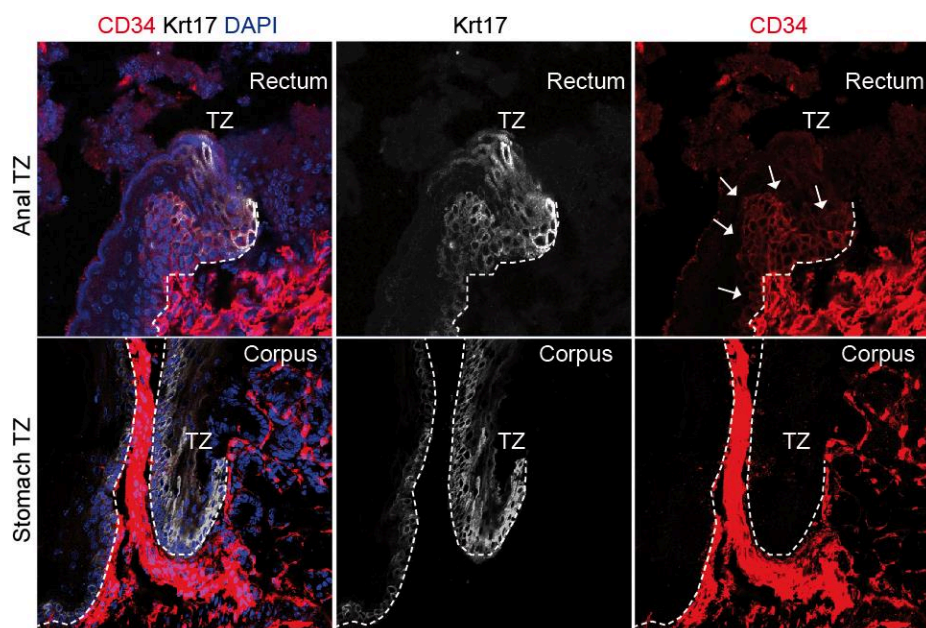
147. Rajendra, S. & Sharma, P. Transforming human papillomavirus infection and the esophageal transformation zone: prime time for total excision/ablative therapy? *Dis. Esophagus* **32**, doz008 (2019).
148. McCauley, H. A., Chevrier, V., Birnbaum, D. & Guasch, G. De-repression of the RAC activator ELMO1 in cancer stem cells drives progression of TGF β -deficient squamous cell carcinoma from transition zones. *eLife* **6**, e22914 (2017).
149. McCauley, H. A. & Guasch, G. Serial Orthotopic Transplantation of Epithelial Tumors in Single-Cell Suspension. in *Stem Cell Niche: Methods and Protocols* (ed. Turksen, K.) 231–245 (Humana Press, 2013). doi:10.1007/978-1-62703-508-8_20.
150. Flesken-Nikitin, A., Choi, K.-C., Eng, J. P., Shmidt, E. N. & Nikitin, A. Y. Induction of Carcinogenesis by Concurrent Inactivation of p53 and Rb1 in the Mouse Ovarian Surface Epithelium. **6**.
151. Nagaraj, N. S. & Datta, P. K. Targeting the transforming growth factor- β signaling pathway in human cancer. **16** (2010).
152. Nam, K. T. *et al.* Gastric tumor development in Smad3-deficient mice initiates from forestomach/glandular transition zone along the lesser curvature. *Lab. Invest.* **92**, 13 (2012).
153. Ijichi, H. *et al.* Aggressive pancreatic ductal adenocarcinoma in mice caused by pancreas-specific blockade of transforming growth factor-beta signaling in cooperation with active Kras expression. *Genes Dev.* **20**, 3147–3160 (2006).
154. Bardeesy, N. *et al.* Smad4 is dispensable for normal pancreas development yet critical in progression and tumor biology of pancreas cancer. *Genes Dev.* **20**, 3130–3146 (2006).
155. Maggio-Price, L. *et al.* *Helicobacter* Infection Is Required for Inflammation and Colon Cancer in Smad3-Deficient Mice. *Cancer Res.* **66**, 828–838 (2006).

156. Zhao, M., Mishra, L. & Deng, C.-X. The role of TGF- β /SMAD4 signaling in cancer. *Int. J. Biol. Sci.* **14**, 111–123 (2018).
157. Liu, F., Yang, X., Geng, M. & Huang, M. Targeting ERK, an Achilles' Heel of the MAPK pathway, in cancer therapy. *Acta Pharm. Sin. B* **8**, 552–562 (2018).
158. Jančík, S., Drábek, J., Radzioch, D. & Hajdúch, M. Clinical Relevance of KRAS in Human Cancers. *J. Biomed. Biotechnol.* **2010**, 1–13 (2010).
159. Waters, A. M. & Der, C. J. KRAS: The Critical Driver and Therapeutic Target for Pancreatic Cancer. *Cold Spring Harb. Perspect. Med.* **8**, a031435 (2018).
160. Tuveson, D. A. *et al.* Endogenous oncogenic K-rasG12D stimulates proliferation and widespread neoplastic and developmental defects. *Cancer Cell* **5**, 375–387 (2004).
161. Lapouge, G. *et al.* Identifying the cellular origin of squamous skin tumors. *Proc. Natl. Acad. Sci.* **108**, 7431–7436 (2011).
162. Dvorak, H. F. TUMORS: WOUNDS THAT DO NOT HEAL. *The New England Journal of Medicine* (1986).
163. DePianto, D. Keratin 17 promotes epithelial proliferation and tumor growth by polarizing the immune response in skin. *Nat. Genet.* **42**, 6 (2010).
164. Khanom, R. *et al.* Keratin 17 Is Induced in Oral Cancer and Facilitates Tumor Growth. *PLOS ONE* **11**, e0161163 (2016).
165. Kim, S., Wong, P. & Coulombe, P. A. A keratin cytoskeletal protein regulates protein synthesis and epithelial cell growth. *Nature* **441**, 362–365 (2006).
166. Marie, J. C., Liggitt, D. & Rudensky, A. Y. Cellular Mechanisms of Fatal Early-Onset Autoimmunity in Mice with the T Cell-Specific Targeting of Transforming Growth Factor- β Receptor. *Immunity* **25**, 441–454 (2006).
167. Long, J. D. & Orlando, R. C. Esophageal submucosal glands: structure and function. *Am. J. Gastroenterol.* **94**, 2818–2824 (1999).

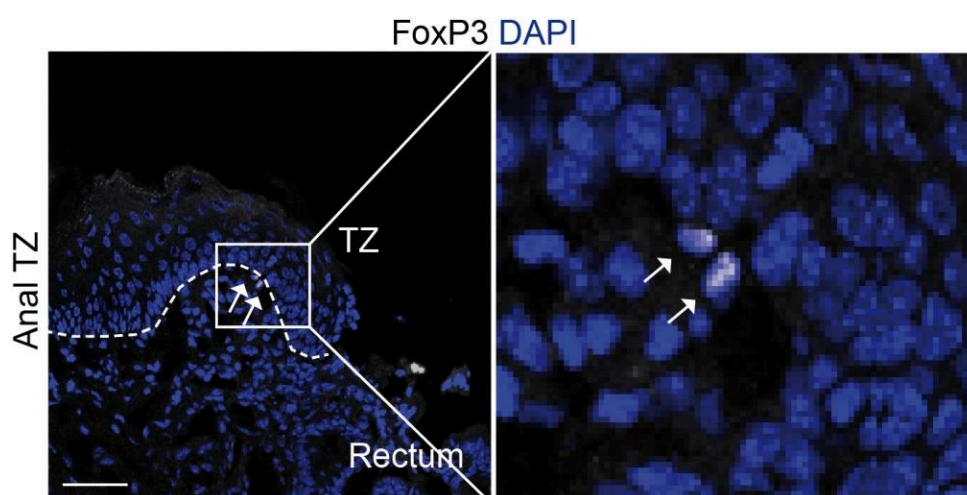
168. Gerbe, F. *et al.* Intestinal epithelial tuft cells initiate type 2 mucosal immunity to helminth parasites. *Nature* **529**, 226–230 (2016).
169. Peck, B. C. E., Shanahan, M. T., Singh, A. P. & Sethupathy, P. Gut Microbial Influences on the Mammalian Intestinal Stem Cell Niche. *Stem Cells Int.* **2017**, 1–17 (2017).
170. Preidis, G. A. *et al.* Probiotics stimulate enterocyte migration and microbial diversity in the neonatal mouse intestine. *FASEB J.* **26**, 1960–1969 (2012).
171. Doucet, Y. S., Woo, S.-H., Ruiz, M. E. & Owens, D. M. The Touch Dome Defines an Epidermal Niche Specialized for Mechanosensory Signaling. *Cell Rep.* **3**, 1759–1765 (2013).
172. Tian, H. *et al.* A reserve stem cell population in small intestine renders Lgr5-positive cells dispensable. *Nature* **478**, 255–259 (2011).
173. Löhmußaar, K. Patient-derived organoids model cervical tissue dynamics and viral oncogenesis in cervical cancer. *24*.
174. Jinnin, M. *et al.* Tenascin-C upregulation by transforming growth factor- β in human dermal fibroblasts involves Smad3, Sp1, and Ets1. *Oncogene* **23**, 1656–1667 (2004).
175. Chittka, A., Wurm, Y. & Chittka, L. Epigenetics: The Making of Ant Castes. *Curr. Biol.* **22**, R835–R838 (2012).
176. Hughes, M. W. *et al.* Disrupted Ectodermal Organ Morphogenesis in Mice with a Conditional Histone Deacetylase 1, 2 Deletion in the Epidermis. *J. Invest. Dermatol.* **134**, 24–32 (2014).
177. Li, J. *et al.* Progressive Alopecia Reveals Decreasing Stem Cell Activation Probability during Aging of Mice with Epidermal Deletion of DNA Methyltransferase 1. *J. Invest. Dermatol.* **132**, 2681–2690 (2012).

178. Kang, S., Chovatiya, G. & Tumbar, T. Epigenetic control in skin development, homeostasis and injury repair. *Exp. Dermatol.* **28**, 453–463 (2019).
179. Spallotta, F. *et al.* Enhancement of lysine acetylation accelerates wound repair. *Commun. Integr. Biol.* **6**, e25466 (2013).
180. Sen, G. L., Reuter, J. A., Webster, D. E., Zhu, L. & Khavari, P. A. DNMT1 maintains progenitor function in self-renewing somatic tissue. *Nature* **463**, 563–567 (2010).
181. Yan, W., Herman, J. G. & Guo, M. Epigenome-based personalized medicine in human cancer. *Epigenomics* **8**, 119–133 (2016).
182. Midwood, K. S. & Orend, G. The role of tenascin-C in tissue injury and tumorigenesis. *J. Cell Commun. Signal.* **3**, 287–310 (2009).
183. Bhattacharjee, O., Ayyangar, U., Kurbet, A. S., Ashok, D. & Raghavan, S. Unraveling the ECM-Immune Cell Crosstalk in Skin Diseases. *Front. Cell Dev. Biol.* **7**, 68 (2019).
184. Han, P. *et al.* Esophageal Microenvironment: From Precursor Microenvironment to Premetastatic Niche. *Cancer Manag. Res.* **Volume 12**, 5857–5879 (2020).
185. Gurung, M. *et al.* Role of gut microbiota in type 2 diabetes pathophysiology. *EBioMedicine* **51**, 102590 (2020).
186. Schirmer, M., Garner, A., Vlamakis, H. & Xavier, R. J. Microbial genes and pathways in inflammatory bowel disease. *Nat. Rev. Microbiol.* **17**, 497–511 (2019).
187. Jain, U. *et al.* *Debaryomyces* is enriched in Crohn's disease intestinal tissue and impairs healing in mice. *Science* **371**, 1154–1159 (2021).
188. Jain, T., Sharma, P., Are, A. C., Vickers, S. M. & Dudeja, V. New Insights Into the Cancer–Microbiome–Immune Axis: Decrypting a Decade of Discoveries. *Front. Immunol.* **12**, 622064 (2021).

ANNEXE



Annexe 1: Krt17 (white) and CD34 (red) expressions in anal and stomach TZ. Arrows denote CD34⁺ cell population.



Annexe 2: Tregulators positive for FoxP3 (white) at the anorectal TZ.